PRODUCTION AND STRUCTURAL STUDIES OF LUNG SURFACTANT PROTEIN B (SP-B) PEPTIDES

MAHZAD SHARIFAHMADIAN

Production and Structural Studies of Lung Surfactant Protein B (SP-B) Peptides

Mahzad Sharifahmadian

July 2011, Memorial University of Newfoundland

Submitted in partial fulfillment of the requirements for the Degree of Master of Science

Department of Biochemistry

Memorial University of Newfoundland

St. John's, NL A1B 3X9

2011

Abstract

Lung surfactant is a mixture of lipids and proteins which is critical for normal breathing by lining the air-water interface to reduce the surface tension. Lung surfactant protein B (SP-B) is the only essential protein component of lung surfactant complex due to the lethality of any SP-B deficiency. It is thought that SP-B functions by enhancing lipid rearrangements at various phases of the breathing cycle. However, the high-resolution structure and mechanism of SP-B are not yet understood. In the first part of this research, SP-B and a 7- residue deletion mutant of SP-B were produced recombinantly and partially characterized. In the second part of this research, circular dichroism, solution and solid-state nuclear magnetic resonance (NMR) methods were used to assess the structure of two SP-B-based peptides, Super-Mini-B and N-terminal insertion sequence ($SP\text{-}B_{1\text{-}7}$). Super-Mini-B is composed of the N-terminal 7-residue insertion sequence and the N-and C-terminal helices of SP-B. Interestingly, it was observed that Super-Mini-B produces greater lipid membrane perturbation than the peptide which lacks the N-terminal insertion sequence (i.e. Mini-B). Comparing the results of structural studies on Mini-B, $SP\text{-}B_{1\text{-}7}$ and Super-Mini-B helps unveil the contribution of the 7-residue insertion sequence to the function of SP-B.

Acknowledgements

I would first like to thank my supervisor, Dr. Valerie Booth for her wonderful guidance and support. I would also like to thank Donna Jackman, Dr. Muzaddid Sarker, Dr. Michael Hayley and Dharamaraju Palleboina who helped me greatly throughout my project. I acknowledge the supportive and encouraging roles of my committee members Dr. Mike Morrow and Dr. Kaushik Nag throughout the whole program. I would like to thank Dr. David Heeley, Craig Skinner, Marie Codner, for their help (Biochemistry Department, Memorial University, NL, Canada), as well Dr. Alan Waring and his colleagues preparing one of the peptide samples used in this work (Department of Medicine, UCLA School of Medicine, CA, USA). The pan-university Core Research Equipment and Instrument Training Network (CREAIT) at Memorial University for facilitating some NMR experiments and performing DNA sequencing experiments. I am also grateful for the funding obtained for this project from Canadian Institutes of Health Research (CIHR) to my supervisor.

I would also like to thank all my lovely friends and people who made living in St. John's like being at home.

Table of Contents

List of Tables

List of Figures

List of Abbreviations

1D	one-dimensional
16-DSA	16-doxyl-stearic acid
2D	two-dimensional
ARDS	acute respiratory distress syndrome
BCIP	5-bromo-4-chloro-3-indolyl-phosphate
CD	circular dichroism
CPP	cell penetrating peptide
DLS	dynamic light scattering
DMF	dimethylformamide
DOSY	diffusion ordered spectroscopy
DPPC	dipalmitoylphosphatidylcholine
DSS	sodium 2,2-dimethyl-2-silapentane-5-sulfonate
EDTA	ethylenediaminetetraacetic acid
Fmoc	9-fluorenylmethyloxycarbonyl
HFIP	hexafluoroisopropanol
HPLC	high-pressure liquid chromatography

IPTG	β-D-1-thiogalactopyranoside
MALDI-TOF MS	matrix assisted laser desorption ionization – time of flight mass spectrometry
NBT	nitro blue tetrazolium
NMR	nuclear magnetic resonance
NOESY	nuclear overhauser-effect spectroscopy
NRDS	neonatal acute respiratory distress syndrome
PC	phosphatidylcholine
PCR	polymerase chain reaction
PG	phosphatidyleglycerol
PMSF	phenylmethanesulfonylfluoride
POPC-d_{31}	deuterated 1-palmitoyl-2-oleoyl-*sn*-glycero-3-phosphocholine
POPG	1-palmitoyl-2-oleoyl-*sn*-glycero-3-phospho-(1'-rac- glycerol)
ppm	parts per million
PVDF	polyvinylidene fluoride
SDS	sodium dodecyl sulphate
SDS-PAGE	sodium dodecyl sulfate polyacrylamide gel electrophoresis

SN	staphylococcus nuclease
SP-A	surfactant protein A
SP-B	surfactant protein B
$SP\text{-}B_{1\text{-}7}$	N-terminal insertion sequence
SP-D	surfactant protein D
TB	terrific broth
TBS	tris buffered saline
TFE	2,2,2-trifluoroethanol
TOCSY	total correlation spectroscopy

1. Introduction

The respiratory system functions as the supplier of oxygen to the blood. Gas diffusion happens at the alveolar level in very close proximity to lung capillaries. There are about 300 million alveoli in the lungs providing a total surface area of about 140 m^2 (Guyton and Hall, 2006). The alveolar walls are lined by alveolar epithelial cells which are in direct contact with respiratory gases (Figure 1).

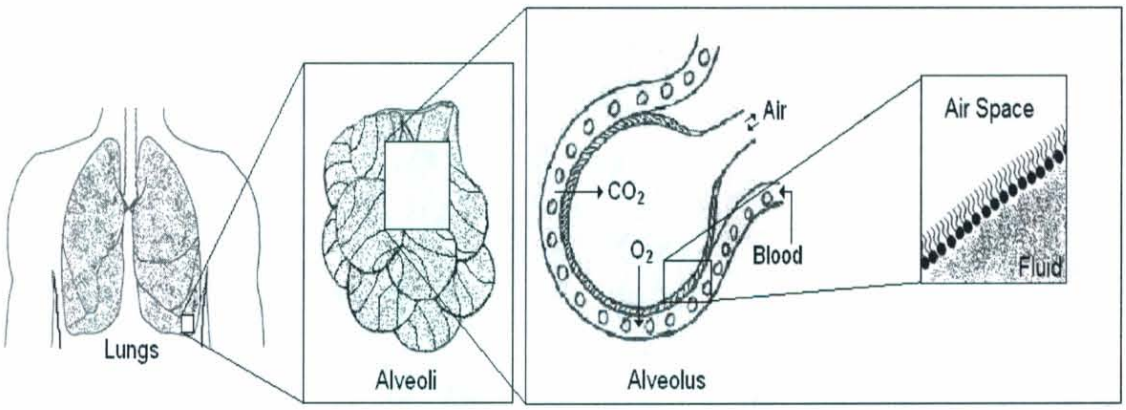

Figure 1. A schematic diagram of the human respiratory system. Lung surfactant, a lipid-protein complex, lines the inner surface of alveoli and reduces the surface tension at the air-water interface to facilitate breathing.

The constant exposure to environmental gases and particles requires the presence of a 0.2 mm thick water layer coating the inner surface of the alveoli. This layer prevents the dehydration (Bastacky et al. 1995).

When water forms a surface with air, water molecules strongly attract each other; the forces of attraction between water molecules are stronger than the forces between water and air that lead to a surface tension at the air-water interface. The surface tension forces air out causing the alveoli to collapse and consequently disrupts respiration (Guyton and Hall, 2006). The natural remedy to decrease the surface tension and maintain inflation is the presence of lung surfactant, a complex mixture of lipids and proteins (Whitsett et al., 2010). Lung surfactant complex decreases the surface tension by formation of the surface active films at the alveolar level and transfer of surface active materials between the air-water interface and hypophases (Serrano et al., 2006).

Deficiency or inactivation of lung surfactant either by premature birth, gene mutation or lung injury leads to severe respiratory disorders. The pathophysiological effect of surfactant deficiency was first diagnosed in premature infants with neonatal respiratory distress syndrome (NRDS). Lung surfactant does not normally begin to be secreted into the alveoli until the sixth or seventh months of pregnancy, in some cases, even later than that. Thus many premature babies have little or no surfactant in the alveoli, which gives rise to a very high tendency for lung collapse (Griese, 1999). NRDS affects about 1 percent of newborn infants; it is the leading cause of death in prematurely born babies (Hallman et al., 2001). The respiratory disorder resulting from the damage and dysfunction of surfactant during

injuries or sepsis is called acute respiratory distress syndrome (ARDS). ARDS has a high rate of fatality, between 36% to 52% (Seeger et al., 1993).

Mutations in the genes encoding surfactant protein B and surfactant protein C (SFTPB and SFTPC, respectively) can lead to acute respiratory failure and interstitial lung diseases. Respiratory failure in mature newborns due to mutation in SP-B and SP-C encoding genes is extremely rare but has been observed repeatedly as an inherited cause of severe respiratory dysfunction (Nogee et al., 2000).

Surfactant replacement therapy has had a proven role in the treatment of NRDS and may have a role in the treatment of patients with ARDS. However, efforts to use replacement surfactant to treat ARDS have not been successful thus far; deactivation of the replacement surfactant reduces the efficiency of endogenous surfactant therapy in these patients (Gunther et al., 1999; Stevens and Sinkin, 2007).

Surfactant based drugs can contain both the phospholipid and protein content. Synthetic surfactants differ remarkably from natural surfactants in their protein composition (Marraro, 2004). The original commercially available surfactant, (Exosurf; Glaxo Wellcome), does not contain any surfactant proteins. Clinical trials have shown artificial surfactants are much more effective if they include surfactant proteins as compared to protein-free preparations (Lewis and Veldhuizen, 2003). Natural surfactants, derived from animal lungs by organic extraction,

contain surfactant proteins and are much more effective in lowering the surface tension (Stevens and Sinkin, 2007).

There are two type of epithelial covering the alveolar surface; type I and type II cells. Type I cells form the structure of an alveolar wall while all lung surfactant components are synthesized by type II alveolar epithelial cells. After secretion to the alveolar space, lung surfactant phospholipids can form distinct physical structures from monolayers to multilayers, including tubular myelin and lamellar bodies, as well as vesicular, protein-lipid structures. Formation of these structures is mainly affected by the stoichiometry of lipids and surfactant proteins, and physical forces generated during respiration (Whitsett, et al., 2010). Although the composition of lung surfactant can vary from one species to another, lung surfactant is composed of around 80% phospholipids, 5–10% neutral lipids –mainly cholesterol–, and 8–10% proteins making up 5–6% of total surfactant mass (Goerke, et al., 1998).

The lipid fraction of mammalian surfactants (by mass) is composed of around 80% phosphatidylcholine (PC), about half of which is the disaturated form dipalmitoylphosphatidylcholine (DPPC) (Veldhuizen, et al., 1998). Different levels of fluidity during the respiration cycle require a balance between the presence of saturated and unsaturated lipids. The most remarkable difference of surfactant composition in humans in comparison to other mammalian membranes is the unusual high content of DPPC and

anionic phospholipids, mostly phosphatidylglycerol (PG) (Wustneck, et al., 2005). DPPC is a rare phospholipid species in other tissues but evolutionary has been chosen. DPPC's saturated chains pack to a high density at the air–water interface at physiological temperature and provide a significant reduction in surface tension at the end of expiration (Hawcoa et al., 1981).

In mice and humans at 37°C, the physiological temperature, pure phospholipids have a slow rate of film formation and weak surfactant activity. Appropriate rate of film formation, stability during respiration cycle and re-spreading capacities are dependent on the presence of the surfactant proteins (Whitsett and Weaver, 2002 ; Halliday, 1996).

Surfactant proteins designated surfactant protein A (SP-A), SP-B, SP-C, and surfactant protein D (SP-D), play critical roles in various aspects of surfactant structure, function, and metabolism (Perez-Gil, 2008). In general they are divided in two main groups; the hydrophilic surfactant proteins SP-A and SP-D, and the hydrophobic surfactant proteins SP-B and SP-C. SP-A is the most abundant protein component of surfactant (Sueishi and Benson, 1981) which is associated with surfactant phospholipids (Schurch et al., 1992; Bi et al., 2001). SP-D is found in a very small amount in the lavage and does not associate with lipid containing structures (Haagsman and Diemela, 2001). The structures of SP-A and SP-D allow them to bind to diverse ligands underlying their role in the innate immune system at the lung surface (Crouch and Wright, 2001). SP-B and SP-C

compose 1–1.5% of total surfactant mass. These hydrophobic proteins interact with the lipids in lung surfactant (Shiffer et al., 1993; Taneva and Keough, 1994).

SP-B is the only lung surfactant protein whose deficiency is lethal (Clark et al., 1995; Tokieda et al., 1997). SP-B exists in different classes of vertebrates including fish (lungfish), amphibians, reptiles and mammals; in human the encoding gene is located on chromosome 2. It belongs to the family of saposin-like proteins, which possess a special fold of around 80 amino acids containing amphipathic alpha-helices and three conserved disulphide bridges in conserved positions (Munford et al., 1995). All saposin-like proteins have activities related to interaction with phospholipid membranes (Patthy, 1991).

The mature SP-B isolated from lung lavages is a highly hydrophobic peptide with 79 amino acids, with ~8 kDa molecular mass; the functional form is a homodimer. It possesses three covalent intramolecular disulphide bonds per monomer and an additional disulphide bond stabilizing the dimer (Serrano et al., 2006) (Figure 2). It is synthesized as a precursor (381 amino acids) followed by proteolytic cleavage of N- and C-terminal propeptides in several different steps that result in the mature sequence (Brasch et al., 2003; Ueno et al., 2004).

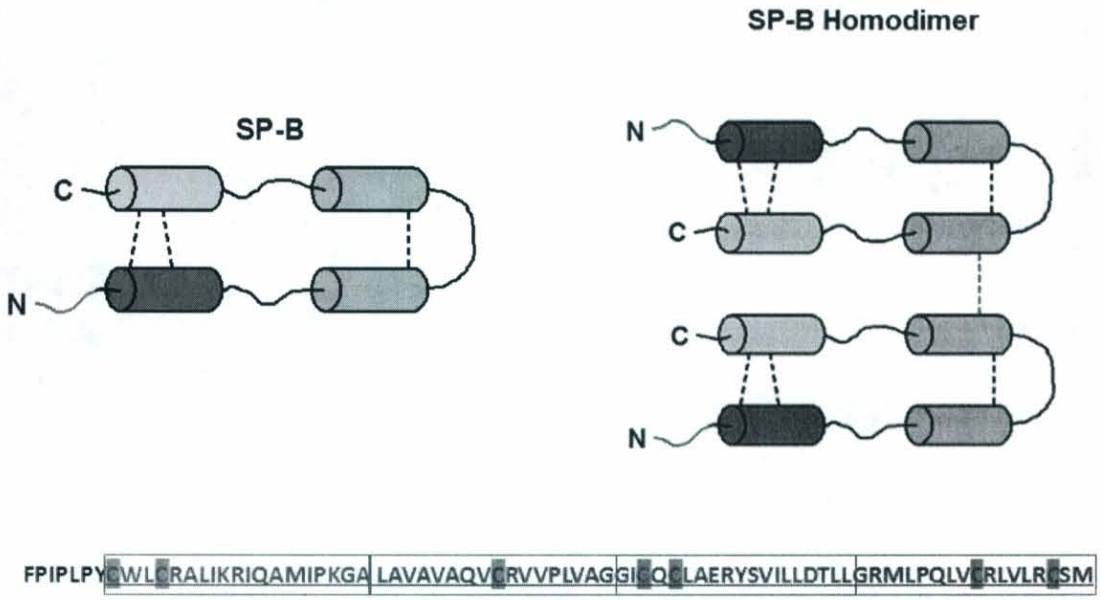

Figure 2. Schematic diagram of mature SP-B and SP-B homodimer. Disulfide bonds connecting the predicted helices are shown by dashed lines. The fourth disulfide bond (red dashed line) stabilizes the dimer. The amino acid sequence and expected helical regions (boxes) are shown, cysteine residues are highlighted in grey.

The synthesized precursor SP-B is transported from the endoplasmic reticulum to the Golgi apparatus and then to multivesicular bodies where it is packed into lamellar bodies. Proteolytic processing of SP-B occurs in type II pneumocytes during the exocytic pathway of surfactant. The active SP- B peptide is stored with SP-C and surfactant phospholipids in lamellar bodies (Voorhout et al., 1992; Korimilli et al., 2000).

Several mechanisms have been suggested to underlie SP-B's function including enhancing the interfacial adsorption of phospholipids from the hypophase to the air–water interface (Cruz et al., 2000 ; Schram and Hall, 2004), stabilizing compressed films at the alveolar surface (Krol et al., 2000), facilitating the re-spread of the surfactant material during expansion and providing lowest surface tension during respiration cycle. It has been proposed that SP-B functions as a link from bilayers (hypophases) to the monolayer (air-water interphase) and back (Taneva and Keough, 1994; Zaltash et al., 2000) (Figure 3).

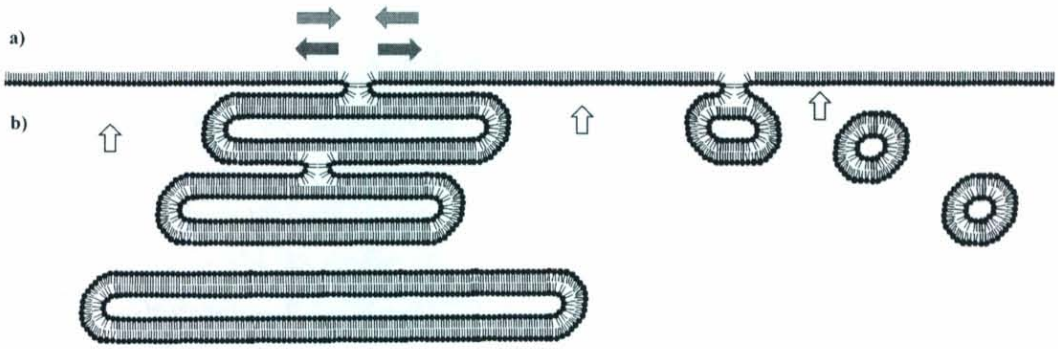

Figure 3. A model representing the role of SP-B during compression (a. pointing in arrows) and expansion (a. pointing out arrows) of breathing cycle. SP-B mediates bilayer–bilayer and bilayer–monolayer transitions.

Previous works have shown that SP-B fragments can retain similar activities to the full-length SP-B. The N-terminal half of SP-B consists of amino acids 1-37, and has a high number of hydrophobic and cationic residues that provides lipid-interaction properties. C-terminal based peptides also showed *in vitro* and *in vivo* surfactant activities (Kang et al., 1996; Baatz et al., 1991; Ryan et al., 2005). Enhancement of oxygenation and lung compliance, dynamic re-spreading in animal models, membrane permeabilization and liposome lysis have been reported for N- or C-terminal helical fragments of SP-B (Revak et al., 1991;Walther et al., 2002) (Figure 4).

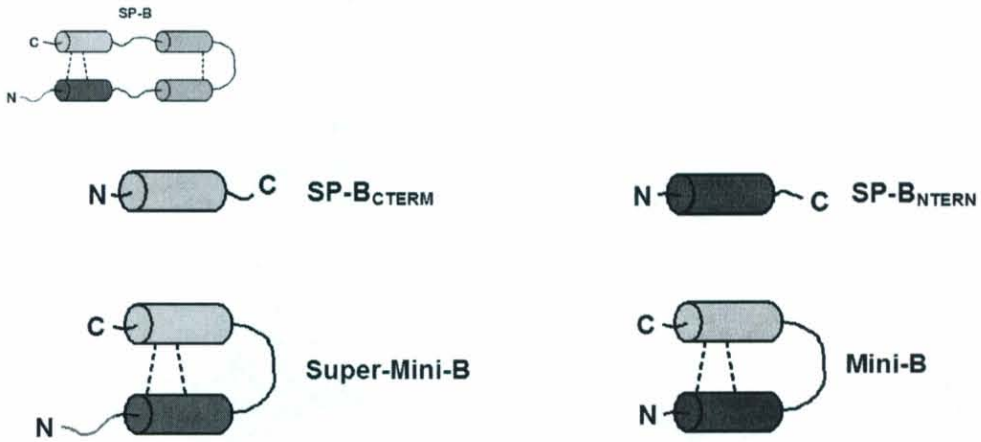

Figure 4. Schematic diagram of SP-B peptides synthesized based on the predicted helical segments of SP-B. SP-B_{NTERM} and SP-B_{CTERM} are designed based on the N- and C-terminal helices of SP-B respectively. Super-Mini-B

and Mini-B are N- and C-terminal containing peptides. The disulfide bonds connecting the helices are shown by dashed lines.

A recent *in vivo* study (Walther et al., 2010) assessed biological activities of a group of SP-B peptides; Mini-B, Super-Mini-B and N-terminal fragment of SP-B ($SP\text{-}B_{1\text{-}8}$). Mini-B is a 34-residue peptide that consists of the N- and C-terminal predicted helical regions of SP-B. Super-Mini-B is a 41-residue peptide with two internal disulfide bonds that contains the N-terminal 7-residue insertion sequence and the predicted N- and C-terminal helices of SP-B. These regions are connected via a loop as well as two disulfide bonds (Waring et al., 2005). Super-Mini-B can be considered as a modified Mini-B since the only difference is the presence of the insertion sequence ($SP\text{-}B_{1\text{-}7}$) (Table 1).

Table1. Amino acid sequences of SP-B, Mini-B and Super-Mini-B. Disulfide bonds are formed between cysteine residues highlighted by gray color.

Protein	Amino acid sequence
SP-B	FPIPLPYCWLCRALIKRIQAMIPKGA----------LAVAVAQVCRVVPLVAGGICQCLAERYSVILLDTLLGRMLPQLVCRLVLRCS-M
Mini-B	-----CWLCRALIKRIQAMIPKG----------GRML-PQLVCRLVLRCS-M
Super-Mini-B	FPIPLPYCWLCRALIKRIQAMIPKG----------GRML-PQLVCRLVLRCS-M

In this study (Walther, et al. 2010), lung lavaged rats were treated by artificial surfactants composed of lipids alone and lipids plus SP-B, Mini-B, Super-Mini-B and N-terminal fragment of SP-B ($SP\text{-}B_{1\text{-}8}$). The study included the measurement of arterial oxygenation and lung dynamic compliance in lung lavaged rats with ARDS and controls. The treatment with lipids alone did not improve the oxygen content in blood. Lipids + $SP\text{-}B_{1\text{-}8}$ improved it only slightly more than lipids alone. Lipids + Mini-B produced higher oxygenation levels than lipids + SP-B. Lipids + Super-Mini-B reached the highest value for arterial oxygenation (Figure 5). The results suggest that the N-terminal insertion sequence ($SP\text{-}B_{1\text{-}7}$), in combination with the N- and C-terminal helices of SP-B, provides greater surfactant activity than either the N- and C-terminal helices alone, or full length SP-B.

Lung dynamic compliance is related to the volume of the air that is exchanged during respiration. Measurement of this value by Walther and co-workers indicated a similar relative activity of the peptides compared to the oxygenation measurements. The only difference was that lipids + Mini-B had a lower activity than lipids + SP-B (Figure 5). This result indicates that the presence of N-terminal insertion sequence ($SP\text{-}B_{1\text{-}7}$) may be important for lung expansion-compression. It also supports the possibility of a different mechanism of function of SP-B for oxygenation compared to lung dynamics.

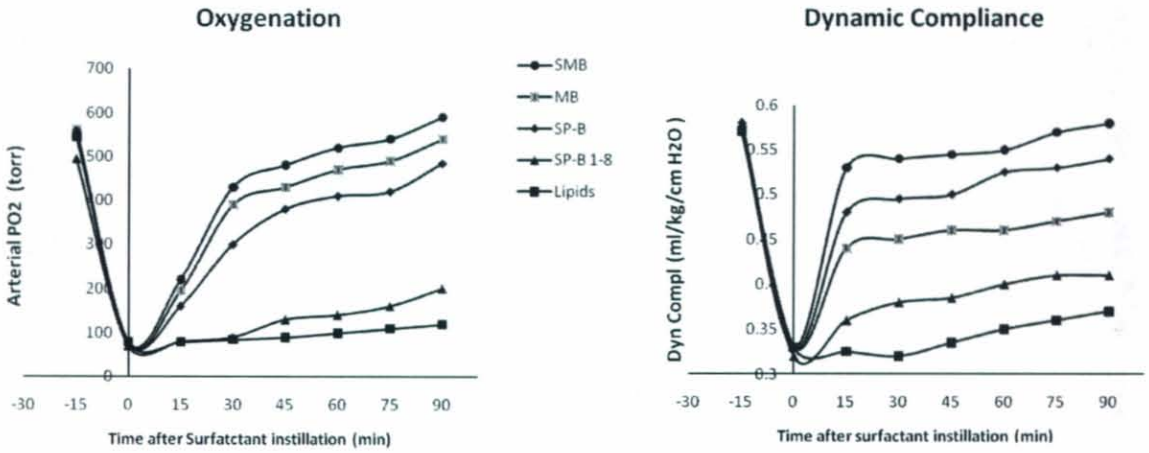

Figure 5. Arterial oxygenation and dynamic compliance in rats subjected to removal of lung surfactant by *in vivo* lavage. Exogenously surfactant replacement was administered by synthetic surfactants prepared from lipids only and lipids plus native SP-B or SP-B peptides. Synthetic lipids + 1.5 mol % Super-Mini-B, Mini-B, or $SP\text{-}B_{1-8}$, synthetic lipids +1.5% porcine SP-B and synthetic lipids alone as a control. Arterial partial pressure of oxygen (PaO_2) and dynamic lung compliance (mL/kg/cm H_2O; calculated by dividing tidal volume/kg body weight by changes in airway pressure) are shown as a function of time after surfactant administration. The plots are self-prepared using the published data of Ref. Walther et al. 2010.

The knowledge of a structure of a protein provides information on its molecular mechanism of function. The exact three-dimensional structure of SP-B is still unknown. Structure of some SP-B peptides have been determined by solution nuclear magnetic resonance (NMR) experiments; the N-terminal peptide ($SP\text{-}B_{11\text{-}25}$) (Kurutz and Lee, 2002), and the C-terminal peptide ($SP\text{-}B_{63\text{-}78}$) (Booth, et al., 2004) (Figure 6). The high resolution structure of Mini-B has also been determined (Sarker et al., 2007) (Figure 6). In order to define the importance of the N-terminal 7 residues of SP-B ($SP\text{-}B_{1\text{-}7}$), results of structural studies on Mini-B and Super-Mini-B, particularly NMR experiments, were compared.

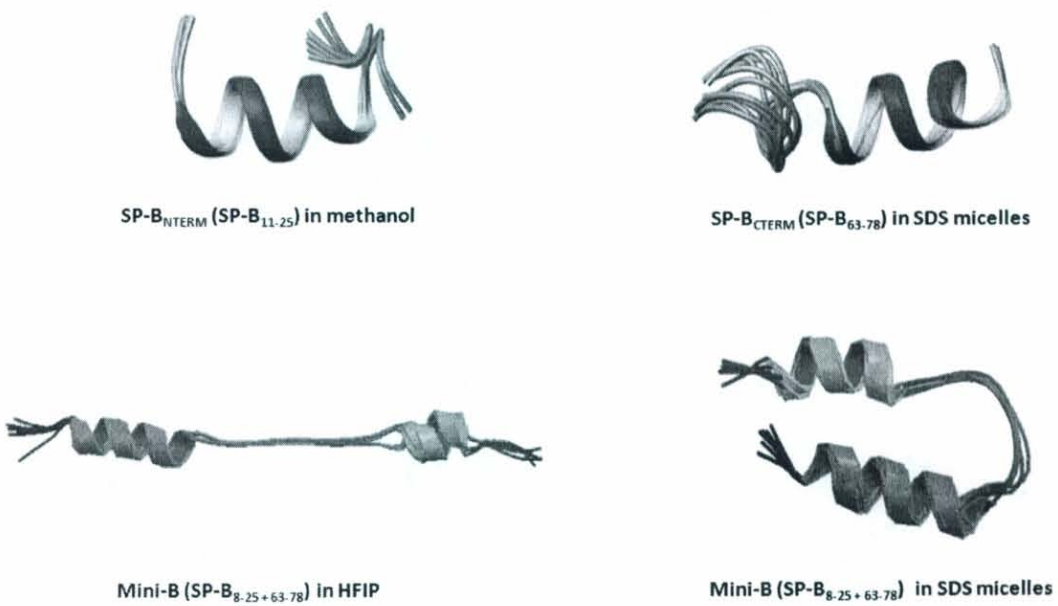

Figure 6. The high-resolution structures of three terminal fragments of SP-B determined by solution NMR. The fragments are $SP\text{-}B_{NTERM}$ ($SP\text{-}B_{11\text{-}25}$) in

methanol (PDB ID 1KMR) (Kurutz and Lee, 2002), SP-B_{CTERM} (SP-B_{63-78}) in sodium dodecyl sulfate (SDS) micelles (PDB ID 1RG3) (Booth et al., 2004), reduced Mini-B (SP-$B_{8-25\ +\ 63-78}$) in hexafluoroisopropanol (HFIP) (PDB ID 2JOU) and oxidized Mini-B in SDS micelles (PDB ID 2DWF) (Sarker et al., 2007). The disulfide bonds are not shown.

NMR is commonly employed in studying three dimensional structures of proteins. One of the advantages of NMR spectroscopy is that data can be acquired in solution. Studying the structure of proteins in solution with the possibility of adjusting conditions (such as temperature, pH and salt concentration) allow us to closely mimic physiological conditions and study *in vivo* functions of proteins (Wüthrich, 1986).

NMR is a property that makes particular nuclei in a magnetic field absorb energy from the applied electromagnetic pulse and radiate this energy back out. These nuclei are called NMR active nuclei or ½ spin nuclei. The energy radiated back out from each nucleus has a specific resonance frequency depending on the strength of the magnetic field and the environment surrounding the nucleus (Pochapsky and Pochapsky, 2007). In proteins purified from natural sources there is only one ½ spin nucleus, ^{1}H.

The axes in NMR spectra are frequency, normally represented as chemical shift. The chemical shift describes the dependency of the radiated

energy level of a magnetic nucleus on the electronic and chemical environment surrounding that particular nucleus. Solution-state NMR experiments provide information about the structure of a protein based on two types of correlations between nuclei; correlations between nuclei with ~3 covalent bonds of each other (from total correlation spectroscopy (TOCSY) experiments), and interactions between nuclei that are close to each other through the space conformation, but not through the chemical bond (from nuclear overhauser effect spectroscopy (NOESY) experiments) (Cavanagh et al., 1996).

One of the limitations of solution NMR is the size issue. Larger molecules have slower tumbling rates and shorter NMR signal relaxation times. This reduces the sensitivity of received signals and result to weak peaks. Also more complexity will introduce to a spectrum by large size molecules because there are more NMR-active nuclei and more interactions among them (Yu, 1999).It is hard to get information of the structure from broad and low intensity peaks. The limitation of solution-state NMR in studying hydrophobic proteins such as SP-B is that, this class of proteins cannot be brought into a sufficiently concentrated solution due to their highly hydrophobic nature (Laws et al., 2002). Detergent or lipid micelles can be used to mimic the lipid environment to solubilize these proteins. A micelle is an aggregate of amphiphilic molecules, in a polar solvent (mostly water). These amphiphilic molecules contain a hydrophilic head group and

one long or two short acyl chains. When the concentration of these molecules in water is greater than a certain value, known as the critical micellar concentration (CMC), spherical structures called micelles are formed which the hydrophilic head groups are exposed to water molecules and burying the acyl chains inside. Nevertheless solubilisation of hydrophobic proteins by lipid containing solutions is not helpful enough for NMR studies since the proteins in complex with lipids tumble very slowly and don't give rise to detectable peaks in solution NMR spectra (Sanders and Sonnichsen, 2006).

Solid-state NMR works based on the resonance of NMR-active nuclei in the magnetic field. In this technique, interactions between nuclei are orientation dependent and take place in media with no or little mobility. It is an alternative technique to give information about the protein structure. However it does not provide high resolution structural data in comparison to solution-state. Solid-state NMR is also a valuable tool to study local dynamics, kinetics and thermodynamics of protein-lipid interactions in protein-membrane systems (Laws et al., 2002). Since SP-B is a membrane associated protein, studying SP-B peptides in lipid bilayers by solid-state NMR provides precious information about SP-B/lipid interactions.

In spite of SP-B's importance, attempts at recombinant expression of the full-length protein and chemical synthesis of a near-full protein have

not succeeded yet, mainly due to its high degree of hydrophobicity and the presence of three intrachain disulfide bonds. However, fragments of SP-B retain much of the function of the full length protein (Kang et al., 1996; Baatz et al., 1991; Ryan et al., 2005), making them helpful to understand the mechanism of the full length protein. Additionally, peptides are of interest as they pose substantial advantages over full length proteins to use as therapeutics, e.g. for NRDS or ARDS.

The main objectives of this work are to produce full/near full length SP-B suitable for NMR studies and to understand the role of the N-terminal 7 residues of SP-B. SP-B based peptides encompass similar activities to the full length protein, this fact raise the hypothesis that particular structural features of SP-B are responsible for particular activities of SP-B. In this research, structural studies on SP-B peptides; Super-Mini-B and N-terminal insertion sequence of SP-B ($SP\text{-}B_{1\text{-}7}$). The research was performed using solution and solid-state NMR spectroscopy in order to characterize the structural changes and membrane interaction properties induced by the by presence of N-terminal insertion sequence in the context of SP-B peptides. Moreover, recombinant expression of SP-B in an attempt to produce the full-length protein and optimizing expression conditions were investigated. In this work also production and expression of a novel near full-length SP-B peptide; N-terminal deleted SP-B (Nd-SP-B) were examined. The overall

result of this research provides a strong foundation for future studies on the production, conformation and interactions of full-length SP-B.

2. Material and Methods

2.1. Sequence identification of SP-B encoded plasmid

The plasmid containing full-length SP-B gene was designed and synthesized by members of the Jesús Pérez-Gil lab at Universidad Complutense (Spain). Starting with this plasmid, it was transformed into DH5α *E. coli* cells. The plasmid was amplified in these cells, the cells were harvested and the DNA isolated using the extraction and purification procedures of QIAprep® Miniprep kit (QIAGEN Inc. Mississauga, ON). Bacterial cells were harvested from a 2 ml cell culture by micro centrifugation. The pellet was subjected to the alkaline-SDS lysis procedure. The solution added to a micro column filled with silica and equilibrated with a high salt concentration. DNA adsorbed onto the column and contaminants were removed by a simple wash step. The bound DNA was eluted in water or Tris-EDTA buffer. The purified DNA was sequenced by the Genomics and Proetomics (GaP) Facility, (Memorial University).

2.2. Transformation of the plasmid to the expression cell line

After confirmation of sequences, 1 µl (0.1 ng/µl) of the purified DNA was added to a 50 µl aliquot of competent C43(DE3) cells. The

transformation reaction was incubated on ice for 30 minutes. The heat shock was applied for 45 seconds at 42°C and then the reaction was placed on ice for 2 minutes. 500 µl of lysogeny broth (LB) medium was added to the transformation reaction and incubated at 37°C for 1 hour. The LB medium consisted of 10 g/L tryptone, 5 g/L yeast extract, 10 g/L NaCl, pH 7. After incubation, the transformation reaction was plated on LB–ampicillin (100 µg/ml) agar plates and the plates were incubated at 37°C for 16 hours. Later in my work to optimize the cell growth, I have used terrific broth (TB) media which is a richer than LB. TB medium is consisted of 12 g/l tryptone, 24 g/l yeast extract, 9.4 g/l potassium phosphate (dibasic), 2 g/l potassium phosphate (monobasic). The final pH was adjusted at 7.

2.3. Recombinant expression of full length surfactant protein B

An isolated colony on the transformed plate was selected and placed in 10 ml LB-ampicillin (100 µg/ml). The mixture was incubated overnight at 37°C. The overnight culture was added to 750 ml LB–ampicillin broth. Cells were grown at 30°C until the OD_{600} reached 0.7, and then isopropyl β-D-1-thiogalactopyranoside (IPTG) (1 mM) was added to induce expression of SP-B. After 4 hours incubation, the cells were harvested by centrifugation at 4000 g for 10 min. The pellet was resuspended in a minimized amount of resuspension buffer (10 mM Tris HCl pH 7.9, 1 mM ethylenediaminetetra acetic acid (EDTA), 0.01 M phenylmethanesulfonylfluoride or

phenylmethylsulfonyl fluoride (PMSF)) and kept in -20°C freezer until needed.

In order to break the cell membranes, pellets were subjected to French press at room temperature, sonication while the sample was kept on ice. The French press container and the sonication probe were cooled down by ice before usage. After the cell rupture, tris buffered saline (TBS) 1% lauroyl sarcosine detergent (TBS= 50 mM Tris, 150 mM NaCl, pH 7.6) were added with the same volume as the cell extract. The cell extract was centrifuged at 18,000 g for 10 min. The fusion protein was purified from the supernatant via immobilized metal affinity chromatography. The cobalt containing resin was used to make a His-Trap column (TALON Metal Affinity Resin, Clontech Laboratories,Inc. Mountain View, CA, USA). The column was equilibrated with TBS 1% lauroyl sarcosine buffer. The supernatant was loaded onto the cobalt column and the column was washed with TBS, 1% lauroyl sarcosine, 75 mM imidazole. The protein was eluted from the column by the elution buffer containing TBS, 1% lauroyl sarcosine and 500 mM imidazole. The eluted protein was dialyzed against water to remove imidazole, buffer and detergent. After dialysis, the solution was freeze-dried and stored at 4°C.

2.4. Production & recombinant expression of the N-terminal deleted SP-B

Site-directed mutagenesis was applied on the full-length SP-B containing plasmid. Stratagene's QuikChange® Site-Directed Mutagenesis kit (Agilent Technologies Canada Inc. Mississauga, ON) was used to delete the N-terminal fragment of SP-B. The forward and reverse primers were designed personally based on the full sequence of the plasmid and considering the desired deletion mutation. Both of the mutagenic primers contained the mutation and anneal to the same sequence on opposite strands of the plasmid (Table 2). The encoding sequence of seven N-terminal residues of SP-B (FPIPLPY) was absent in mutagenic primers. The synthesized mutagenic primers were ordered and purchased from Sigma-Aldrich Co. (St. Louis MO). 5 µl of 10× reaction buffer was mixed with 2 µl (5–50 ng) dsDNA template (the purified plasmid DNA of the bacteria before the mutation), 2 µl (125 ng) forward primer, 2 µl (125 ng) reverse primer and 1 µl deoxyribonucleotide triphosphate (dNTP) mix. Double distilled water was added to bring the volume to 50 µl. Then 1 µl of *Pfu* DNA polymerase (2.5 U/µl) was added to reaction mixture.

Polymerase chain reaction (PCR) was to used to amplify the mutation reaction. The PCR reaction was as follows: a pre-denaturation step, 30 seconds heat treatment at 95°C. The reaction was followed by 18 cycles of denaturation, 30 seconds at 95°C, annealing for 1 minute at 55°C and extension for 20 minutes at 68°C. The second part of the PCR reaction was repeated for 18 cycles. After completion of the reaction, 1 µl of the *Dpn*

I restriction enzyme (10 U/μl) was added to the amplification product and incubated at 37°C for 1 hour to digest the parental (unmutated) DNA. *Dpn* I is an endonuclease, specific for methylated and hemimethylated DNA. It is used to digest the parental DNA. DNA isolated from almost all *E. coli* strains is methylated and therefore susceptible to *Dpn* I digestion. The sequencing of mutation products confirmed the efficiency of *Dpn* I. The mutated product was transformed into C43(DE3) *E. coli* cells. The same procedures, as described in 2.1 to 2.3, were applied to prepare a sample for DNA sequencing and expression.

Table 2. The sequences of forward and reverse primers designed for site directed deletion mutation on the N-terminal of SP-B.

Primers	The sequence
Forward Primer	5'-GTTCCACGGGGCCCATGCTGGCTCTGCAGG
Reverse Primer	5'-CCTGCAGAGCCAGCATGGGCCCCGTGGAAC

2.5. Identification of the expressed peptide

The recombinantly expressed peptides were identified using western blotting by immunoblotting of anti-histidine antibody. The histidine

tag was inserted at the N-terminal of the desired peptide, the purpose was to facilitate the purification process through metal affinity chromatography and also the anti-histidine antibody was used to detect the expression of the desired peptide. Since the desired peptide is a novel construct using a synthesized antibody is not convenient. For western blotting, first the eluted protein from column chromatogram (described in 2.3) was loaded on a SDS-PAGE, sodium dodecyl sulfate polyacrylamide gel electrophoresis, gel. The SDS-PAGE gel consists of both stacking gel and separating gel. Gels were solidified in a gel caster. To prepare a 12% SDS-PAGE gel, first the 10 ml separating gel was poured and polymerized. The separating gel is made of 4 ml 30% acrylamide mix (acrylamide 29.2% + 0.8% N,N'-methylenebisacrylamide), 6 ml 0.75 M Tris pH 8.8, 0.2 % SDS, 100 µl 10% ammonium persulfate (APS) and 20 µl tetramethylethylenediamine (TEMED). The 5 ml stacking gel was made of 650 µl 30% acrylamide mix, 4.35 ml 0.13 M Tris pH 6.8, 0.12% SDS, 100 µl 10% APS and 10 µl TEMED. Chemicals were purchased from Sigma-Aldrich Co., St. Louis MO and Fisher Scientific Co. Ottawa, ON. After the separating gel was thoroughly solidified, the stacking gel solution was added to the caster and a plastic comb was inserted to form wells. Then the gel was placed in a running chamber filled with 1× SDS running buffer (25 mM Tris pH 8.3, 250 mM glycine, 0.1% SDS). The protein sample was dissolved in sample buffer (65 mM Tris-HCl pH 6.8, 1.3% SDS, 13% glycerol, 1% β-

mercaptoethanol, 0.02% sodium azide and 0.02% bromophenol blue), boiled for 1 minute and loaded into one of the wells. The electrophoresis at 180 V was completed when the sample buffer dye (bromophenol blue) reached to the bottom of the gel.

Electrophoretic transfer of the protein from the gel to a polyvinylidene fluoride (PVDF) membrane (Millipore Corporation, MA, USA) was carried out by electrophoresis at 60 V for 120 minutes. The membrane was then kept for 1 hour at room temperature in a solution of 5% non-fat milk in TTBS; TBS (20 mM Tris, 0.5 M NaCl, pH 7.6) and 0.05% Tween-20. The membrane was then incubated with a primary antibody against the histidine tag, monoclonal Mouse IgG1, at room temperature for 2 hours, and then the antibody solution was washed from membrane in TTBS for several times. The membrane was incubated with the secondary antibody (polyclonal Goat Anti-Mouse IgG Alkaline Phosphatase conjugated) for 1 hour at room temperature followed by several wash steps. The dilution time for the primary antibody (anti-histidine) was 1:5000 (1 µl in 5000 µl) and the secondary antibody is 1:3000. Antibodies were purchased from Sigma-Aldrich Co., St. Louis, MO. To visualize the bound antibodies, BCIP/NBT color reaction was employed. BCIP (5-bromo-4-chloro-3-indolyl-phosphate) in conjunction with NBT (nitro blue tetrazolium) are used as chromogenic substrates for the colorimetric detection of alkaline phosphatase activity. BCIP as a color generator and

NBT for signal enhancement, they are ideal for immunoblotting while alkaline phosphatase is conjugated to the secondary antibody. 5ml of alkaline phosphatase buffer (100mM Tris-HCl [pH 9.0], 150mM NaCl, 1mM MgCl2), 75 mg/ml NBT in 70 % dimethylformalmamide (DMF) and 50 mg/ml BCIP in 100% DMF were mixed, the solution were applied to the PVDF membrane that was treated with the primary antibody in the previous step. NBT and BCIP were bought from Sigma-Aldrich Co.

2.6. Chemical synthesis and purification of N-terminal fragment of SP-B ($SP\text{-}B_{1\text{-}7}$)

N-terminal insertion sequence of SP-B (FPIPLPY) was produced by solid-phase synthesis using 9-fluorenylmethyloxycarbonyl (Fmoc) chemistry. Amino acids were weighed out in 5× excess and placed into a CS Bio peptide synthesizer (model CS336X, CS Bio Company Inc, Menlo Park, CA) using 0.43 g of a 0.47 mmol/g Rink amide resin (CS Bio Company Inc, Menlo Park, CA). Dissolution and de-blocking of amino acids were facilitated using a 0.4 M 1-hydroxy-benzotriazole dissolved in dimethylformamide (DMF), and a 20% peperidine/DMF solution (Sigma-Aldrich Co., St. Louis, MO). The resin was washed with DMF. After completion of synthesis, the resin containing synthesized $SP\text{-}B_{1\text{-}7}$ was transferred to a 10 ml syringe equipped with a filter, and washed with methanol. Then the resin was air dried for 30 minutes followed by vacuum

drying for 60 minutes. The peptide was cleaved from the resin by a cocktail consisting of 9 ml trifluoroacetic acid (TFA), 0.25 ml 1,2-Ethanedithiol, 0.1 ml thioanisole (Sigma-Aldrich Co.), and 0.25 ml distilled water. The peptide was precipitated from the solution by addition of 50 ml of -20°C diethyl ether. The precipitate was pelleted down by centrifugation at 4°C, 4,000 rpm, 5 min. The precipitant was collected and allowed to air dry overnight.

Purification procedure was carried out by using high-pressure liquid chromatography (HPLC) (Varian ProStar HPLC, Varian Inc., St. Laurent, QC). The HPLC was equipped with a reverse-phase DYNAMAX C8 preparatory column (Varian Inc., St. Laurent, QC), and a spectrophotometer operating at a wavelength of 215 nm. The peptide was eluted using an acetonitrile gradient (80/20% HPLC grade water/acetonitrile – 0/100% acetonitrile; Sigma-Aldrich Co). The mass and sequence of the peptide were confirmed through matrix assisted laser desorption ionization – time of flight mass spectrometry (MALDI-TOF MS) by Genomics and Proteomics (GaP) facility (Memorial University).

2.7. Solution nuclear magnetic resonance (NMR)

The structure of Super-Mini-B and SP-B_{1-7} were assessed by solution-state nuclear magnetic resonance (NMR). The peptides were investigated in an organic solvent (HFIP) and a membrane mimicking environment (detergent containing solution). 1 mM Super-Mini-B or 2 mM

SP-B_{1-7} were dissolved in 40% HFIP (hexafluoroisopropanol), 50% H_2O and 10% D_2O with 0.4 mM 4,4- dimethyl-4-silapentane-1-sulfonic acid (DSS). For detergent containing solution, 1 mM Super-Mini-B were dissolved in 90% H_2O, 10% D_2O, 0.2 mM DSS, and 150 mM deuterated SDS (Sodium dodecyl sulfate). Values were the same for 2 mM SP-B_{1-7} SDS sample except the peptide was dissolved in 300 mM deuterated SDS. Deuterated SDS, DSS and D_2O were purchased from Cambridge Isotope Laboratories, Inc. (Andover, MA). For all experiments, DSS was used to obtain the proton reference signal at 0 ppm and water-gate water suppression was used with a 3-9-19 pulse. All two dimensional experiments used a recycle delay of 1 second. One dimensional (1D) and two-dimensional (2D) NOESY, TOCSY and diffusion ordered spectroscopy (DOSY) experiments were carried out using a TXI probe on a Bruker Avance 600 MHz at Centre for Chemical Analysis, Research and Training (C-CART) (Memorial University).

For 1D ^{1}H NMR, 32 scans were recorded. A mixing time of 200 ms was used with 160 scans for the 2D NOESY. For the 2D TOCSY, a DIPSI2 sequence was used, and the mixing time was 80 ms, with 128 scans. Acquisition of spectra was performed using TopSpin (Bruker, Milton, ON).

Spectra were processed using iNMR (http://www.inmr.net) and analyzed using SPARKY (Goddard and Kneller, 2005). For NMR structural studies, each peak needs to be assigned as a specific nucleus in the molecule under investigation. Resonance assignments also have to be sequence-

specific, i.e., each peak must be assigned to a nucleus or correlation of nuclei in a particular amino acid in the protein sequence. ^{1}H peaks were assigned to a chemical group type on the basis of their chemical shifts. Amide protons (HN) resonate between 10.0 and 7.0 ppm, the backbone α-protons (Hα or HA) resonate between 6.0 and 3.5 ppm, the aliphatic side-chain protons resonate between 3.5 and 1.0 ppm and the methyl protons resonate at chemical shifts less than 1.5 ppm (Cavanagh et al., 1996).

The diffusion experiments were performed on 150 mM SDS in H_2O and D_2O with 1 mM Super-Mini-B at pH 5 and 30 °C, with the same sample used for other solution NMR experiments. The pulse sequence for diffusion measurement used stimulated echo with bipolar gradient pulses, followed by 3-9-19 pulse for water suppression. DOSY spectra were collected in 32 steps, attenuating signals to about 5% of the initial value by increasing the gradient strength from 2% to 95% of the maximum amplitude, for a constant diffusion time of 100 ms and an optimized gradient pulse length of 4 ms. The spectra were processed using iNMR and the diffusion constants calculated using the "DOSY" package in DOSYToolBox08 (Nilsson, 2009).

16-doxyl-stearic acid (16-DSA) was added from a 2 mM DSA in NMR SDS containing buffer to Super-Mini-B and SP-B_{1-7} samples, the final concentration of DSA was 0.6 mM. The samples were used for DSA-TOCSY experiments. DSA was purchased from Sigma-Aldrich Co., (St. Louis MO).

2.8. Solid-state nuclear magnetic resonance (NMR)

The oriented lipid/lipid-protein samples were prepared using Rainey and Sykes procedure (Rainey and Sykes, 2005). Muscovite mica (grade V-4, dimension: 75 × 25 × 0.26 mm^3), purchased from Structure Probe (West Chester, PA), was cut into small pieces to prepare 12 plates with dimensions of 12.5 mm × 5 mm and thickness of ~40 μm. Deurterated 1-palmitoyl-2-oleoyl-sn-glycero-3-phosphocholine, POPC-d_{31}, and 1-palmitoyl-2-oleoyl-sn-glycero-3-phospho-(1'-rac-glycerol), POPG, were purchased from Avanti Polar Lipid (Alabaster, AL). For the lipid only sample, 4 mg of POPC-d_{31} and POPG at a ratio of 7:3 were dissolved in a solvent composed of $CH_3OH/CHCl_3$ (1:1 by volume). For the lipid-peptide sample, 1 mol % (by weight) of Super-Mini-B was added to the lipid-organic solvent solution. The solution, with a total volume of ~250 μl, was spread over mica plates. The plates were dried for ~2 h in a fume hood and then placed in a vacuum chamber overnight. A few microliters of deuterium depleted water were spread on each plate and the plates were kept in a hydration chamber with saturated ammonia phosphate solution at 4°C for 3 days. Then the plates were stacked together, wrapped with a plastic film, and sealed with polystyrene plastic. Samples were stored at 4°C. The ^2H spectra were acquired at a temperature of 296 K on a spectrometer operated at a resonance frequency of 61.4 MHz.

2.9. Circular dichroism (CD) spectroscopy

Samples prepared for structural studies by solution NMR (preparation described in 2.7) were also investigated by circular dichroism (CD) spectroscopy. The secondary structural characteristics of Super-Mini-B, Mini-B and SP-B_{1-7} were assessed in aqueous (HFIP containing samples) and lipid mimicking environment (SDS samples). The CD spectra were obtained using a Jasco J-810 spectropolarimeter. Experiments were carried out at 25°C using 1 mm quartz cuvette. The spectra were acquired as the result of 4 repeated scans from 260 to 200 nm, using scan intervals of 1 nm and an integration time of 1 s at each wavelength. Secondary structure content was calculated from the spectra using CDPro software (http://lamar.colstate.edu/~ssreeram/CDPro) developed by Woody and co-workers (Sreerama and Woody, 1993). CD values were converted to mean residue ellipticity (MRE). Basis set 2 of the CDPro software was used and analysis was completed using CONTIN/LL method (Johnson, 1999: Sreerama and Woody, 2000; 2004).

3. Results

3.1. Detection of expressed recombinant full length SP-B

The starting point of this study was the plasmid DNA provided by Jesús Pérez-Gil's research group at Universidad Complutense (Spain). The plasmid was designed to contain the full-length SP-B gene fused to

staphylococcus nuclease (SN). SN as a fusion protein is attached to SP-B through a linker sequence. A recognition site for protease digestion (thrombin digestion) was provided to separate SP-B from the fusion part. Six histidine residues were added to the N-terminus of SN sequence to facilitate purification of the expressed protein by metal affinity chromatography.

The plasmid was amplified in DH5α *E. coli* cells in an overnight culture of LB media. The DNA sequencing of multiple clones confirmed the expected sequence for the designed plasmid [DNA sequencing–genomics and proteomics (GaP) facility, Memorial University]. The plasmid was then transformed into the C43(DE3) cell line. This specific strain of *E. coli* is genomically modified to provide the optimum over expression of toxic and hydrophobic proteins (Dumon-Seignovert et al. 2004).

Transformed cells were cultivated in LB media and induced by 1 mM IPTG. After the overnight induction, cells were centrifuged down and the pellet was collected. 10% Lauryl sarcosine was added to the pellet before the cell disruption procedure in order to enhance cell membrane disruption and to solubilise the hydrophobic expressed protein. Cells were then disrupted by French press and sonication.

The expressed protein was purified from the cell extract by the affinity of the histidine tag to a cobalt column. Detection of the purified protein on a Comassie stained gel was not promising because three bands

were detected in the purified sample while we were expecting only one band (Supplementary material, Figure S1.). In Western blot analysis a single immunopositive band was observed (Figure 7), as probed by an antibody specific for the histidine tag (since an antibody against SP-B is not available). The apparent molecular mass of the expressed fusion protein was estimated by comparison to the molecular mass markers run on the same SDS-PAGE gel used for Western blotting. The expected molecular mass for SN-SP-B is ~27 kDa while the estimated size of the detected band is approximately 22 kDa.

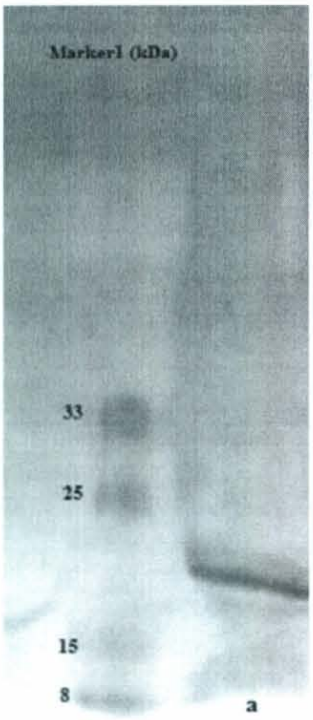

Figure 7. Western blot analysis of the cell extract harvested from the overnight culture of cells encoding SN-SP-B plasmid. a) The band

represents antigen–antibody reaction upon applying anti-Histidine antibody. The histidine tag is located at the N-terminal of SN-SP-B sequence.

While a large difference in apparent molecular weight via SDS-PAGE is not unexpected for a hydrophobic protein (see Discussion) - characterization of the expressed construct by an alternative method was desirable. For this, MALDI-TOF MS was used [genomics and proteomics (GAP) facility, Memorial University]. The purified sample was digested by trypsin that cleaves peptide chains at the amino acids lysine or arginine, except when either is followed by proline. The trypsin digestion is a helpful step to allow an efficient tandem mass spectroscopy. Tandem (MS/MS) mass spectroscopy is a technique to use more than one analyzer and so can be used for the peptide sequencing. First the mass spectrometer ionization source (MALDI) ionizes the sample molecules. The mass analyzer (TOF analyzer) separates the ions formed in the ionization source of the mass spectrometer based on their mass-to-charge (*m/z*) ratios. In the tandem-type mass spectrometer, two mass spectrometers are connected in tandem. Between the two mass spectrometers is an ion selector for selecting only a specific ion. For example in TOFTOF mass spectrometers, ions are separated in the first TOF stage. Just before a specific ion reaches the ion selector, the selector voltage is turned off. Then, after the ion of interest passes the ion selector, its voltage is turned on to allow only the ion of

interest to pass. The MS/MS spectrum can provide information about the amino acid sequence of the peptide of interest.

Results confirmed the sequence of some fragments from the fusion protein and SP-B (Figure 8 and Table 3). While the presence of the N-terminal residues of SP-B was detected by mass spectroscopy, I was not able to detect the remaining portions of SP-B using this method.

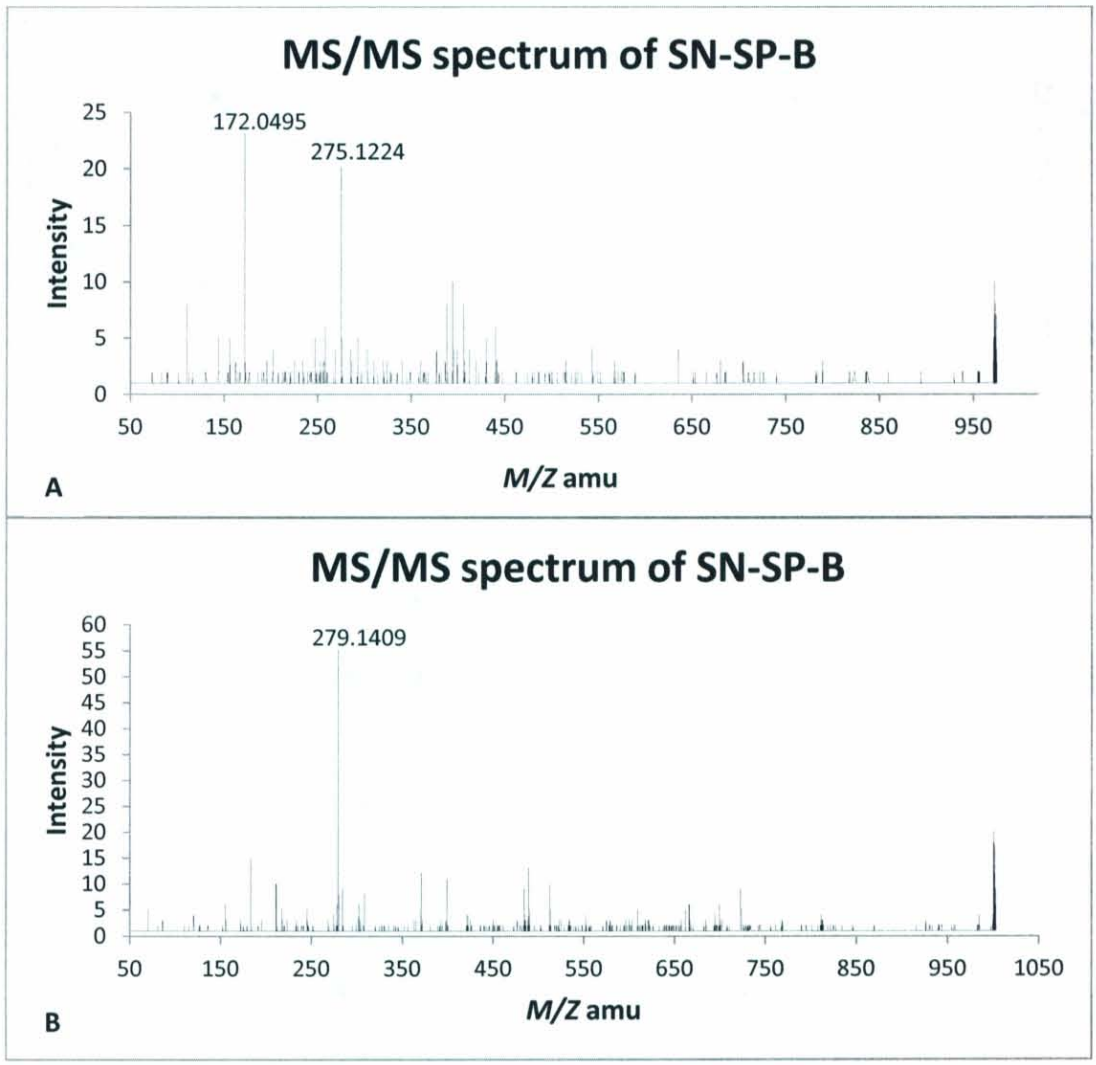

Figure 8. MS/MS spectra of SN-SP-B sample produced using MALDI-TOF mass spectroscopy. A) The mass/charge ratios of the fragment corresponding to histidine tag sequence is labeled. B) Peaks corresponding to the sequence of N-terminal fragment of SP-B are labeled. The amino acid sequences of these detected fragments are shown in Table 3.

Table 3. MS/MS analysis confirmed the presence of two fragments with the from the SN-SP-B construct (indicated by gray highlighting). Red represents the SP-B sequence and blue represents the fusion part consisting of the sequence of histidine tag, SN and the linker. [RG] is the action site of thrombin. Trypsin potential cleavage sites are underlined.

SN-SP-B expected amino acid sequence
MHHHHHHATSTKKLHKEPATLIKAIDGDTVKLMYKGQPMTFRLLLVDTPE TKHPKKGVEKYGPEASAFTKKMVENAKKIEVEFDKGQRTDKYGRGLAYIY ADGKMVNEALVRQGLAKVAYVYKPNNTHEQHLRKSEAQKKEKLNIWSED NADSGLGGGGGLVP[RG]PFPIPLPYCWLCRALIKRIQAMIPKGALAVAVAQ VCRVVPLVAGGICQCLAERYSVILLDTLLGRMLPQLVCRLVLRCSM
A. Detected Sequence of the fusion part
MHHHHHH
B. Detected Sequence of SP-B
GPFPIPLPY

3.2. Investigating disruption of protein synthesis and proteolysis induced by stress-activated proteins

The electrophoresis and mass spectroscopy work in the previous section brought up the possibility that either SP-B may be produced by the bacteria in a truncated form, or may be proteolyzed during its expression. To investigate these possibilities, cell cultures were collected 1 hour, 3 hours, 5 hours and 18 hours (overnight) after induction by IPTG. After the cell disruption, Western blotting of the cell extract showed bands at the same molecular mass (~22 kDa) for all time points. Results showed that the expressed SN-SP-B did not change at different time points after induction (Figure 9).

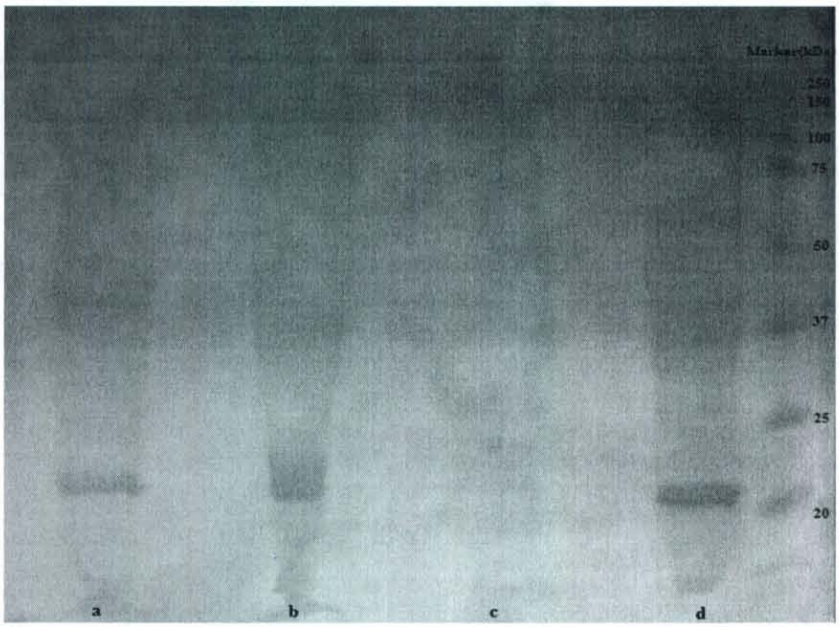

Figure 9. Western blot representation of time course collected cultures after induction. a) 1 hour; b) 3 hours; c) 5 hours; d) 18 hours (overnight) after induction. Protein concentration was not equal in samples; the presence and the size of the band were only investigated.

3.3. Investigating effect of cell disruption techniques on the expressed protein

Another possible explanation for the low molecular weight observed for the expressed protein was peptide breakage by mechanical forces during cell disruption. Although sonication usually does not break covalent peptide bonds, the possible destructive effect of French press and sonication were investigated (Figure 10). A combination of these techniques were applied to the cell pellet; two times French press and two times

sonication, one time French press and two times sonication, two times French press, one time French press, and five times freeze and thaw as a control. The detected band in western blot analysis was identical in apparent size under all conditions (~22 kDa) confirming that expressed SN-SP-B was not cleaved by cell disruption forces.

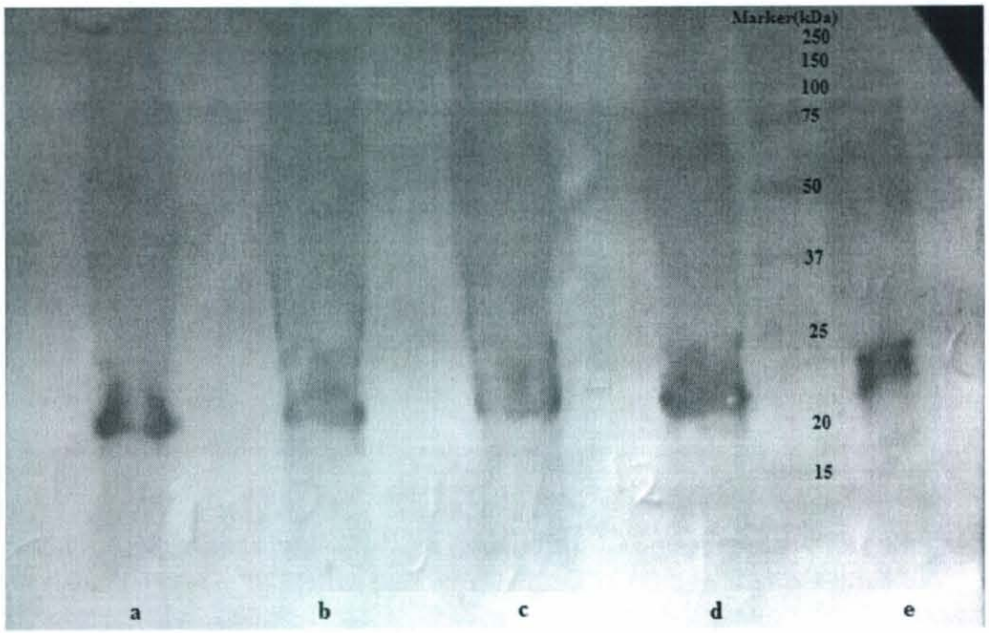

Figure 10. Western blot analysis of 100 ml cell extracts subjected to different cell disruption techniques. a) 2 times French press and 2 times sonication; b) 1 time French press and 2 times sonication; c) 2 times French press; d) 1 time French press; and e) 5 times freeze and thaw. Protein concentration was not adjusted in samples; the presence and the size of the band only were investigated. Diffusion of bands is due to sample overloading.

3.4. Optimizing growth conditions

Increasing the levels of SN-SP-B expression was important both for better confirming the sequence of the expressed protein, as well as for future structural studies. Therefore I next worked to optimize bacterial growth and protein expression conditions. The type of the media and concentration of IPTG for induction were investigated (Table 4). First, the total protein concentration was measured for 500 ml cell cultures grown in TB (Terrific Broth) and LB media. The cultures were induced by 1 mM IPTG. The total protein yield Protein concentration increased significantly in TB which is a richer media than LB.

A previous study showed that protein expression can be improved by decreasing the concentration of IPTG used to induce expression (Romano, et al. 2009). I examined the effect of IPTG concentration on SN-SP-B expression by the transformed cells. Protein content was measured after inducing LB cultures by a gradient of IPTG concentrations. Results showed that up to 0.4 mM IPTG, the total protein concentration is increasing. Decreases in protein concentration were evident at higher concentrations of IPTG. Both 0.4 mM and 1 mM IPTG were tested in TB media cultures. Total protein content was significantly higher for cultures inducted by 0.4 mM IPTG compared to 1 mM IPTG.

Table 4. Optimizing IPTG concentration to maximize protein expression. Total protein concentration of samples with equal volume, resulting from cell extracts of 500 ml overnight cultures was measured by the Bradford assay. LB cultures were induced by four different IPTG concentrations. TB media cultures were induced only by 0.4 mM and 1 mM IPTG. X means these concentrations of IPTG in TB were not investigated.

IPTG(mM)	**0.1**	**0.4**	**0.7**	**1**
LB (mg/ml)	1.183	1.904	1.476	0.932
TB (mg/ml)	X	6.685	X	2.288

3.5. Production of a novel SP-B peptide; N-terminal deleted SP-B peptide

The difficulties in confirming the full sequence of the recombinantly expressed SN-SP-B by mass spectroscopy are likely related to the highly hydrophobic nature of SP-B. Parallel studies with fragments of SP-B (see section 3.9) indicated the N-terminal 7 residues of SP-B might be particularly problematic. Even if we could confirm the full sequence, we would face similar difficulties in further structural studies on the sample. In order to produce a novel near full-length SP-B peptide without affecting its expected helical structure, seven amino acids from N-terminal end of SP-B were removed by site directed mutagenesis (Figure 11). The resulting gene

had a histidine tag followed by SN (as the fusion protein) and N-terminal deleted SP-B (Nd-SP-B). DNA sequencing of multiple transformed clones confirmed the success of mutation.

MHHHHHHATSTKKLHKEPATLIKAIDGDTVKLMYKGQPMTFRLLLVDTPE
TKHPKKGVEKYGPEASAFTKKMVENAKKIEVEFDKGQRTDKYGRGLAYIY
ADGKMVNEALVRQGLAKVAYVYKPNNTHEQHLRKSEAQKKEKLNIWSED
NADSGLGGGGGLVP[RG]PCWLCRALIKRIQAMIPKGALAVAVAQVCRVVP
LVAGGICQCLAERYSVILLDTLLGRMLPQLVCRLVLRCSM

Figure 11. The expected amino acid sequence of N-terminal deleted SP-B peptide. Blue represents the sequence of the fusion protein; staphylococcus nuclease (SN). Red is the expected sequence for N-terminal deleted SP-B (-7AA), [RG] is the recognition site of thrombin.

3.6. Identification of expressed recombinant N-terminal deleted SP-B

The mutated plasmid containing SN-Nd-SP-B was transformed into the C43 *E. coli* strain. The cell extract from an overnight induced culture was purified on a cobalt column (Figure 12). Western blot analysis identified two bands ~ 21 and 22 kDa with the histidine tag. Since bands are

very close they can be result of the partial reduction of disulfide bonds in the protein. The fraction of protein remaining with disulfide bonds move slower through the gel than the reduced fraction of protein. C43(DE3) are mutants that allow over-expression of some globular and membrane proteins unable to be expressed at high-levels in the parent strain BL21(DE3). Cysteines in the *E. coli* cytoplasm (including C43(DE3)) are actively kept reduced by pathways involving thioredoxin reductase and glutaredoxin. The disulfide bond dependent folding of heterologous proteins is improved in some strains (the Origami strains by Novagen) (Sorensen, H. P. & Mortensen, K. K., 2005). In my work the represented bands are from post cell disruption steps. After the rupture, most likely disulfide bond formation happens. However the molecular mass for both bands is less than expected for Nd-SN-SP-B (~26 kDa). The sample was purified through cobalt column and was digested by trypsin for MALDI-TOF MS [genomics and proteomics (GaP) facility, Memorial University]. Mass spectroscopy could detect fragments from SN and the linker part of SN-Nd-SP-B (Figure 13 and Table 5).

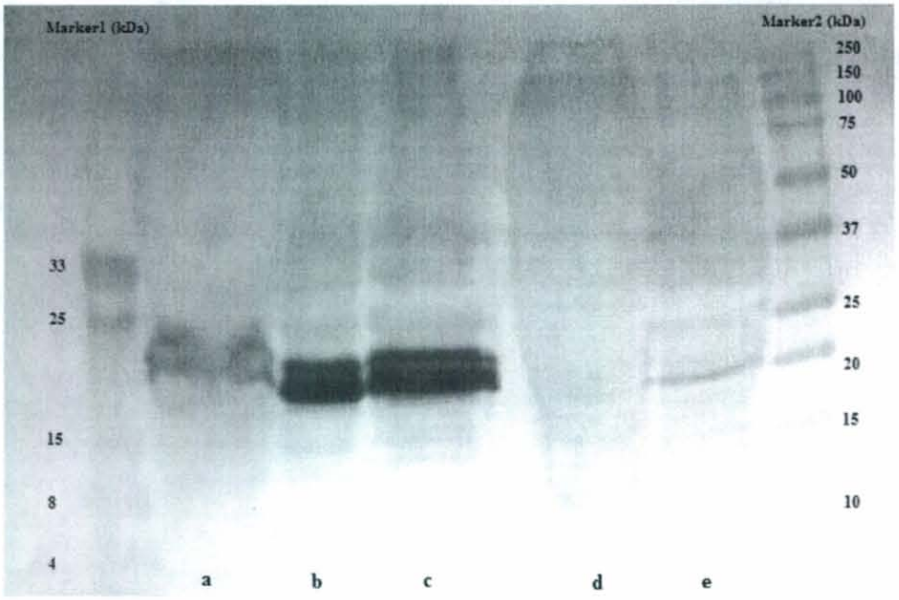

Figure 12. Western blot analysis of the cell extract from an overnight induced culture encoding SN-Nd-SP-B. Bands represent antigen–antibody reaction upon applying anti-Histidine antibody. The histidine tag is located at the N-terminus of SN-Nd-SP-B. Samples from different stages of protein extraction were loaded on the gel a) supernatant after cell disruption and solubilisation (1% lauroyl sarcosine) b) 30 µl of SN-Nd-SP-B resulting from the elution step of cobalt affinity chromatography (applying 200 mM imidazole) c) 60 µl of eluted SN-Nd-SP-B d) flow through after loading the sample and e) wash after loading the sample (75 mM imidazole). Protein concentration was not adjusted in samples; the presence and the size of the band were investigated.

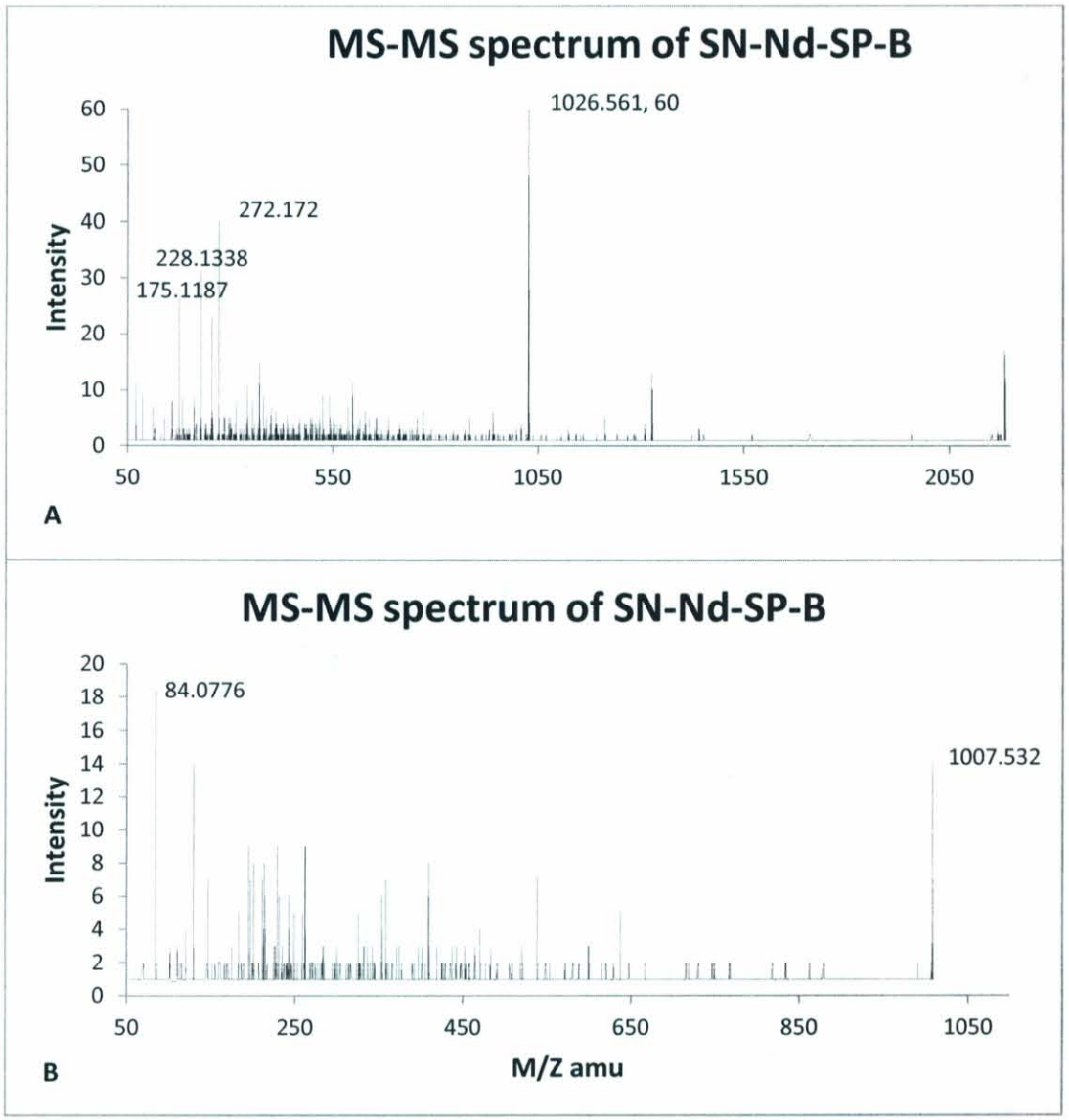

Figure 13. MS-MS spectra resulting from MALDI-TOF mass spectroscopy of SN-Nd-SP-B trypsin digested sample. A) The mass/charge ratio of a fragment of SN is labeled. B) Peaks corresponding to the sequence of SN and the linker are labeled. The amino acid sequences of the detected fragments are shown in Table 5.

Table 5. MS/MS analysis of SN-SP-B trypsin digested sample identified two fragments with the expected sequence (indicated by gray highlighting). No fragment was detected from Nd-SP-B. Red represents the SP-B sequence and blue represents the fusion part consisting of the sequence of histidine tag, SN and the linker. [RG] is the recognition site of thrombin. Trypsin potential cleavage sites are underlined.

SN-Nd-SP-B expected amino acid sequence
MHHHHHHATSTKKLHKEPATLIKAIDGDTVKLMYKGQPMTFRLLLVDTPE KHPKKGVEKYGPEASAFTKKMVENAKKIEVEFDKGQRTDKYGRGLAYIYA DGKMVNEALVRQGLAKVAYVYKPNNTHEQHLRKSEAQKKEKLNIWSEDN ADSGLGGGGGLVP[RG]PCWLCRALIKRIQAMIPKGALAVAVAQVCRVVPL AGGICQCLAERYSVILLDTLLGRMLPQLVCRLVLRCSM
Detected Sequence of the fusion part
KIEVEFDK LNIWSEDNADSGLGGGGGLVPR
Detected Sequence of Nd-SP-B

3.7. Production and characterization of N-terminal insertion sequence (SP-B_{1-7})

The first 7 residues of SP-B (the insertion sequence) were produced by chemical synthesis for structural studies. SP-B_{1-7} was synthesized by Fmoc chemistry (section 2.6). The peptide was purified by using reverse-phase HPLC. The HPLC was equipped with a reverse-phase DYNAMAX C8 preparatory column (Figure 14). The purified peptide was collected for further studies by mass spectroscopy. The mass and sequence of the peptide were confirmed through MALDI-TOF MS [Genomics and Proteomics (GAP) facility, Memorial University].

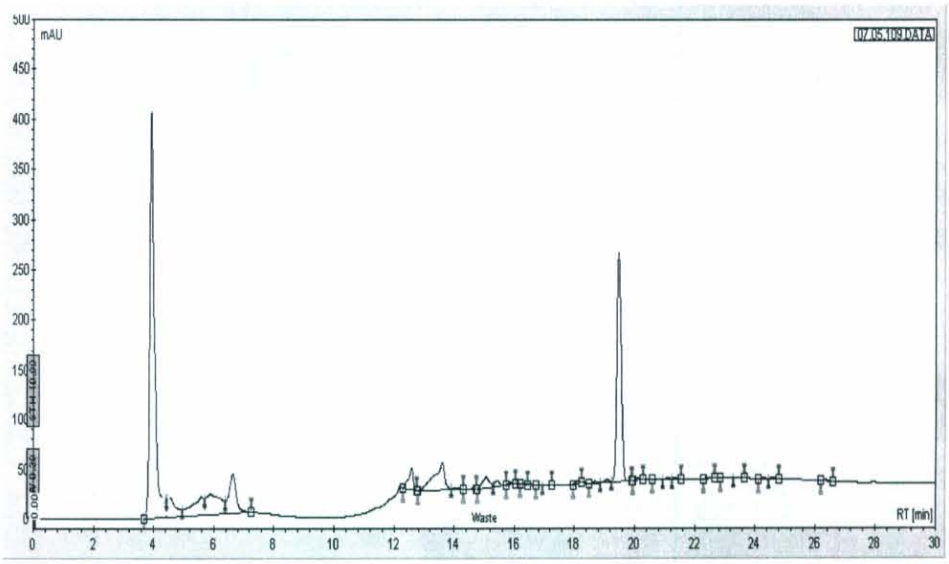

Figure 14. HPLC spectrum of SP-B_{1-7} eluted with an increasing acetonitrile gradient. Samples were run through a preparatory reverse-phase HPLC

chromatographer equipped with a DYNAMAX C-8 column. The strongest [highest absorbance in milli-absorbance units (mAU) at 215 nm] peak (~ 19 min) was collected for sequencing by mass spectroscopy. The strong peak at the beginning of the spectrum belongs to water.

Circular dichroism studies were carried out to assess secondary structural characteristics of SP-B_{1-7}. CD spectra of 2 mM Super-Mini-B were recorded at 25°C and pH 5 in aqueous solution with 40% HFIP (plus 50% H_2O and 10% D_2O), as well as membrane-mimetic environments (90% H_2O, 10% D_2O, 0.2 mM DSS, and 300 mM deuterated SDS). Efforts to solubilize the peptide either in 40% HFIP or SDS buffer were not successful; most of the sample was insoluble and precipitated. Secondary structural features of the soluble portion were calculated from the CD spectra using CDPro software (http://lamar.colstate.edu/~ssreeram/CDPro) and CONTIN/LL analysis method (Sreerama and Woody, 1993; 2004). The results for SP-B_{1-7} in 40% HFIP and SDS buffer were similar; the curves did not have the typical pattern for a helical conformation (Figure 15). The calculated secondary structural content were similar for HFIP and SDS containing samples; mostly unordered structures (45.8% in HFIP, 46.1% in SDS) and β-structures (27.3% in HFIP, 26.7% in SDS). A very small portion was detected for α-helical structures (0.3% and ~1.5% 3_{10}-helix in 40% HFIP and SDS, 3_{10}-helix is a right-handed helical structure), the

peptide retains the same content of 13% polyproline II structure in 40% HFIP and SDS (Table 6).

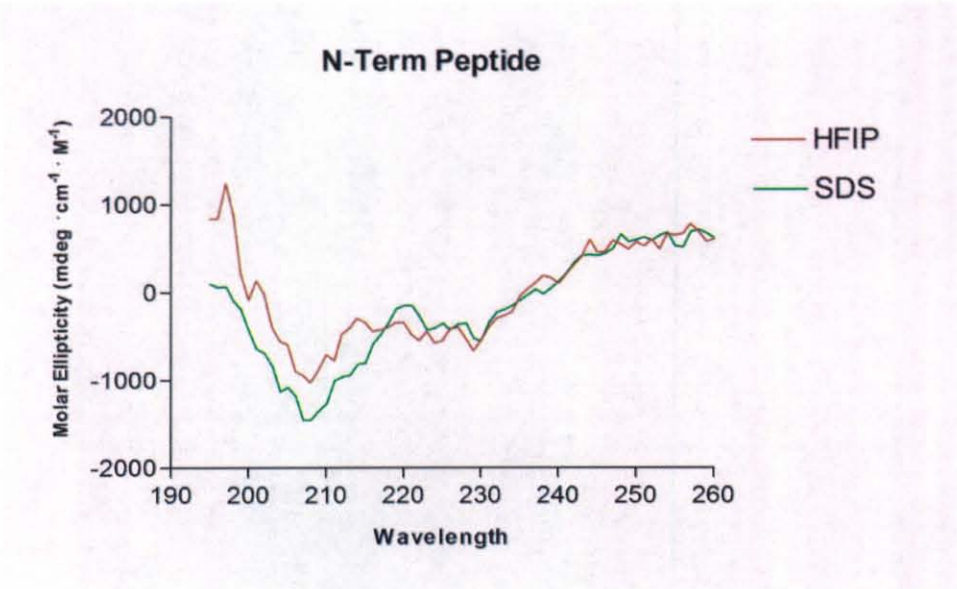

Figure 15. Far-UV CD spectrum of 2 mM N-terminal SP-B peptide dissolved in 40% HFIP (plus 50% H_2O and 10% D_2O) at pH 5 (red) as well as in the presence of 300 mM SDS NMR buffer containing 90% H_2O, 10% D_2O, 0.2 mM DSS, and 300 mM deuterated SDS (green). All spectra were taken using a 1 mm path-length quartz cuvette from 193 nm to 260 nm at 25°C.

Table 6. Secondary structural content of 2 mM SP-B_{1-7} in the presence of 300 mM SDS NMR buffer, and 40% HFIP NMR buffer at pH 5 and 25°C. Structural content percentages were calculated from CD spectra data using Woody and co-workers method (Sreerama and Woody 1993; 2000; 2004).

Secondary Structure (%)	α-Helix	3/10	β-Sheet	Turn	PolyprolineII	Unordered
SP-B_{1-7} in HFIP	0.3	1.6	27.3	11.9	13.2	45.8
SP-B_{1-7} in SDS	0.3	1.5	26.7	12.1	13.3	46.1

3.8. Solution nuclear magnetic resonance spectroscopy (NMR) preliminary structural characterization of N-terminal insertion peptide

The structural characteristics of SP-B_{1-7} were studied by solution NMR experiments. The 2D TOCSY and NOESY are the standard experiments to identify interactions between spin systems.

2D NMR experiments with SP-B_{1-7} in SDS micelles could detect only a few peaks with low intensities. Even though between spin systems SP-B_{1-7} is a small peptide, the number of observed peaks was still fewer than expected. This could be because the peptide forms large aggregated particles which do not give rise to solution NMR peaks (Figure 16).

As was mentioned in section 2.7, in a NMR spectrum each peak is associated with a specific magnetic (½ spin) nucleus in the investigated molecule. In a 2D NMR spectrum, each cross-peak is associated with 2 nuclei. In order to assign the peaks in the NMR spectra of SP-B_{1-7}, first the TOCSY was employed to indicate which peaks were in the same spin system and hence in the same amino acid residue. The spin systems were then assigned to an amino acid type based on comparison to the random coil values (Wuthrich, 1986). The majority of the peaks in the TOCSY spectrum were assigned within ±0.7 ppm off the expected proton resonance frequencies. I have designated proton nuclei in order of proximity to backbone HN nucleus, HA, HB, HC.... (Table 7). All of the 7 residues (SP-B_{1-7}) were assigned, however some of their protons did not produce any observable correlation peaks in order to be assigned. For prolines, because of the resonance similarity it was not possible to assign their resonances to particular prolines within the sequence. The remaining unassigned peaks likely originated from peptide impurities. Changes in intensity of peaks were used to assess the position of SP-B_{1-7} in the micelle. 16-doxyl-stearic acid (16-DSA) was added to the peptide/micelle sample, DSA is a paramagnetic detergent-soluble reagent. The proximity to this reagent leads to a marked intensity reduction of all NMR signals of nearby protons (Hilty et al. 2004).

A linewidth broadening and thus a height reduction of signals were observed for the entire spectrum. The level of proton intensity reduction indicates the proximity of proton groups to the center of micelle. The intensity reduction of peaks was monitored in TOCSY spectra, and then peak intensities were used to prepare a plot (Figure 17). Data analysis showed a substantial decrease in peak intensities and disappearance of peaks corresponding to residues 1 and 2 suggesting these residues are deeply inserted in the micelle. However unexpectedly several peaks showed increase in intensity.

Table 7. ^{1}H Chemical shifts of the N-terminal insertion sequence of SP-B from the TOCSY experiment on SP-B_{1-7}. HA, HB, ... respectively stand for proton nuclei in order of proximity to backbone HN nucleus.

Residues	HN (ppm)	HA (ppm)	HB (ppm)		HC (ppm)		HD (ppm)		HE (ppm)	HF (ppm)	HG (ppm)
F1	Not found	4.518	2.739	3.084	7.292		7.672		6.865	7.375	7.277
P2/4/6	---	3.847 4.382 4.531	1.781 1.771 2.038	2.122 2.283 2.141	1.292 1.941 1.544	1.545 1.778 1.160	3.659 3.474 3.788	3.176 3.236 3.449	---	---	---
I3	Not found	4.089	1.937		0.994	0.998 1.134	Not found		1.786	---	---
L5	Not found	4.421	1.559	1.786	1.547		0.933	0.951	---	---	---
Y6	Not found	4.397	3.071	2.745	7.044		6.798		7.116	6.798	7.116

A

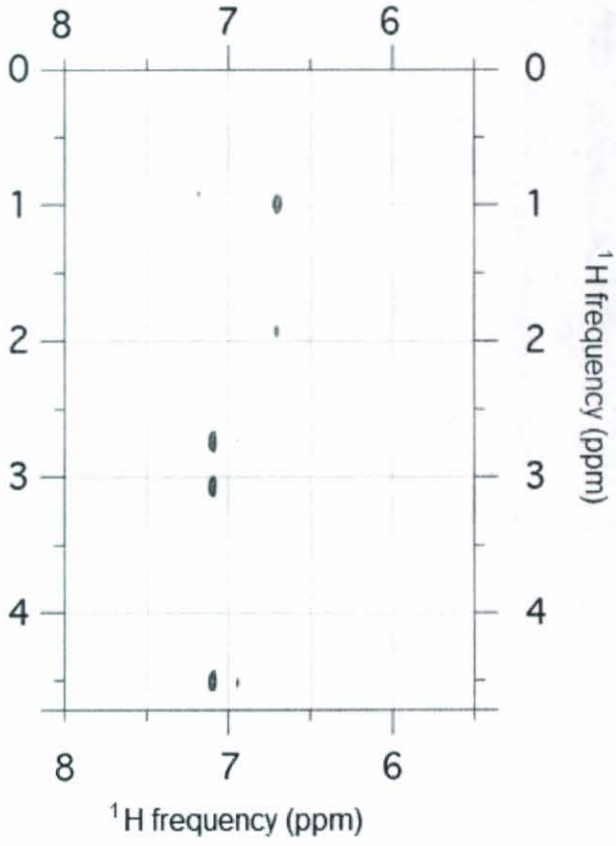

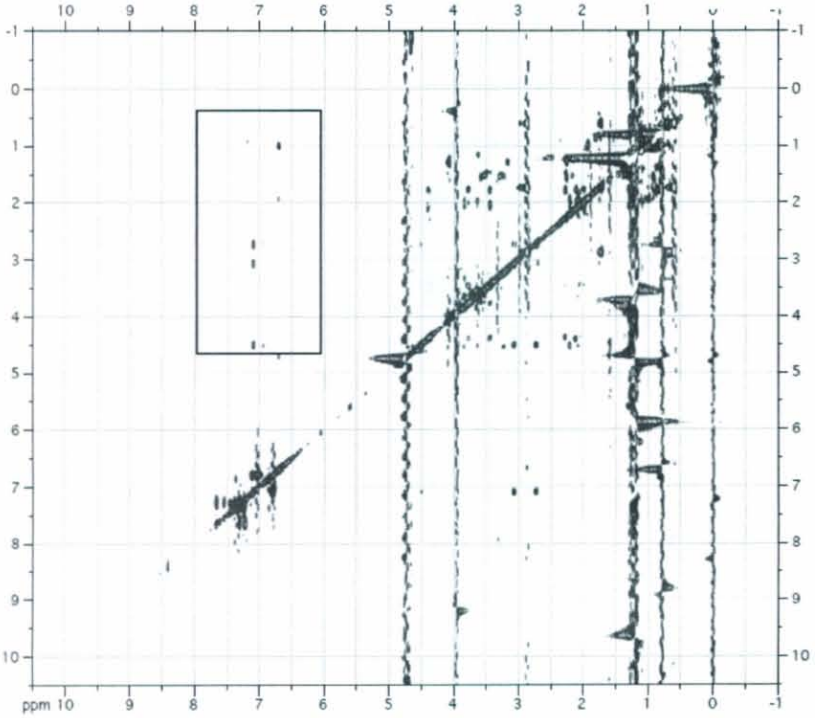

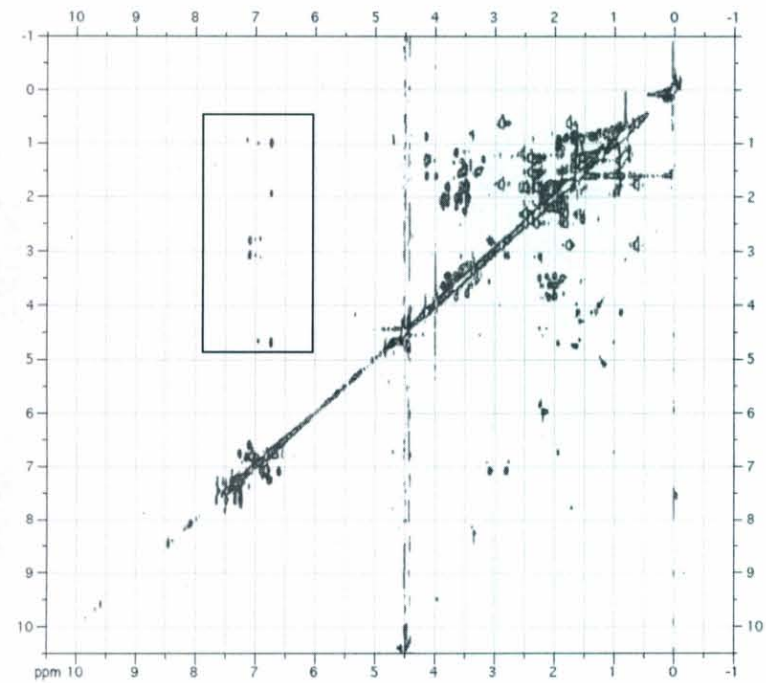

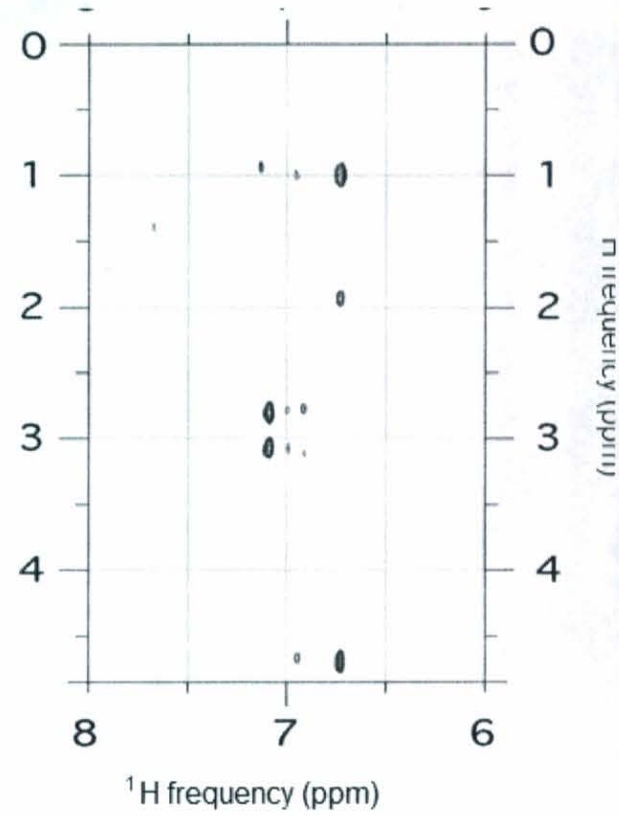

Figure 16. (A) 2D TOCSY spectra of 2 mM SP-B_{1-7} in 300 mM SDS, at pH 5 and 45°C, The HN-HX correlation region is pointed out through the panel coming off the spectra. HX could be any type of proton nuclei except HN. (B) at pH 5 and 45°C after addition of 0.6 mM 16-DSA. 128 scans were recorded for each experiment at 80 ms mixing time.

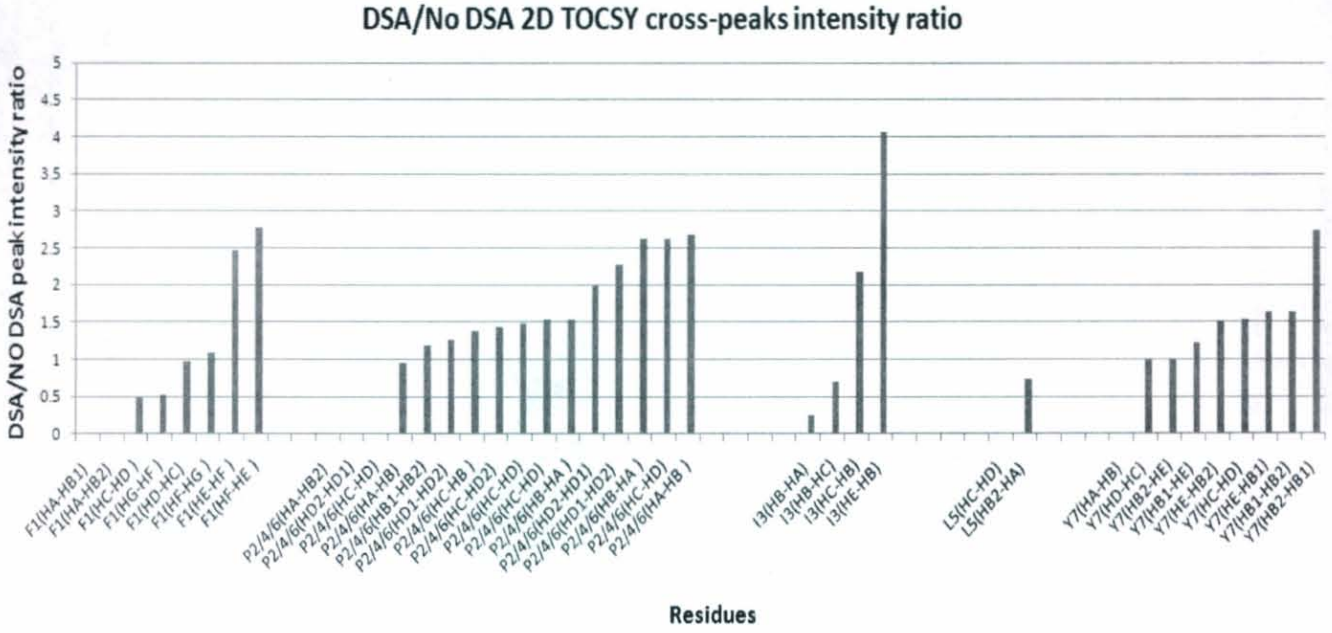

Figure 17. Effect of 0.6 mM 16-DSA on N-terminal insertion peptide of SP-B. The ratio of 2D TOCSY cross-peak intensity with and without 16-DSA is plotted. X axis represents the amino acid and corresponding proton groups of each correlation peak. HA, HB, ... respectively stand for proton nuclei in order of proximity to backbone HN nucleus. Note that it was not possible to assign the proline resonances to particular prolines within the sequence.

3.9. Characterising the structure of Super-Mini-B

Super-Mini-B was chemically synthesized and purified by Alan Waring Lab at UCLA, USA (Walther et al., 2010) following a similar procedure to that used for SP-B_{1-7} (Section 2.6). None of the residues were isotope labeled. The peptide is in the oxidized form, containing four cysteines with a disulfide bond between pairs of cysteines.

CD studies were carried out to assess secondary structural characteristics of Super-Mini-B. CD spectra of 1 mM Super-Mini-B were recorded at 25°C and pH 5 in aqueous solution 40% HFIP (plus 50% H_2O and 10% D_2O), as well as membrane-like environments (90% H_2O, 10% D_2O, 0.2 mM DSS, and 150 mM deuterated SDS). Efforts to solubilize the peptide in either 40% HFIP or SDS buffer were nearly successful; however a small portion of the sample was precipitated. Secondary structural features of the soluble portion were calculated from the CD spectra using CDPro software (http://lamar.colstate.edu/~ssreeram/CDPro) and CONTIN/LL analysis method (Sreerama and Woody, 1993; 2004). In 40% HFIP the structure content was 21.8% α-helix, 13% ß-structure and 38.8% random coil. In SDS buffer, the α-helical content increased to 24.3%, ß-structure content did not change while the unordered structures decreased (ß-structures 13% and unordered structures 35.5%). The tendency of Super-Mini-B to form a polyproline II helical structure was similar in HFIP and SDS (~ 6%). However, this tendency was severely higher (to 13% for SP-

B_{1-7}) in the absence of the helical portions of Super-Mini-B (SP-$B_{1-25, 63-78}$) (Figure 18 and Table 8). The CD spectra were acquired from a high concentration (1 mM) of the peptide because later I need to compare results of NMR and secondary structural studies. As a result, I used the same samples for both studies, however diluting the sample when I was repeating my work (to 0.5mM) did not show any difference in secondary structural contents with 1 mM concentration (data for 0.5 mM are not represented in the thesis).

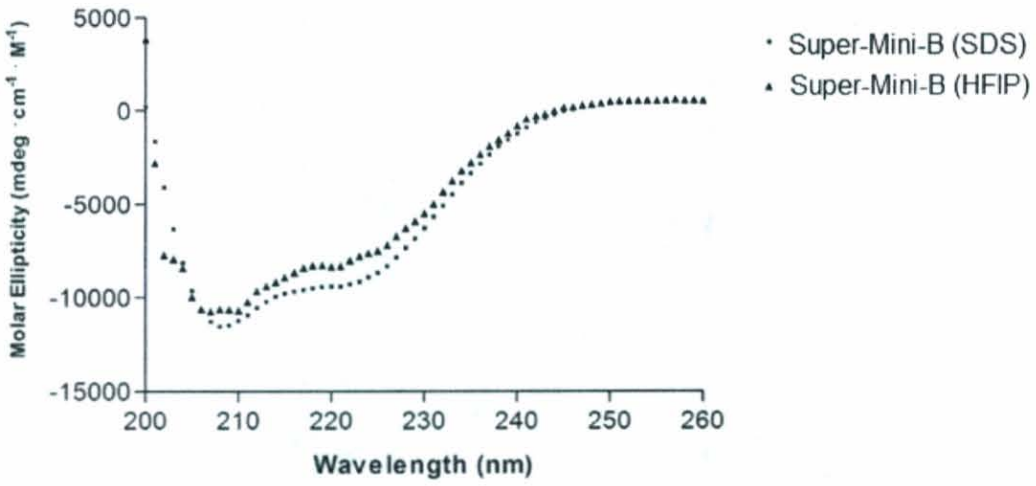

Figure 18. Far-UV CD spectrum of 1 mM Super-Mini-B dissolved in 40% HFIP (plus 50% H_2O and 10% D_2O) at pH 5 as well as in the presence of 150 mM SDS (90% H_2O, 10% D_2O, 0.2 mM DSS, and 150 mM deuterated SDS). All spectra were taken using a 1 mm path-length quartz cuvette from 200 nm to 260 nm at 25°C.

Table 8. Secondary structural content of 1 mM Super-Mini-B, in the presence of 150 mM SDS (plus 90% H_2O and 10% D_2O) as well as in 40% HFIP (plus 50% H_2O and 10% D_2O) at pH 5. Structural content percentages were calculated from CD spectra data using Woody and co-workers method (Sreerama and Woody 1993; 2000; 2004).

Secondary Structure (%)	α-Helix	3/10	β-Sheet	Turn	Polyproline II	Unordered
Super-Mini-B in SDS	**24.3**	**6.7**	**13.0**	**14.4**	**6.1**	**35.5**
Super-Mini-B in HFIP	**21.8**	**6.2**	**13.0**	**14.2**	**6.0**	**38.8**

Secondary structural content of Mini-B were calculated and compared to Super-Mini-B. The α-helix content was significantly greater in Mini-B compared to Super-Mini-B. Moreover Mini-B possesses lower values for ß- and unordered structures than Super-Mini-B (Figure 19). A small value is calculated for polyproline helix II structures in Mini-B, while the peptide does not have the N-terminal insertion sequence that forms polyproline helix II (PPII). This PPII helix content is negligible and is calculated because of using basis set 2 from CDPro software (Johnson, 1999).

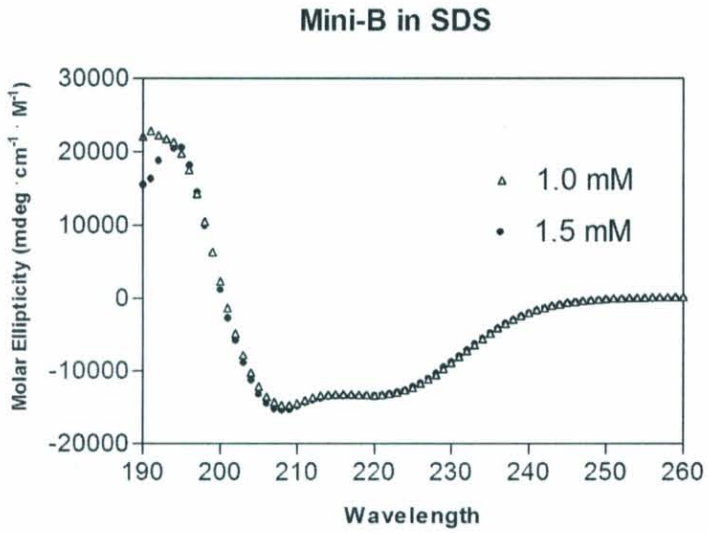

Secondary Structure (%)	α-Helix	3/10	β-Sheet	Turn	Polyproline II	Unordered
Mini-B	**37.0**	**8.9**	**6.8**	**12.6**	**4.7**	**30.0**

Figure 19. Far-UV CD spectrum of 1.5 and 1 mM Mini-B dissolved in 90% H_2O, 10% D_2O, 0.2 mM DSS, and 150 mM deuterated SDS. Both spectra were taken using a 1 mm path-length quartz cuvette from 190 nm to 260 nm at 25°C. Table: corresponding percentages of secondary structural content of 1 mM Mini-B in the presence of 150 mM SDS. Structural contents were calculated from CD spectra data using Woody and co-workers method (Sreerama and Woody 1993; 2000; 2004).

3.10. Solution nuclear magnetic resonance spectroscopy (NMR) structural characterization of Super-Mini-B

NMR studies were carried out to assess structural characteristics of Super-Mini-B. 1 mM of the peptide was dissolved in HFIP buffer (40% HFIP plus 50% H_2O and 10% D_2O, 0.2 mM DSS) as well as in the presence of 150 mM SDS (90% H_2O, 10% D_2O, 0.2 mM DSS, and 150 mM deuterated SDS). Results of 1D ^1H NMR experiments in HFIP and SDS were similar in terms of the spread of NMR signals (dispersion) over 6.8-7.8 ppm. The dispersion was poor in both solvents indicating that the peptide is not well structured.

In order to find the conditions corresponding to the best protein signal, the solvent, temperature and pH were varied. First the 1D ^1H NMR experiments were carried out on different concentrations of Super-Mini-B in 40% HFIP buffer. The peptide was titrated into the buffer to determine the peptide concentration corresponding to the best protein signal, and to look for evidence of peptide-peptide interactions and dimerization in the soluble part of the sample. No changes were observed in the appearance of the spectra (i.e. relative peak intensities, chemical shifts, etc.) with different peptide concentrations (Figure 20).

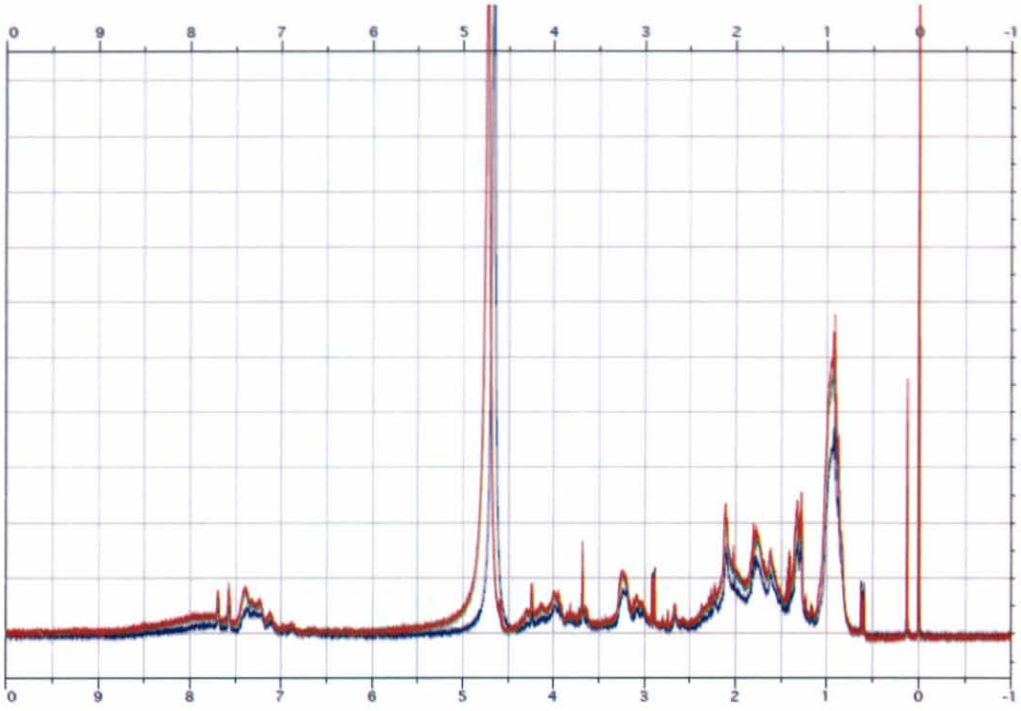

Figure 20. A) ^{1}H NMR spectra of Super-Mini-B were dissolved at three concentrations (blue 0.3 mM, green 0.6 mM, red 0.9 mM) at pH 5 and 25°C in a solution of 40% HFIP buffer (plus 50% H_2O, 10% D_2O, 0.2 mM DSS) 32 scans were used, spectra were processed using iNMR (http://www.inmr.net). Note that the intensity was normalized using the height of the DSS peak (peak at 0 ppm frequency).

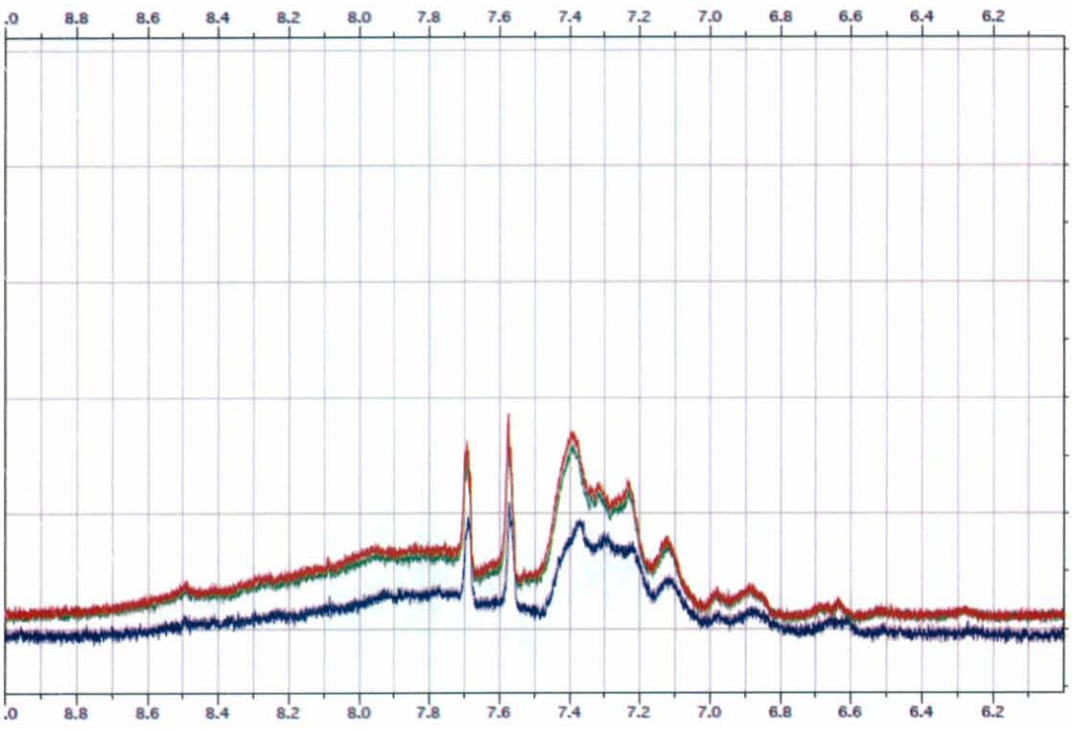

Figure 20. B) HN region of ^{1}H NMR spectra of Super-Mini-B dissolved at three concentrations (blue 0.3 mM, green 0.6 mM, red 0.9 mM) at pH 5 and 25 °C in 40% HFIP (plus 50% H_2O, 10% D_2O, 0.2 mM DSS).

In order to determine the temperature corresponding to the best protein signal, 1D 1H NMR experiments were acquired at different temperatures on 1 mM peptide sample. In 40% HFIP buffer the best signal intensity was acquired at 40°C. At higher temperatures the peptide looks more structured than at low temperatures, as evidenced by the greater peak dispersion in the HN region (Figure 21). Similar results were obtained from 1mM Super-Mini-B in SDS micelle containing buffer; by increasing the temperature the peak dispersion in the HN region (~7-9 ppm) increased. The greatest intensity was recorded at 45°C (Figure 22). Thus the temperatures which the peptide had optimum signal intensity in HFIP and SDS buffer were overlaid for comparison (Figure 23). The appearance of the HN region (i.e. peak intensities and chemical shifts) for the SDS sample looks more structured than the HFIP spectra (Figure 23B). As a result this condition, 1 mM Super-Mini-B dissolved in a solution of 90% H_2O, 10% D_2O, 0.2 mM DSS, and 150 mM deuterated SDS at pH 5 and 45°C, was selected for running the 2D NMR spectra.

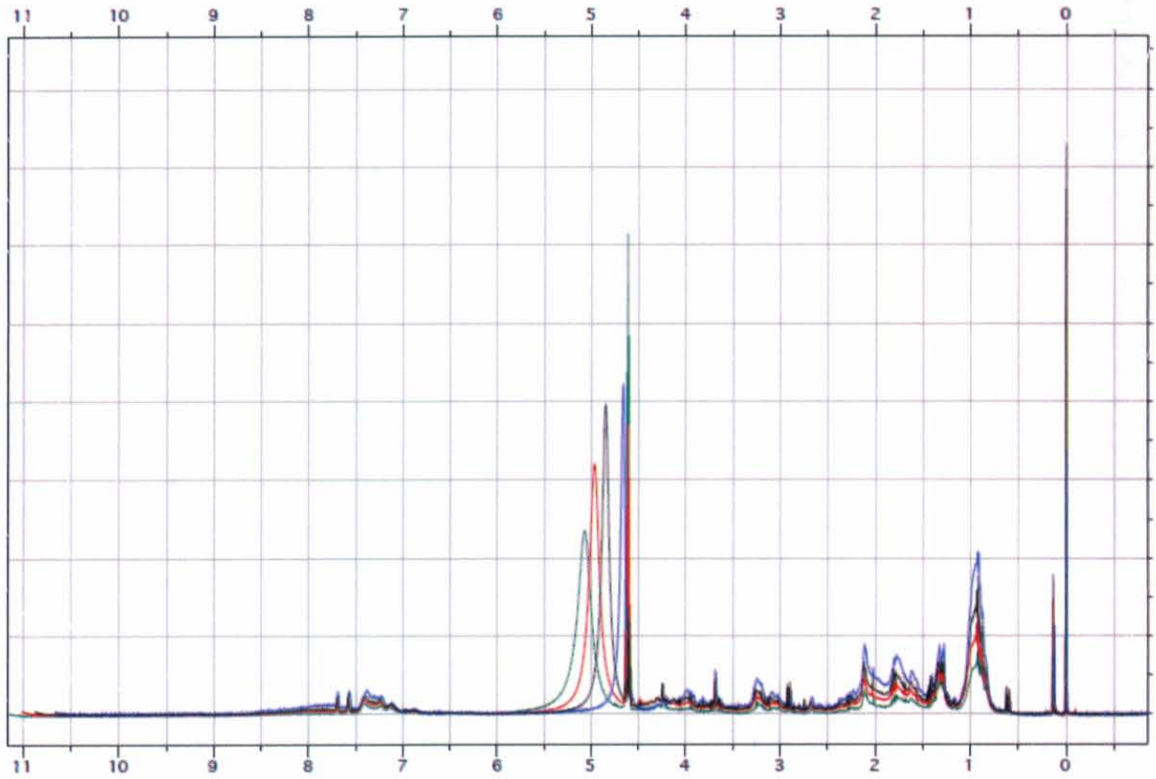

Figure 21. A) ^{1}H NMR spectra of 0.9 mM Super-Mini-B in 40% HFIP buffer at pH 5 and varying temperatures (red 5°C, green 15°C, black 25°C and blue 40°C) recorded with 32 scans. Spectra were processed using iNMR (http://www.inmr.net).

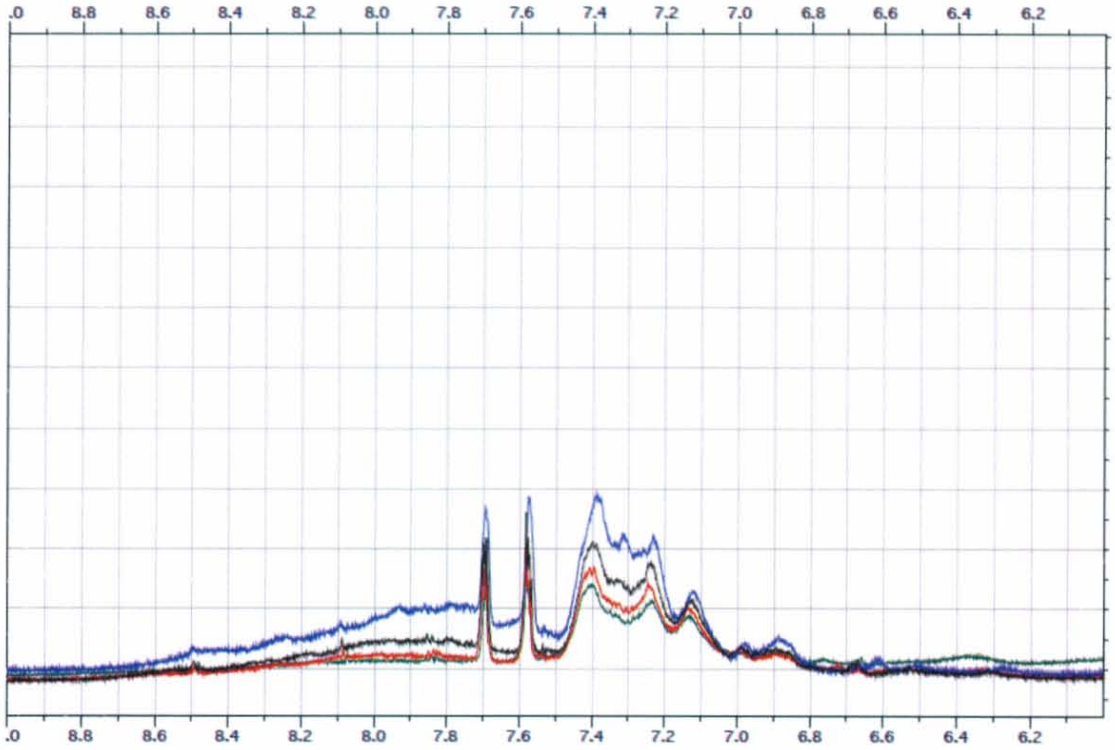

Figure 21. B) HN region of ^{1}H NMR spectra of 0.9 mM Super-Mini-B in 40% HFIP buffer at pH 5 and varying temperatures (red 5°C, green 15°C, black 25°C and blue 40°C).

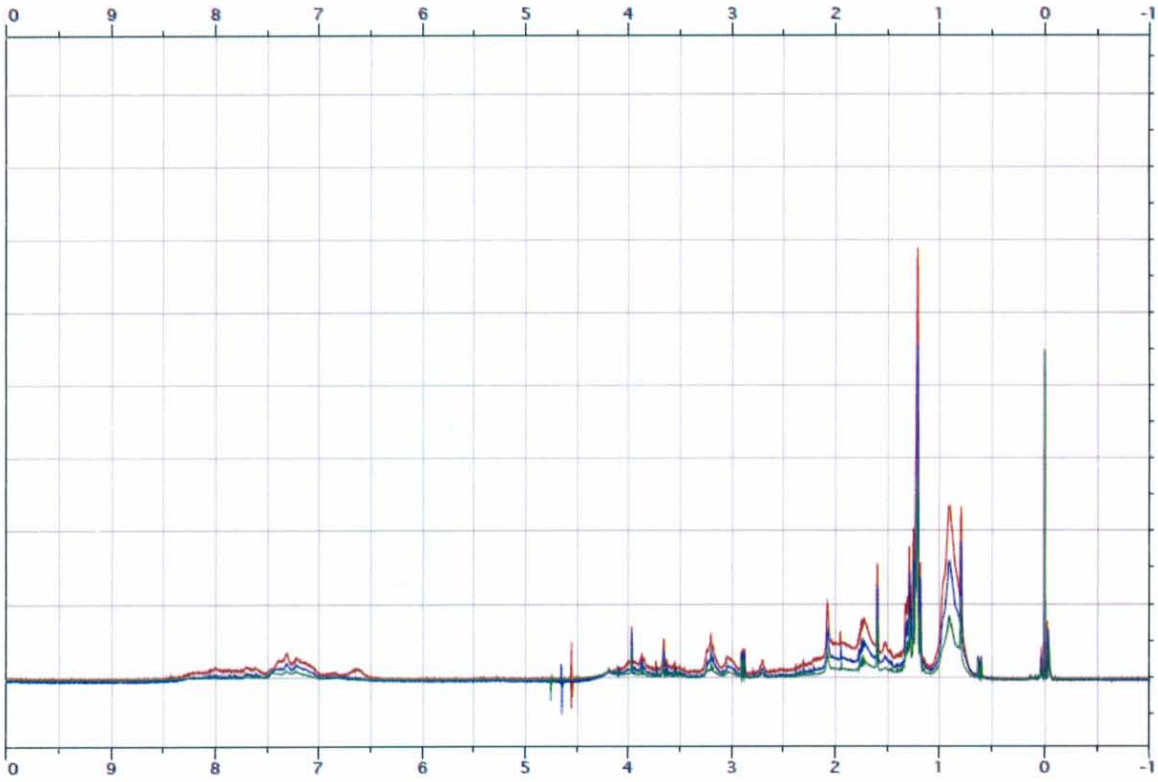

Figure 22. A) ^{1}H NMR spectra of 1 mM Super-Mini-B at pH 5, dissolved in a solution of 90% H_2O, 10% D_2O, 0.2 mM DSS, and 150 mM deuterated SDS at 25°C (green), 35°C (blue) and 45°C (green). For 1D ^{1}H NMR, 32 scans were used; spectra were processed using iNMR (http://www.inmr.net).

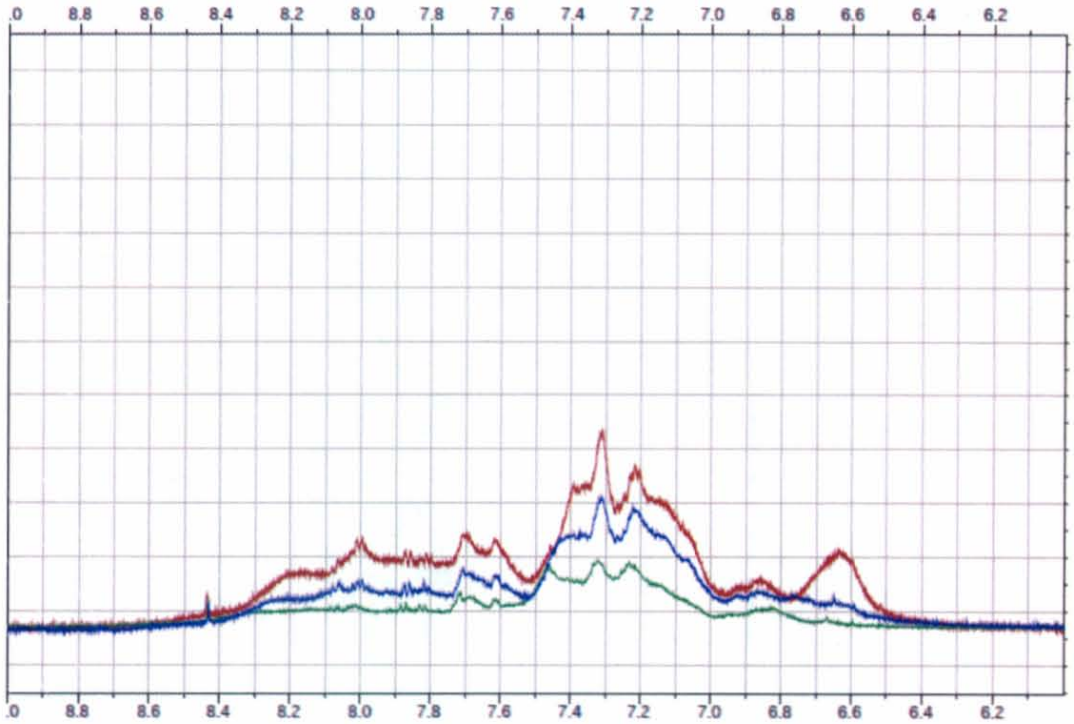

Figure 22. B) HN region of ^{1}H NMR spectra of 1 mM Super-Mini-B dissolved at pH 5 in a solution of 90% H_2O, 10% D_2O, 0.2 mM DSS, and 150 mM deuterated SDS at 25°C (green) , 35°C (blue) and 45°C (green).

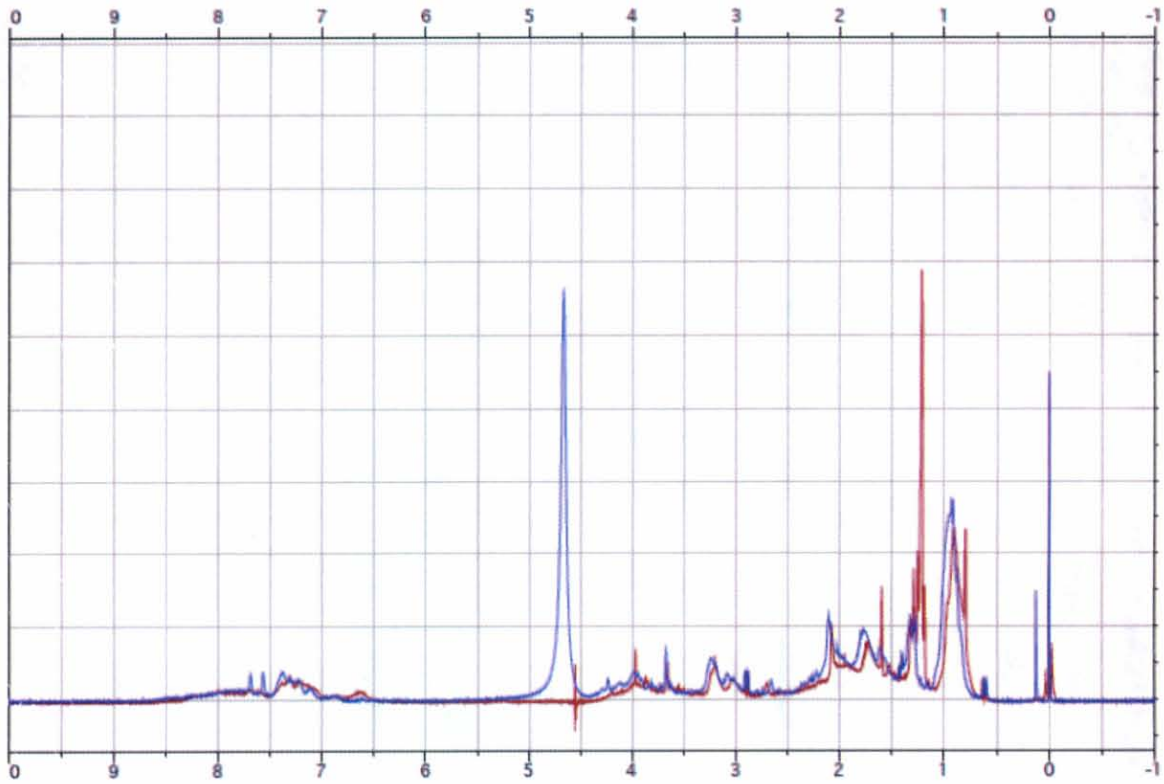

Figure 23. A) ^{1}H NMR spectra of 1 mM Super-Mini-B in 150 mM SDS buffer at pH 5, 45°C (red) and in 40% HFIP, pH 5, 40°C (blue). For 1D ^{1}H NMR, 32 scans were used.

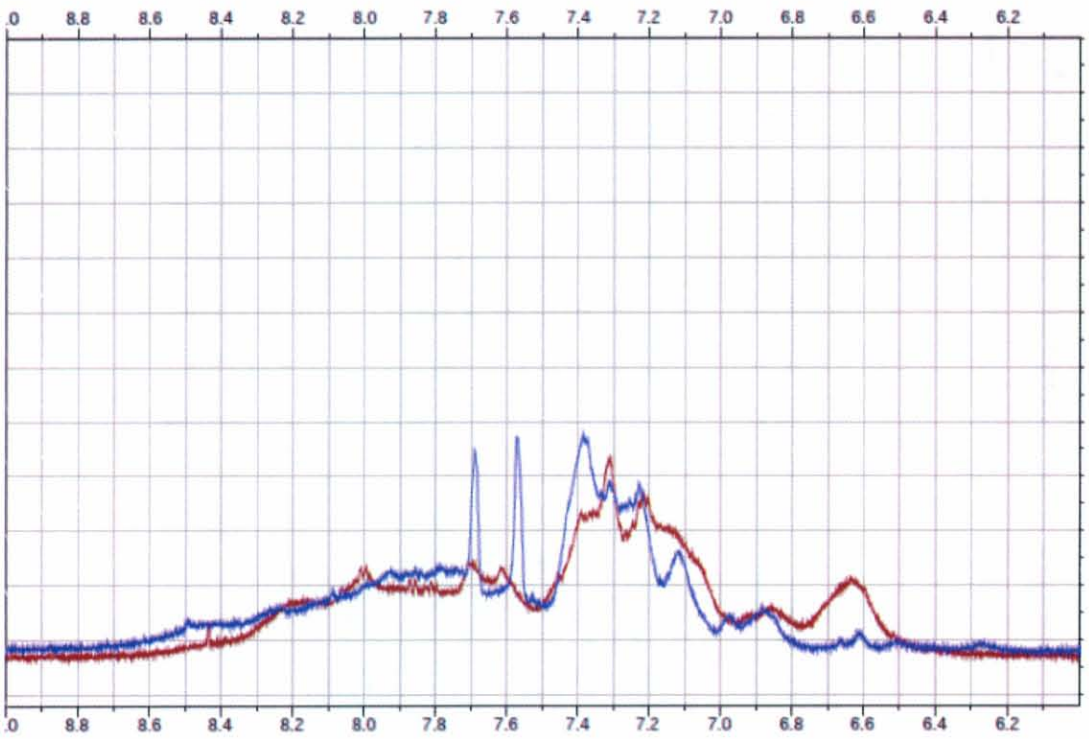

Figure 23. B) HN region of ^{1}H NMR spectra of 1 mM Super-Mini-B in 150 mM SDS buffer at pH 5, 45°C (red) and in 40% HFIP, pH 5, 40°C (blue).

An important goal of structural studies of Super-Mini-B is to characterize its structure and function under physiologicaly relevant conditions. In this study the physiological condition was approximated by a buffer with SDS micelles at pH 7 and 37°C temperature. 1D and 2D NMR experiments on 1 mM Super-Mini-B in SDS micelles were acquired at pH 7 and 37°C and the results were compared to the spectra from acquisition of the sample at pH 5 and 45°C. Peaks intensity was significantly greater at pH 5 and 45°C than at pH 7 and 37°C (Figure 24). Overlaid 1D spectra of Super-Mini-B and Mini-B shows a similarity in dispersion over the HN region suggesting a similar level of structuring for both peptides (Figure 25). However a decrease in peak intensity and broadening for Super-Mini-B suggests an increase in size of the particles (Mini-B results; Courtesy of Muzaddid Sarker).

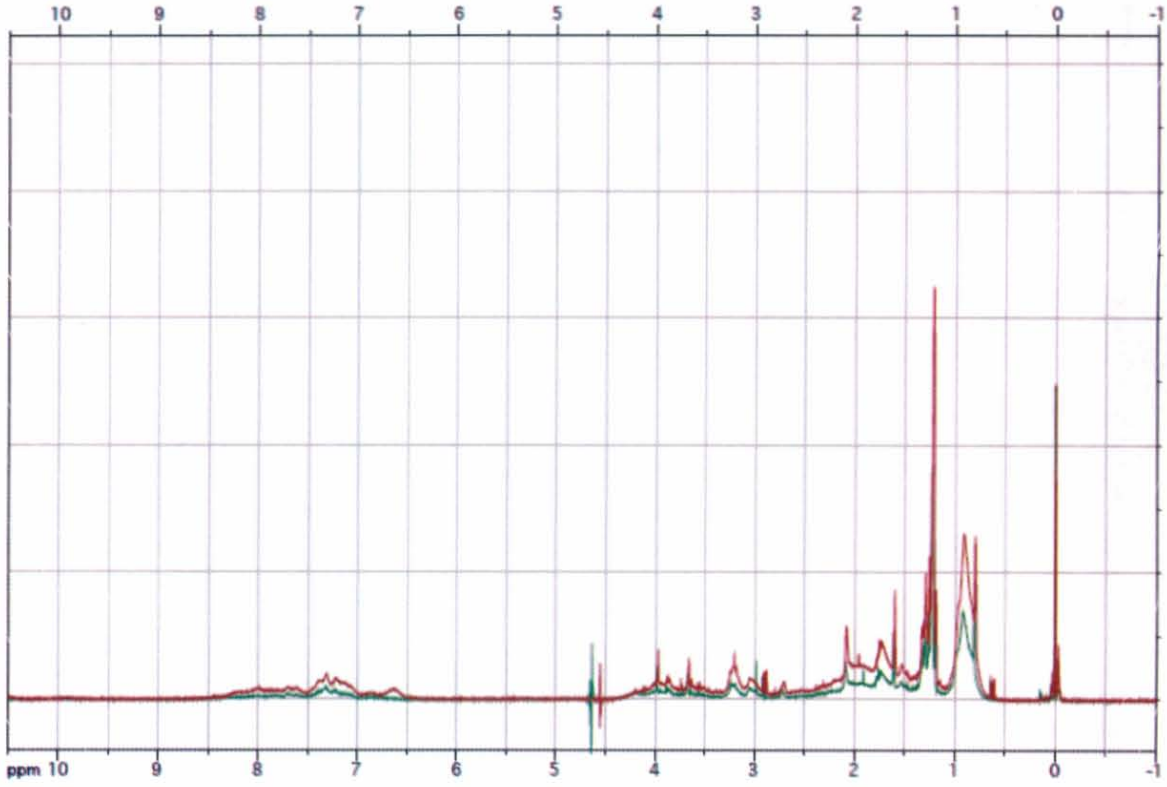

Figure 24. A) ^{1}H NMR spectra of 1 mM Super-Mini-B in SDS buffer (90% H_2O, 10% D_2O, 0.2 mM DSS, and 150 mM deuterated SDS) at pH 5, 45°C (red) and pH 7, 37°C (green).

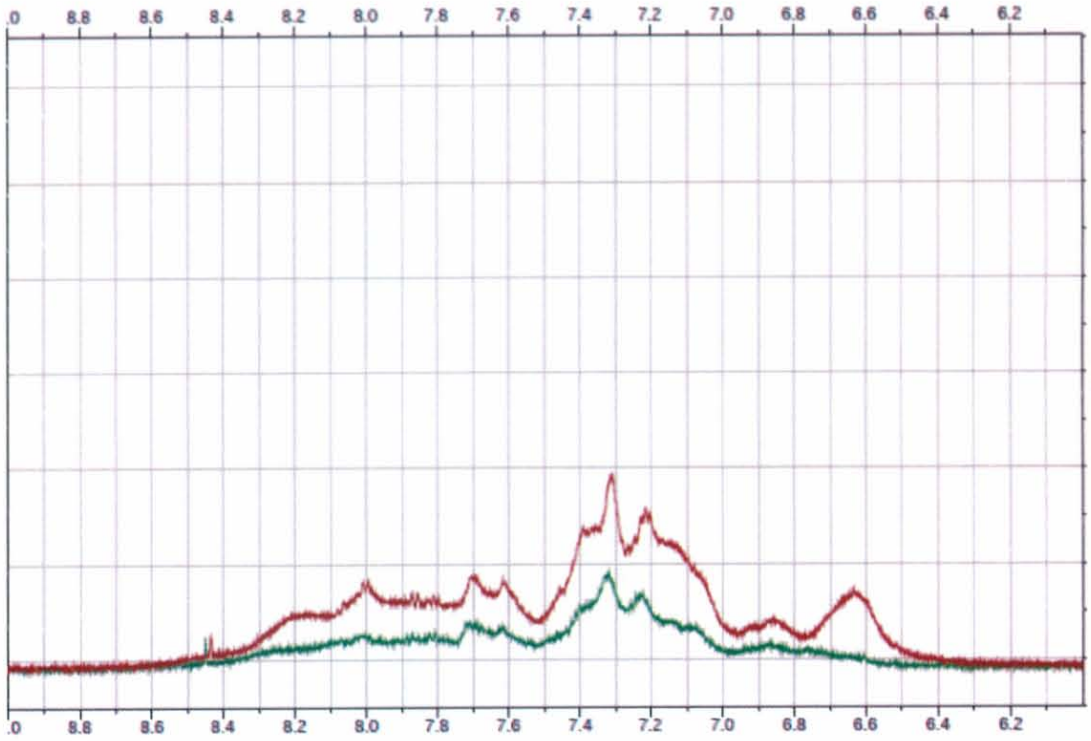

Figure 24. B) HN region of ^{1}H NMR spectra of 1 mM Super-Mini-B in SDS buffer (90% H_2O, 10% D_2O, 0.2 mM DSS, and 150 mM deuterated SDS) at pH 5, 45°C (red) and pH 7, 37°C (green).

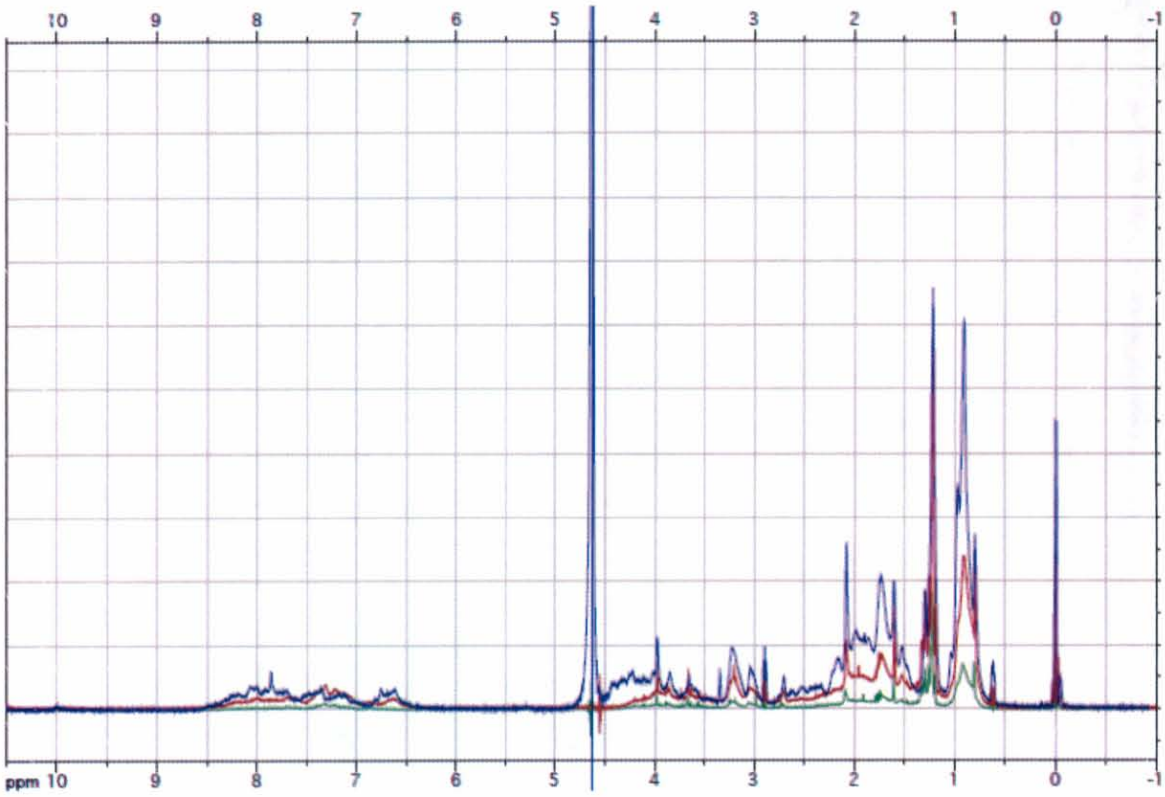

Figure 25. A) ^{1}H NMR spectra of 1.5 mM Mini-B at pH 7 and 37°C (blue), 1 mM Super-Mini-B at pH 7 and 37°C (green) and at pH 5 and 45°C (red). Spectra were recorded with 32 scans. Results show more intense peaks in the HN region for Mini-B compared to Super-Mini-B.

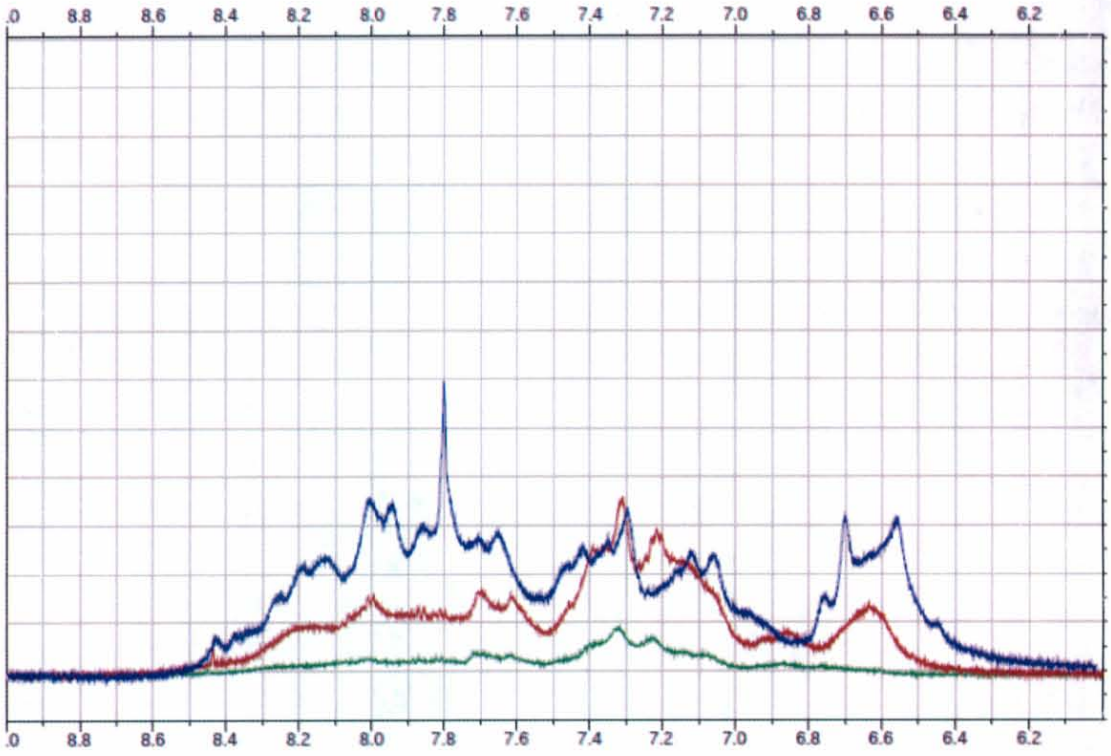

Figure 25. B) HN region of ^{1}H NMR spectra for 1.5 mM Mini-B at pH 7 and 37°C (blue), 1 mM Super-Mini-B at pH 7 and 37°C (green) and at pH 5 and 45°C (red)

After using the 1Ds to optimize the sample conditions, 2D NMR experiments were next carried out to determine the structural features of the peptide. The NOESY experiment on Super-Mini-B in SDS buffer at pH 7 and 37°C had a very small number of broad cross peaks. This may be due to aggregation and a consequent increase in tumbling time under these conditions (Figure 26). In spite of the lower number of peaks observed at pH 7 and 37°C compared to pH 5 and 45°C (Figure 27), overlaying their 2D NOESY spectra did not show any significant changes in chemical shift (Figure 28). The absence of changes in chemical shift indicates that the local structure is likely similar in the two conditions, however, the changes in peak shape are consistent with differences in overall complex size.

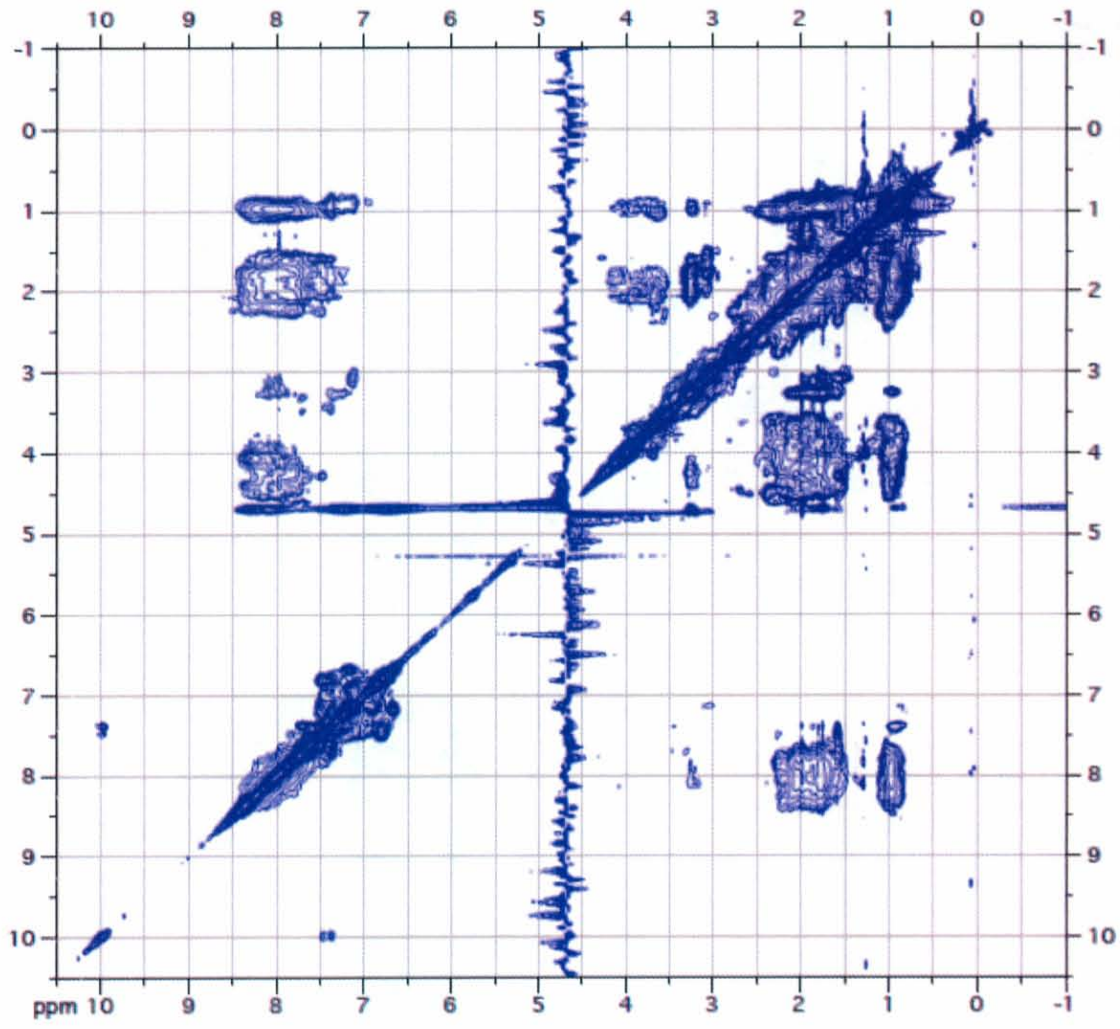

Figure 26. Solution NMR 2D NOESY spectrum of 1 mM Super-Mini-B dissolved in a solution of 90% H_2O, 10% D_2O, 0.2 mM DSS, and 150 mM deuterated SDS at pH 7 and 37°C. For the 2D NOESY, 128 scans were used with a mixing time of 200 ms.

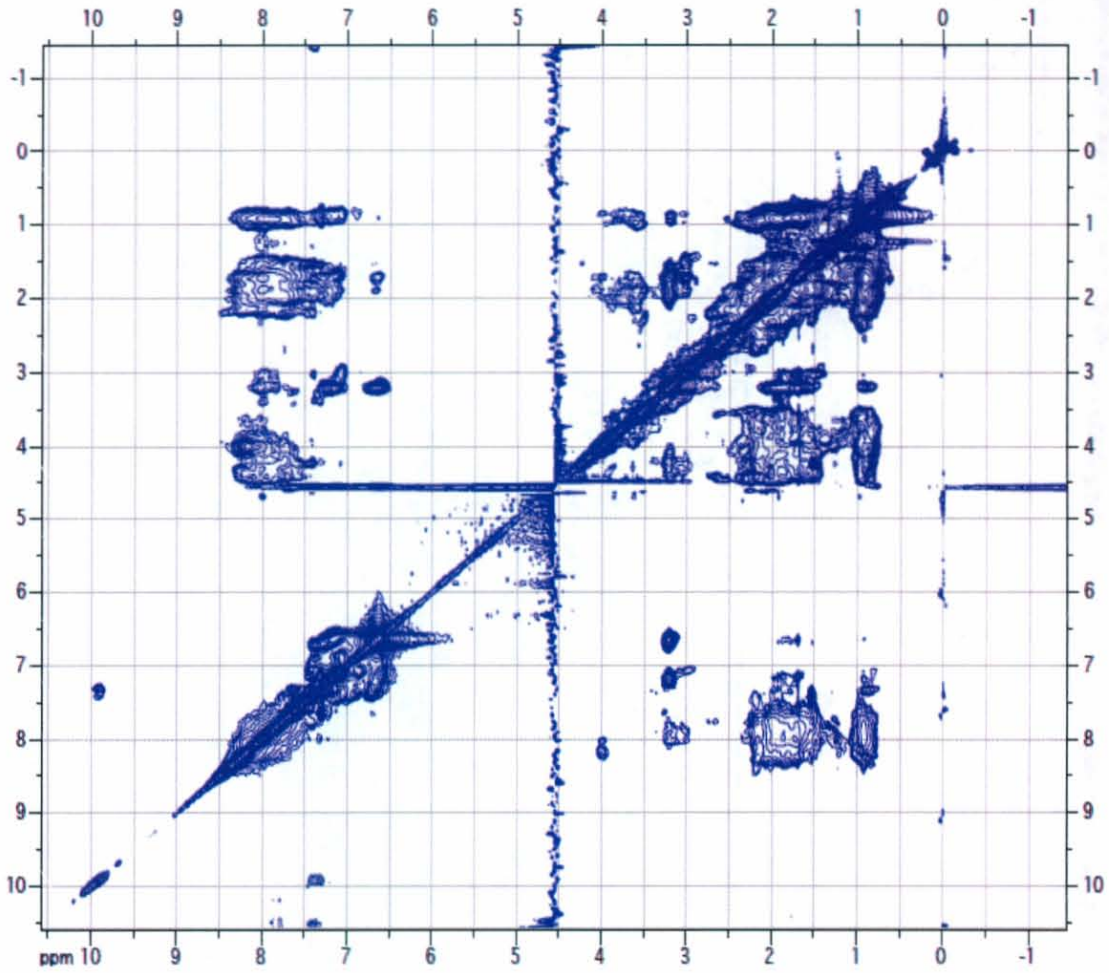

Figure 27. Solution NMR 2D NOESY spectrum of 1 mM Super-Mini-B dissolved in a solution of 90% H_2O, 10% D_2O, 0.2 mM DSS, and 150 mM deuterated SDS at pH 5 and 45°C. For the 2D NOESY, 128 scans were used with a mixing time of 200 ms.

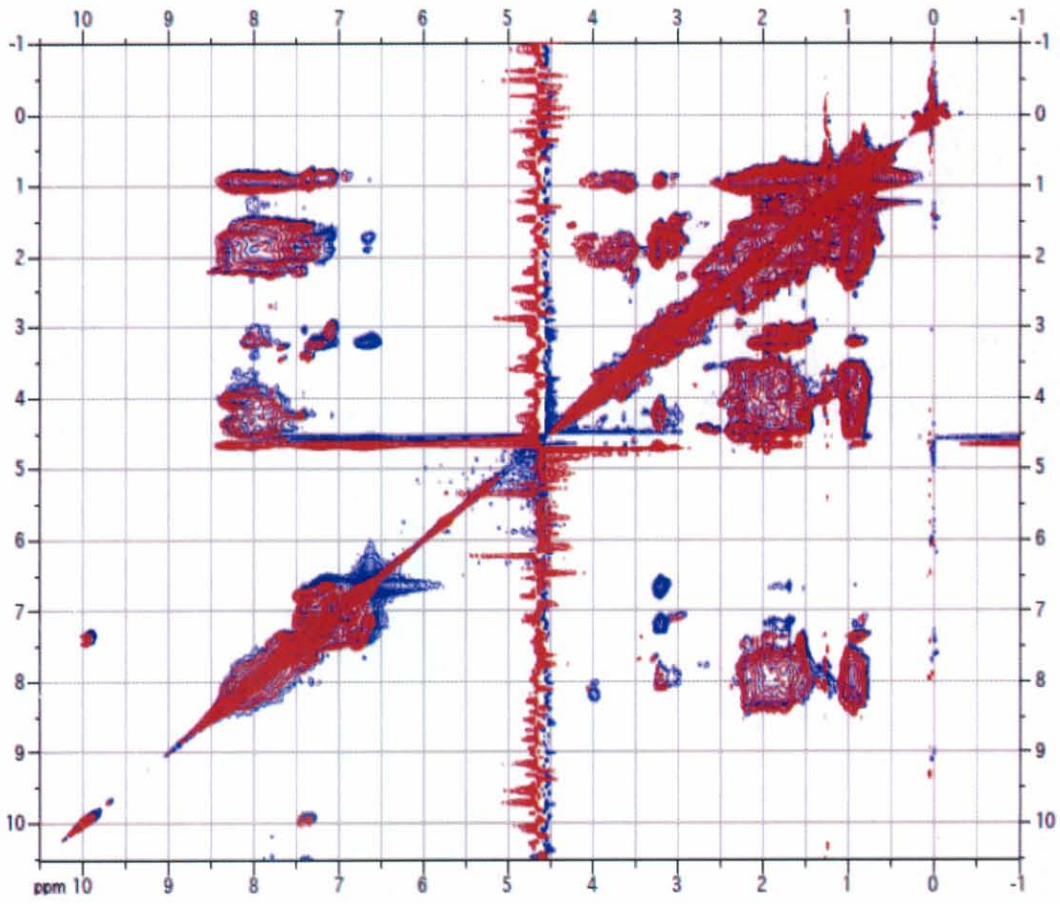

Figure 28. A) Overly of 2D NOESY spectra of 1 mM Super-Mini-B in 150 mM SDS solution at pH 7 and 37°C (red) and pH 5, 45°C (blue) under same acquisition parameters; 128 scans were used with a mixing time of 200 ms.

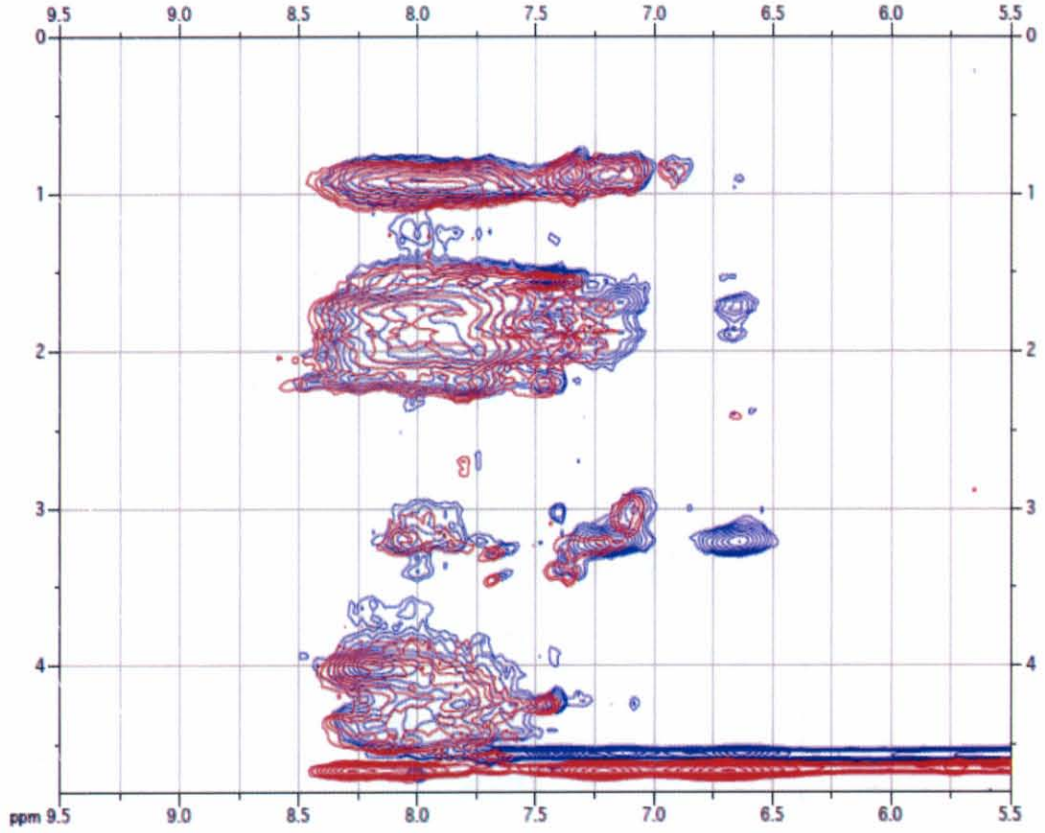

Figure 28. B) Overly of HN-HX correlation region from 2D NOESY spectra of 1 mM Super-Mini-B in 150 mM SDS solution at pH 7 and 37°C (red) and pH 5, 45°C (blue).

The Overlaid 2D NOESY spectra of Super-Mini-B with Mini-B shows the positions of Mini-B's peaks did not appear to change greatly in the context of Super-Mini-B. However Super-Mini-B's peaks are broader and some of the weaker peaks apparent in the Mini-B spectrum are absent from the Super-Mini-B spectrum. The broadening and weakening of the intensity in Super-Mini-B compared to Mini-B is consistent with a substantially slower tumbling time for Super-Mini-B, that is likely related to an increase in aggregation (Figure 29).

The overall results of 2D NOESY experiments in Mini-B and Super-Mini-B indicate that the additional 7 residues do not induce any major changes in the structure of the helical regions of the peptide. However, there are small changes in peak positions that are to be expected based on the differences in temperature (Figure 29B).

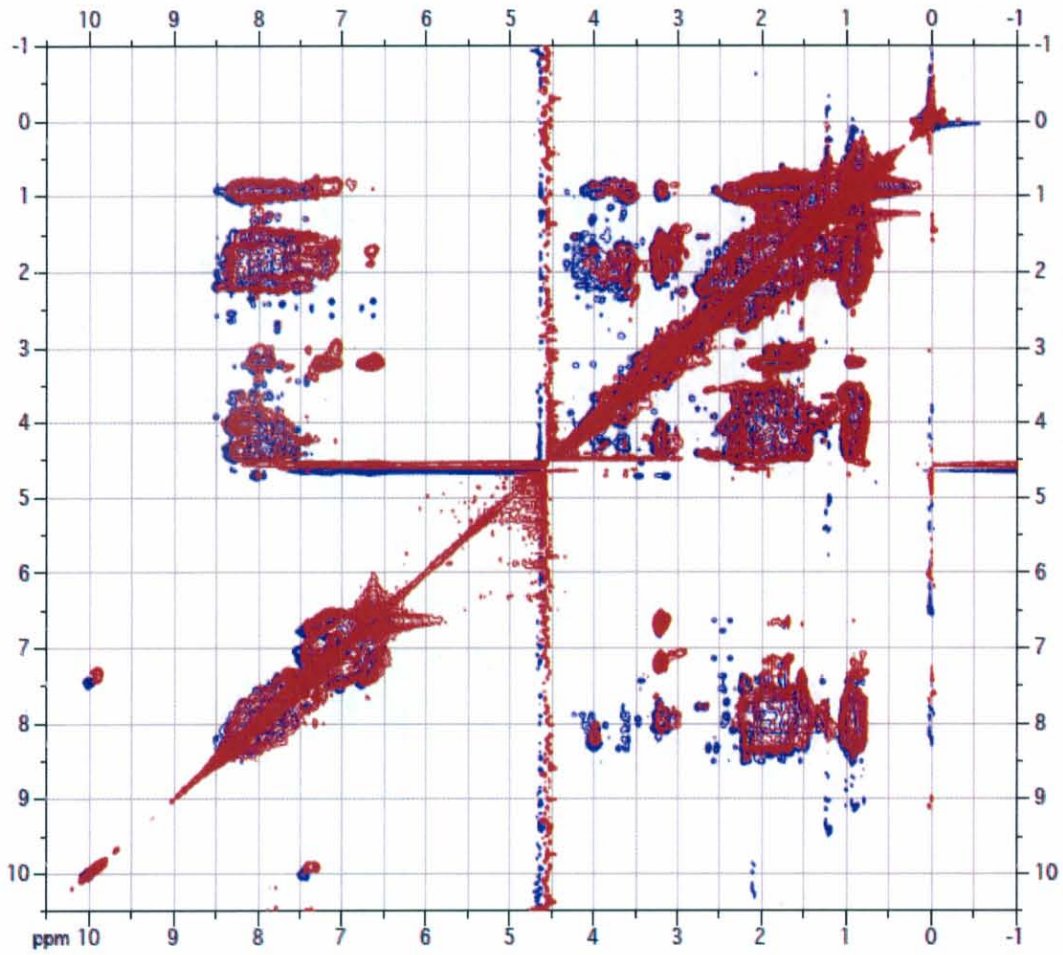

Figure 29. A) Overly of 2D NOESY spectra of 1 mM Super-Mini-B in 150 mM SDS solution at pH 5 and 45°C (red) and 1.5 mM Mini-B in 150 mM SDS pH 5 and 37°C (blue) under similar acquisition parameters; 128 scans were used with a mixing time of 200 ms.

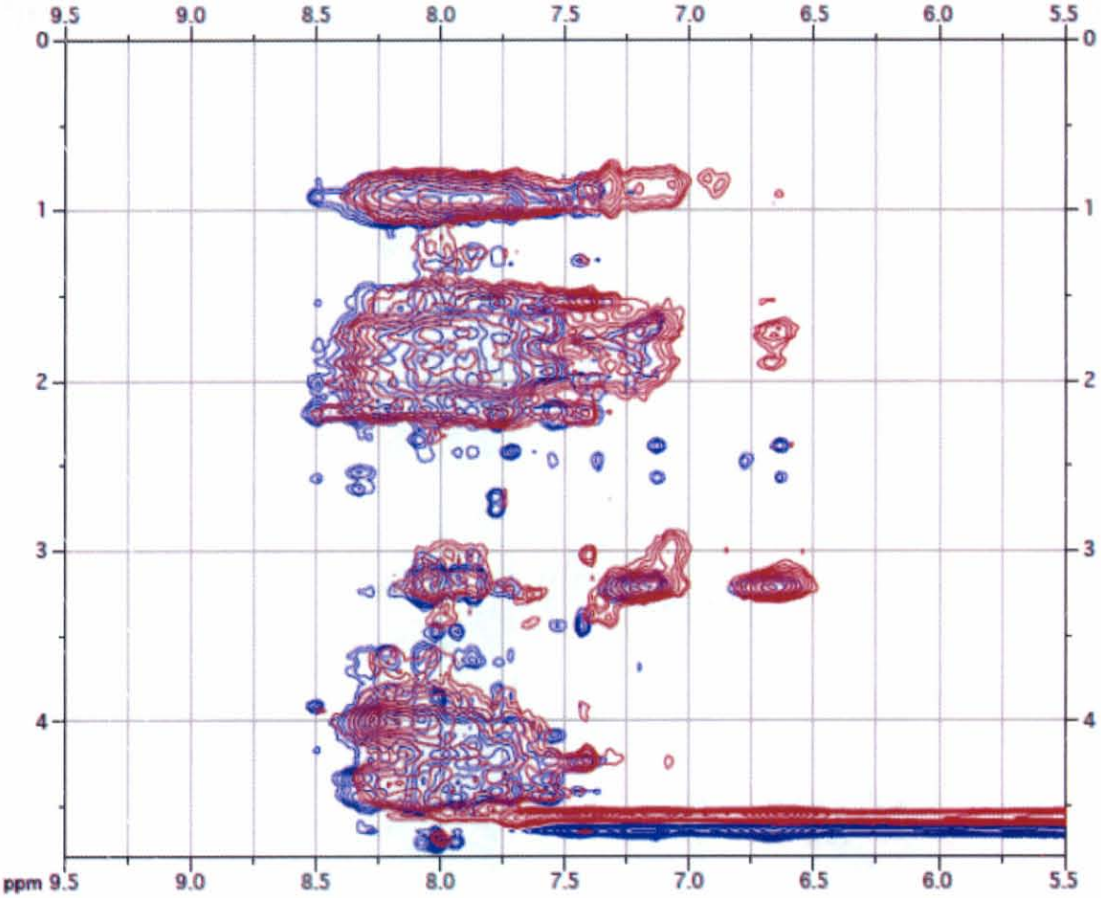

Figure 29. B) Overly of HN-HX correlation region from 2D NOESY spectra of 1 mM Super-Mini-B in SDS solution at pH 5 and 45°C (red) and 1.5 mM Mini-B at pH 5 and 37°C (blue).

The position of the N-terminal insertion sequence of SP-B (SP-B_{1-7}) in the micelle, as a fragment in the context of Super-Mini-B, was assessed by addition of DSA to the peptide/micelle sample. A procedure that is similar to what mentioned before for the DSA TOCSY on SP-B_{1-7} (section 3.8) was carried out to analyze changes in Super-Mini-B peaks. The N-terminal insertion sequence peaks in the TOCSY spectrum of Super-Mini-B were assigned (Table 9). The number of observable peaks for the N-terminal 7 residues in Super-Mini-B was less than SP-B_{1-7}, however, protons associated with the N-terminal residues retained chemical shifts similar to protons at the same spin systems in SP-B_{1-7}. Peaks intensity reduction in presence of DSA was monitored for the N-terminal 7 residue associated peaks. A decrease in intensities was detected for some peaks. The disappearance of peaks corresponding to residues 1 and 2 indicates the peptide is deeply inserted in the micelle (Figure 30).

Table 9. ^{1}H Chemical shifts of the N-terminal insertion sequence of SP-B from the TOCSY experiment on Super-Mini-B. HA, HB, ... respectively stand for proton nuclei in order of proximity to backbone HN nucleus.

Residues	HN (ppm)	HA (ppm)	HB (ppm)		HC (ppm)		HD (ppm)		HE (ppm)	HF (ppm)	HG (ppm)
F1	Not found	Not found	Not found		7.317		7.627		6.906	7.375	7.324
P2/4/6	---	Not found	2.284 2.257	2.194 2.306	1.595 1.340	1.595 1.167	3.618 3.844 3.861	3.506 3.738 3.632	---	---	---
I3	Not found	4.113	1.316		Not found		Not found		Not found	---	---
L5	Not found	3.606	1.595	1.530	Not found		Not found		---	---	---
Y6	Not found	Not found	Not found		7.037		6.808		Not found	Not found	Not found

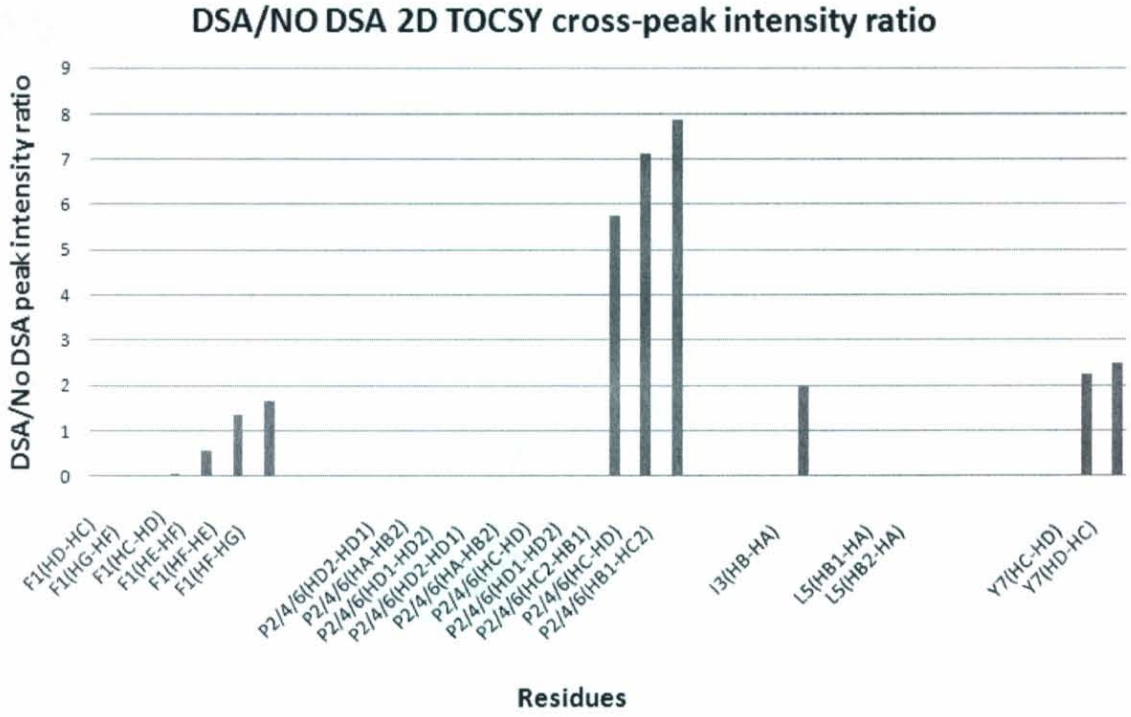

Figure 30. Effect of 0.6 mM 16-DSA on N-terminal residues of 1 mM Super-Mini-B in 150 mM SDS, pH 5 and 45°C. The ratio of 2D TOCSY cross-peak intensity with and without 16-DSA is plotted along the amino acid sequence and corresponding proton groups. The analysis process was described in section 3.8. Note that it was not possible to assign the proline resonances to particular prolines within the sequence.

DOSY experiments provide a measure of the size of particles, such as micelles or protein-micelle complexes by determining the diffusion coefficients. DOSY results can be affected by protein-lipid and protein-protein interactions since the size would change upon binding (Price, 1997). In order to assess the size of particles, the diffusion coefficients of Super-Mini-B in SDS micelles were determined from the DOSY experiment at 30°C. The spectra were processed using iNMR and the diffusion constants calculated using the "DOSY" package in DOSYToolBox08 (Nilsson, 2009). The corresponding hydrodynamic diameter calculated using the Stokes-Einstein equation for spherical particles undergoing free diffusion in solution,

$$D = k_B T/3\pi \eta d_H$$

, that k_B is the Boltzmann constant, T is the absolute temperature, η is the viscosity of the solution and d_H is the hydrodynamic diameter of the particle. The hydrodynamic diameter corresponds to the diameter of a sphere that would be diffusing at the same rate. The apparent hydrodynamic diameter for 1 mM Super-Mini-B was 7.06 nm at pH 7, 30°C while for 1.5 mM Mini-B was 7.02 nm at pH 7, 37°C (Sarker, PhD Thesis, Booth lab) (Figure 31).

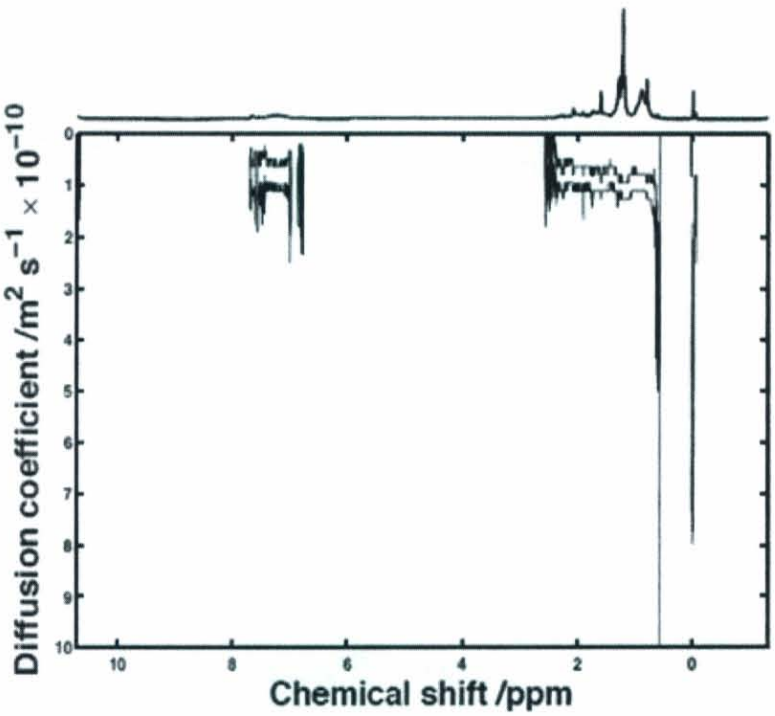

Figure 31. 2D DOSY spectrum of 1 mM Super-Mini-B in SDS at 30°C. The conventional 2D DOSY spectra show approximate measures of the translational diffusion coefficients of various species present in the sample (along Y axis) with respect to their 1H chemical shifts (X axis).

3.11. Solid-state nuclear magnetic resonance (NMR) characterization of lipid-protein interactions of Super-Mini-B

Solid-state NMR experiments were used to assess interactions of Super-Mini-B with membranes. In this study, solid-state NMR experiments were performed with lipid bilayers mechanically oriented on a solid substrate. The inclusion of the peptide into the samples can lead to disruptions in the overall orientation of the bilayers, as well as changes in acyl chain order. These changes reveal aspects of Super-Mini-B/lipid interactions.

^{2}H solid state NMR experiments were performed with Super-Mini-B in oriented lipid bilayers composed of POPC-d_{31}:POPG (7:3, w/w). In the absence of the peptide, deuterium peaks are well resolved with the widest splittings at ±27.08 kHz showing that the lipid bilayers are well aligned. The NMR spectrum after addition of the peptide (1 mol %) shows changes. The signal intensity on the shoulders and the splitting significantly decreased, and the spectra become superpositions of more than one component. One component exhibits larger splittings, corresponding to bilayers oriented with bilayer normal parallel to the magnetic field and the second component displays features with splittings that are half of the oriented component splittings. The second component is most likely due to randomly oriented bilayers (see the arrows in Figure 32). Thus, the presence of Super-Mini-B causes a small fraction of the bilayers to lose their orientation (Figure 32).

By increasing the temperature the splitting did not change, but more signals at half the width of the oriented spectrum were observed. This observation indicates a greater level of bilayer perturbation at higher temperatures (Figure 33).

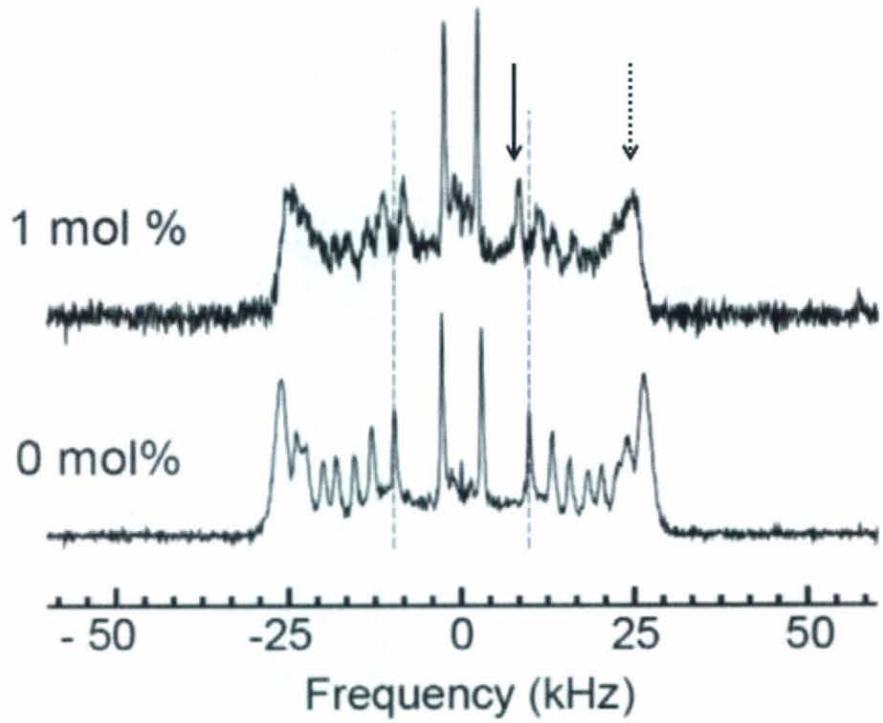

Figure 32. ^{2}H spectra of mechanically oriented POPC-d_{31}:POPG 7:3 with (upper panel) and without (lower panel) 1 mol % Super-Mini-B. The spectra were acquired with 60000 scans at 23°C. The dashed line arrow," -->" indicates oriented and the black arrow "→" indicates randomly orientated species.

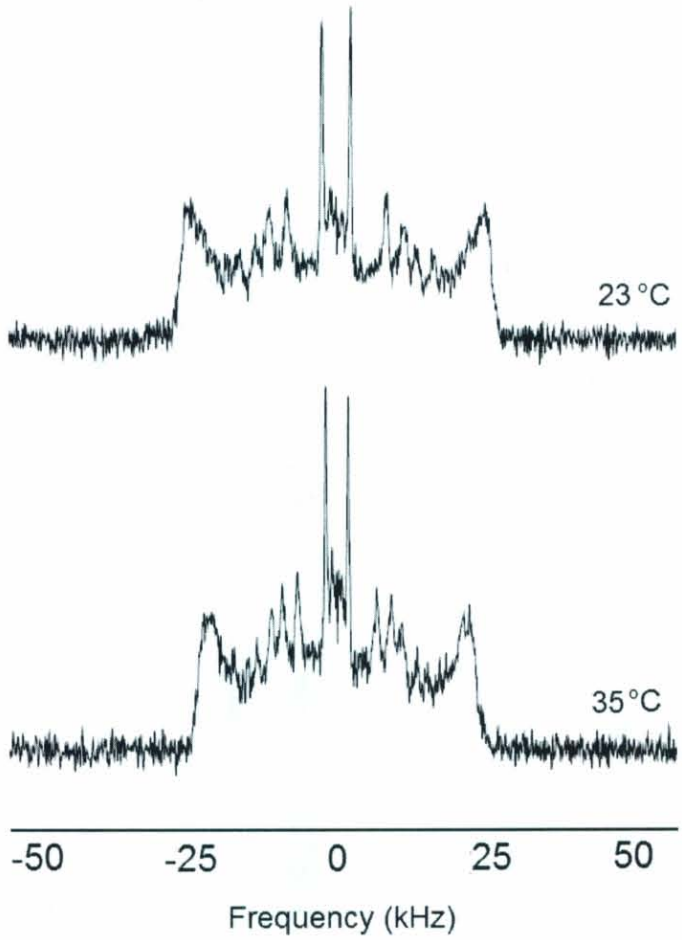

Figure 33. ^{2}H NMR spectra of mechanically oriented bilayers composed of POPC-d_{31}:POPG (7:3, w/w) in the presence of Super-Mini-B (1 mol %) at 23°C and 35°C.

The order parameter profile approach indicates the effect of the peptide on the oriented fraction of the lipid bilayer by measuring the effect of the peptide on chain order at different positions along the chain. The Sternin, et al. method (Sternin et al., 1988) was used to extract order

parameter profiles from ^{2}H NMR spectra of POPC-d_{31}:POPG (7:3, w/w) in the absence and presence of the Super-Mini-B and Mini-B (1 mol %). Analyzed data showed a greater disruption of lipids chain order in presence of Super-Mini-B than Mini-B (Figure 34). However the order parameter profiles will not be absolutely accurate. To calculate the order parameters for the regions of the spectrum where the peaks are not well resolved, the total area under the curve is used for the calculation. Since this area includes the area under signals from both the oriented and unoriented peaks, this will not be entirely accurate for spectra that contain a substantial unoriented portion (Mini-B results and calculations; Courtesy of Dharamaraju Palleboina, Booth lab).

The echo decay time measurement experiment gives some information about the rates of lipid motions. Adding a peptide tends to increase the echo decay rate and shorten the echo decay time. This indicates that the peptide affects the dynamics of the bilayer lipids. The echo decay time for POPC-d_{31}:POPG sample was 1.019 ms in the absence of the peptide and 0.564 ms in the presence of Super-Mini-B. Thus, the presence of the peptide causes a large increase in lipid motions (Figure 35).

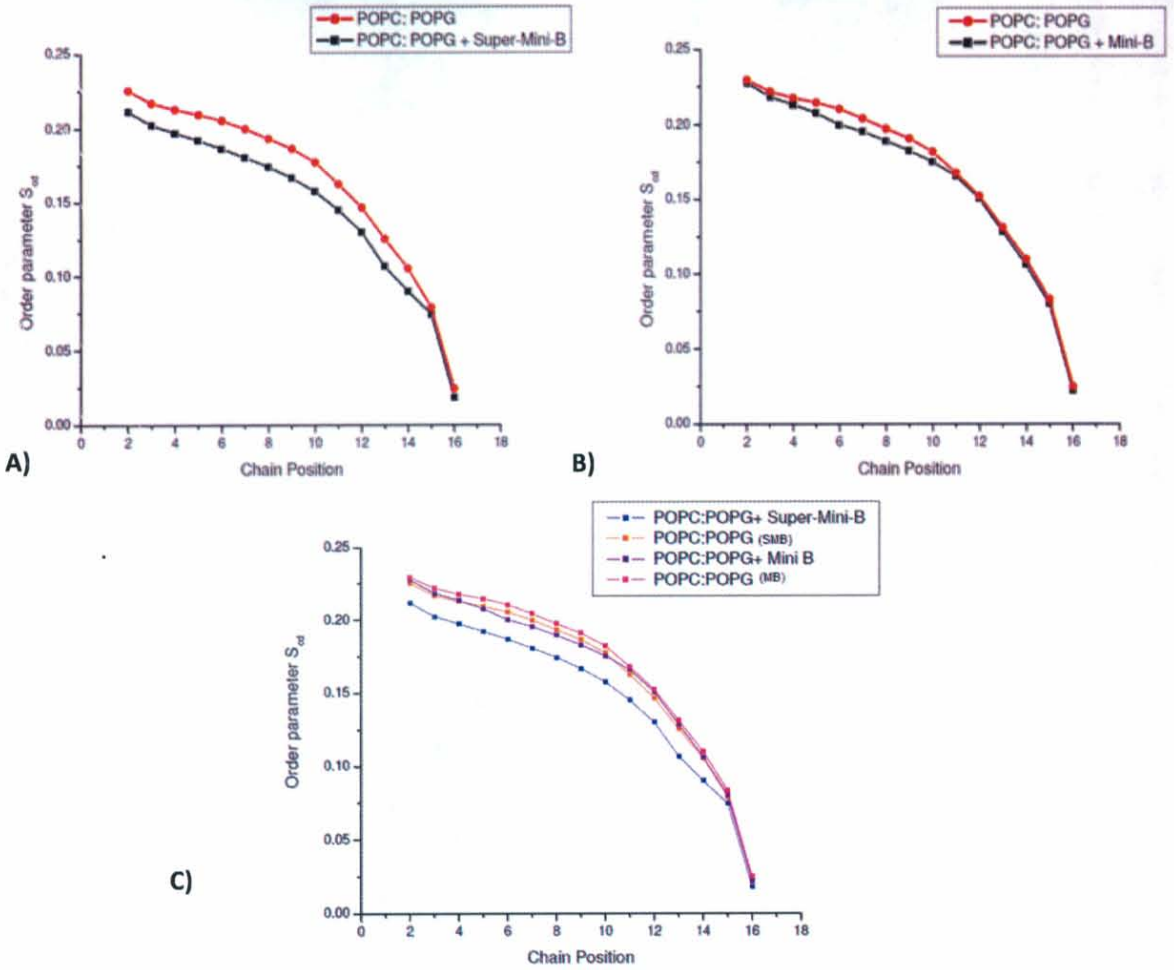

Figure 34. Order parameter profiles of POPC-d_{31}:POPG with and without Super-Mini-B (a), Mini-B (b). (c) Shows the data from (a) and (b) overlaid. Data points extrapolated from ^{2}H NMR experiments on POPC-d_{31}:POPG (7:3, w/w) in the absence and presence of the peptides (1 mol %). SMB and MB stand for the lipid-only samples prepared to compare with Super-Mini-B and Mini-B containing samples respectively. Samples were prepared with the same lipid composition and preparation condition. The slight difference in order parameter of lipid only-samples is due to the expected differences in similar samples with different preparation time. Parameters for Super-Mini-B extracted with help from Dharamaraju Palleboina, Booth lab.

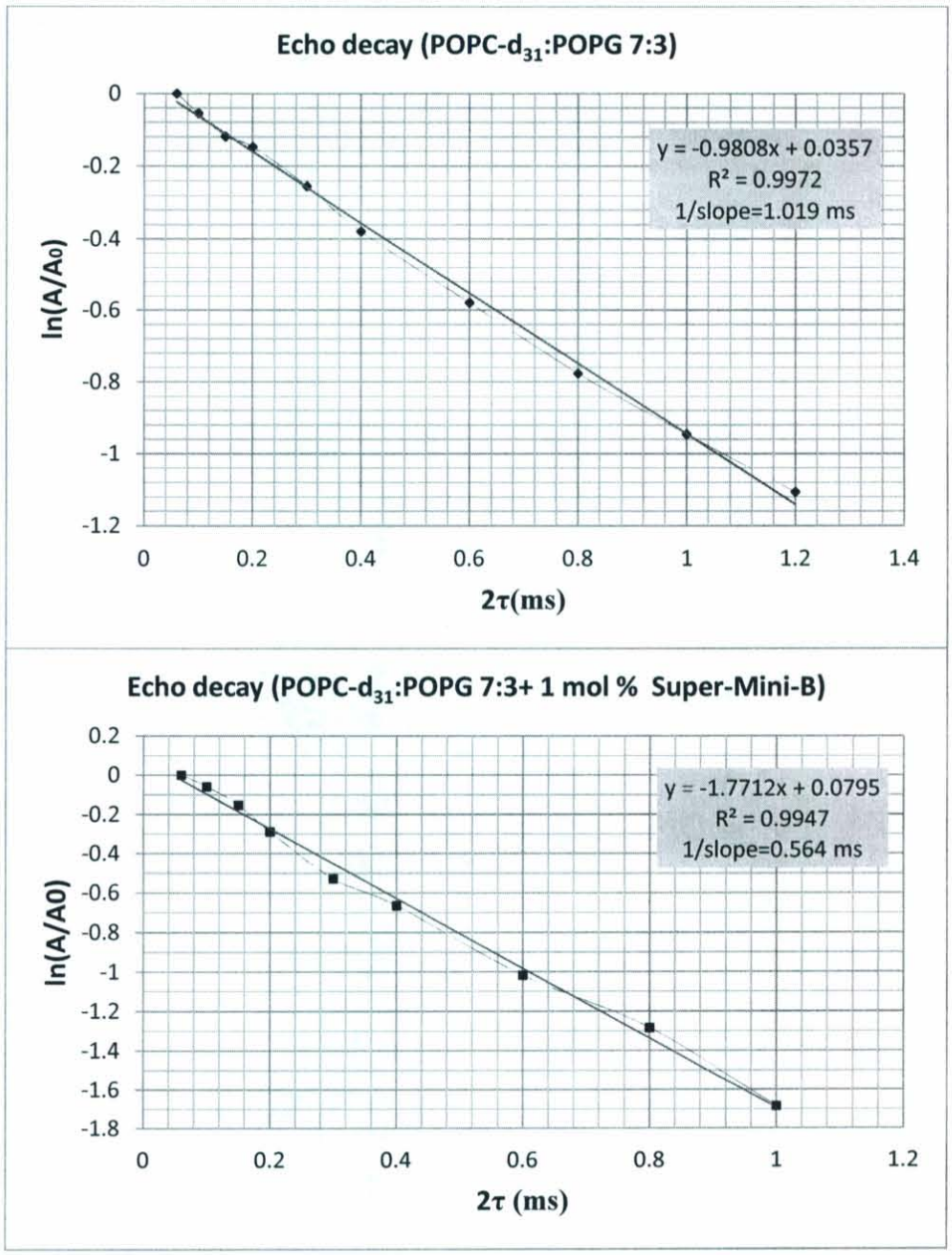

Figure 35. Echo Decay value for POPC-d_{31}:POPG (7:3, w/w) in the absence (A) and presence (B) of 1 mol % Super-Mini-B at 35°C. Echo decay time is calculated based on the slope. Results were extracted with help from Dharamaraju Palleboina, Booth lab.

4. Discussion

To understand the exact mechanism of SP-B's function, we need to know the structure of the protein. The extraction and purification of SP-B from natural sources have been accomplished (Baatz et al., 2001), however, studies to define the structure of SP-B have not been successful yet. Isotope labeling of amino acids is one of the techniques employed to obtain more information on protein structure in NMR studies. For a protein the size of SP-B, isotope labelling is essential to obtain an atomic resolution structure. In order to label amino acids, the protein needs to be produced recombinantly or, in the case of short peptides, synthesized chemically.

The hydrophobic nature of proteins like SP-B poses many difficulties in recombinant expression (Kiefer, 2003). As a result these proteins are often produced in heterologous systems as fusions with soluble proteins. Due to SP-B's hydrophobicity, as well as lytic and fusogenic properties (Ueno et al., 2004), in this study SP-B was fused to SN (staphylococcus nuclease). A plasmid containing the full encoding sequence of SP-B was expressed in C43 strain of *E. coli*.

DNA sequencing analysis of the cloned construct confirmed the expected sequence of the SN-SP-B encoding gene. Attempts to detect the full sequence of the expressed protein were only partially successful. SDS-PAGE has been reported promising for most likely all proteins (including

hydrophobic ones). Since I know that my desired protein is highly hydrophobic, I tried Urea-SDS-PAGE as well by adding up 8 M urea to all of the SDS-PAGE buffers (loading, running and gel preparing buffers. Data are not shown since the pictures of the gel does not have the publishable quality but results were pretty similar to the regular SDS-PAGE. I have repeated expression and SDS-PAGE for several times and got similar resultsThe apparent size of the purified expressed SN-SP-B on SDS gel was less than the expected molecular mass, although Western blotting confirmed presence of the histidine tag in the expressed peptide. This observation may result from the fact that hydrophobic proteins travel through the gel but their dynamics is altered because of their hydrophobic surfaces, resulting to run at different positions than the expected molecular weight (Clark and Pazdernik, 2008).

The chance of activation of proteases at the cell disruption steps is almost zero EDTA and PMSF were used as protease inhibitors EDTA binds the metal ions that the metalloproteases need to function.The half-life of PMSF is 110 min at pH 7 and 55 min at pH 7.5, all at 25°C. During cell rupture samples were kept on ice and for the next steps after cell rupture till the end of purification, all of the procedure was accomplished in a cold room.

Several parameters were assessed to probe other possibilities for the apparently low molecular weight of SP-B on the gel. The possibility of

translation interruption or proteolysis at induction step was investigated; this could happen due to the lack of nutrients (Reeve et al., 1984; Groat et al., 1986). The possibility of breakage at the cell disruption steps was also assessed. No evidence of any of these possibilities was detected; the apparent size of the expressed SN-SP-B peptide did not change under any conditions.

Identification of the amino acid sequence of the expressed protein by mass spectroscopy was limited to a fragment of the fusion protein and the N-terminal fragment of SP-B. The analysis of hydrophobic proteins is a challenge to mass analysis (Lubec and Afjehi-Sadat, 2007; Cech and Enke, 2000). In addition to hydrophobicity, despite reducing the protein prior to mass spectroscopy, it is still possible that some disulfide bonds remain which could limit the ionization. Since no changes were detected in the expressed protein under varying conditions, future works can be focused on overcoming limitations in detecting this highly hydrophobic peptide.

Nd-SP-B (N-terminal deleted SP-B) is a novel near full-length SP-B peptide that was produced by deletion mutation at the N-terminal end of SP-B, SP-B_{1-7} was removed from the peptide. The size of the expressed peptide on the gel was less than the expected molecular weight and ion search analysis could only identify fragments of SN. Again the high hydrophobicity of the peptide limited the sequence identification. However

the structural studies on this near full-length peptide would give valuable information on structure and function of SP-B.

Even if the sequence of the expressed SP-B cannot be confirmed by other methods, if conditions can be found which allow for high resolution NMR data, it will be apparent from this NMR data if the expressed protein has the expected sequence or not. In order to confirm the sequence of constructs in the sample, the subjects that should be studied in future works regarding to expression and purification of SP-B and Nd-SP-B are expression of the protein in minimum media for isotope labelling of the selected amino acids and using the organic extraction method to purify the expressed protein in later purification steps after cleavage from the fusion part or to purify it from remained impurities.

While working on the full-length SP-B pose many difficulties, fragments containing individual helices or pairs of helices of SP-B were shown to retain biological activities of the full-length protein (Revak et al., 1991; Veldhuizen et al., 2000; Walther et al., 2002). Super-Mini-B retained higher values for surfactant activities (e.g. arterial oxygenation and dynamic compliance) than full-length SP-B and Mini-B (Walther et al., 2010). Since Super-Mini-B and Mini-B have the same amino acid sequence except for the presence of the N-terminal insertion sequence ($SP\text{-}B_{1\text{-}7}$) in Super-Mini-

B, Walther's study (Walther et al., 2010) showed the importance of SP-B_{1-7} in surfactant activity of SP-B for the first time.

The N-terminal insertion sequence of SP-B (SP-B_{1-7}) is a short peptide consisting of 7 amino acids. SP-B_{1-7} retains polyproline helix structure (Table 6) and resembles a group of cell penetrating peptides (CPPs) (Pujals and Giralt, 2008). In this group of CPPs, the polyproline helix works as a scaffold to keep hydrophobic and cationic groups close together that promote membrane penetration and destabilization respectively (Ragin and Chmielewski 2004; Shai, 1999). A similar order of amino acids; hydrophobic residues, polyproline helix and cationic residues, are set at the N-terminal fragment of SP-B (SP-B_{1-24}). This similarity of (SP-B_{1-24}) with CPPs may explain the lytic and fusogenic properties of N-terminal based SP-B peptides (Ryan et al., 2005) and also can be considered in models to explain mechanism of function of SP-B.

Structural studies on SP-B_{1-7} alone and in the context of Super-Mini-B helped to define its structure and function within the context of Super-Mini-B. The depth of insertion in SDS micelle was calculated based on DSA-TOCSY experiment. Similar results were acquired for SP-B_{1-7} fragments of Super-Mini-B and SP-B_{1-7} individually; the N-terminal peptide is located superficially in the micelle and may anchor SP-B to the lipid bilayer (Figures 17 and 30). However in this study, results of DSA experiments were brought into question by the unexpected increase in

intensity of some peaks after addition of DSA. The increase in intensity can be due to a contamination or induced changes in the micelle by DSA (Mravljak et al., 2006). Use of another paramagnetic substance such as manganese is an alternative way to confirm or refute the DSA results of this study (Gayen et al., 2011). Other approaches such as tryptophan fluorescence spectroscopy can also give information on insertion of Super-Mini-B in the micelle (McKnight et al., 1991).

In order to assess structural features induced by the presence of SP-B_{1-7}, structural studies on Mini-B (Sarker, et al., 2007) were compared to studies on Super-Mini-B. Although similar conditions were used for the acquisition of the NMR data, the spectra of Mini-B and Super-Mini-B demonstrated considerable differences. The positions of the 2D NOESY peaks of Mini-B did not appear to change greatly in the context of Super-Mini-B, however the Super-Mini-B peaks are broader and some of the weaker peaks apparent in the Mini-B spectrum are absent from the Super-Mini-B spectrum. The overall results of NOESY experiments in Mini-B and Super-Mini-B indicate that the additional 7 residues do not induce any major changes in the structure of the helical regions of the peptide, however the broadening and disappearance of peaks suggests formation of large particles in Super-Mini-B.

The size of particles for Super-Mini-B and Mini-B was determined based on diffusion coefficient values in DOSY experiments. The

hydrodynamic diameter for Super-Mini-B particles was greater than Mini-B. The broadness and low number of peaks in Super-Mini-B can be evidences for formation of large size particles and resulting slow tumbling. Unfortunately it was not possible to obtain high quality DOSY data under the same experimental conditions as were used for the 2D NOESY and TOCSY spectra. Likely due to turbulence in the sample, it was only possible to acquire reliable DOSY spectra at lower temperatures, i.e. 30°C. At this temperature, the measured translational diffusion is similar to that measured for Mini-B at a higher temperature (1 mM Super-Mini-B at pH 7, 30°C was 7.06 nm and 1.5 mM Mini-B at pH 7, 37°C was 7.02 nm) which is puzzling considering the much broader linewidth observed in the NOESY and TOCSY for Super-Mini-B compared to Mini-B. However, this controversy may be due to the fact that rotational diffusion (which is reflected in linewidth) is more sensitive to the complex size than translational diffusion (measured by DOSY), as well as the fact that the protein/micelle complexes may change shape substantially by changes in the temperature. Other approaches to measure size and shape of particles are dynamic light scattering (DLS) (Ghosh, 2005) and small angle neutron scattering (SANS) (Egelhaaf et al., 2003) that can be used to provide additional information on the size of Super-Mini-B.

Further studies by circular dichroism gave us a better view of the structure of the peptides. The presence of N-terminal insertion sequence of

SP-B induced greater contents of β- and unordered structures and also less α-helical structures in Super-Mini-B than Mini-B. This observation can be considered as a transition from α-helices to unordered and later β-structures. Proteins rich in β-structures are prone to aggregate and produce large size particles (Chiti et al., 2003).

Further studies by solid-state NMR assessed lipid bilayer perturbation properties of Super-Mini-B and Mini-B. The lipid interactive property of the N-terminal helix of SP-B (Mini-B and Super-Mini-B as well) has been reported before, the tryptophan residue has the key role of this property (Sarker et al., 2011). Results of the current study show the additional SP-B_{1-7} provides Super-Mini-B a greater level and probably a tryptophan-independent mechanism of lipid interaction. This level of lipid layer perturbation by Super-Mini-B confirmed the assumption that SP-B_{1-7} does not work only as an anchor but also it has a critical role in SP-B's interference with surfactant lipid layers (Figure 34). SP-B_{1-7} can be crucial for mediating transfer of lipids by SP-B at extension and compression phases of respiration.

The effect of SP-B_{1-7} on SP-B's surfactant activity was underestimated until a study showed this short peptide could provide significant changes in surfactant activities (Walther et al., 2010). Structural influences of SP-B_{1-7} were also unexpected. Molecular dynamics simulation suggested that SP-B_{1-7} provides a surface for homodimerization (Walther et

al., 2010). NMR studies in this research did not show any evidences for dimerization (Figure 20). Instead of dimerization, large size particles and β-structures were detected (Figure 29 and Table 8).

One of the goals of this research was to learn more about the structure of the full-length SP-B by studying the structures of its fragments. The structure of Super-Mini-B was composed of helical regions of Mini-B in a smaller portion and a larger portion of β- and unordered structures than Mini-B. I suggest that the extended polyproline helix exposes the hydrophobic residues of SP-B_{1-7} to interact and form unordered and cross-β structures with hydrophobic helical regions of Super-Mini-B. Circular dichroism of Super-Mini-B in a membrane-like environment such as liposomes can provide extra evidence that the β- and unordered structures may provide the essential property of Super-Mini-B and SP-B for lipid/membrane interactions.

SP-B is the only essential protein component of lung surfactant (Clark et al., 1995; Tokieda et al., 1997). The current research will provide some basis for production, structure and understanding the mechanism of function of SP-B. Knowledge of the molecular mechanism of SP-B can improve the current aspects in surfactant replacement therapy and suggest new perspectives for ARDS treatment as well.

References

Baatz, J.E., Sarin, V., Absolom, D.R., Baxter, C., Whitsett, J.A. Effects of surfactant-associated protein SP-B synthetic analogs on the structure and surface activity of model membrane bilayers (1991) Chemistry and Physics of Lipids, 60 (2), pp. 163-178.

Baatz, J.E., Zou, Y., Cox, J.T., Wang, Z., Notter, R.H. High-yield purification of lung surfactant proteins SP-B and SP-C and the effects on surface activity (2001) Protein Expression and Purification, 23 (1), pp. 180-190.

Bastacky, J., Lee, C.Y.C., Goerke, J., Koushafar, H., Yager, D., Kenaga, L., Speed, T.P., Chen, Y., Clements, J.A. Alveolar lining layer is thin and continuous: Low-temperature scanning electron microscopy of rat lung (1995) Journal of Applied Physiology, 79 (5), pp. 1615-1628.

Bi, X., Taneva, S., Keough, K.M.W., Mendelsohn, R., Flach, C.R. Thermal stability and DPPC/Ca2+ interactions of pulmonary surfactant SP-A from bulk-phase and monolayer IR spectroscopy (2001) Biochemistry, 40 (45), pp. 13659-13669.

Booth, V., Waring, A.J., Walther, F.J., Keough, K.M.W. NMR structures of the C-terminal segment of surfactant protein B in detergent micelles and hexafluoro-2-propanol (2004) Biochemistry, 43 (48), pp. 15187-15194.

Brasch, F., Ochs, M., Kahne, T., Guttentag, S., Schauer-Vukasinovic, V., Derrick, M., Johnen, G., Kapp, N., Muller, K.M., Richter, J., Giller, T., Hawgood, S., Buhling, F. Involvement of napsin A in the C- and N-terminal processing of surfactant protein B in type-II pneumocytes of the human lung (2003) Journal of biological chemistry, 278 (49), pp. 49006-49014.

Cavanagh, J., Fairbrother, W.J., Palmer, A.G. & Skelton, N.J. Protein NMR Spectroscopy Principles and Practice (1996) Academic Press, Inc., (ISBN-10: 0121644901 / ISBN-13: 978-0121644901)

Cech, N.B., Enke, C.G. Relating electrospray ionization response to nonpolar character of small peptides (2000) Analytical Chemistry, 72 (13), pp. 2717-2723.

Chiti, F., Stefani, M., Taddel, N., Ramponi, G., Dobson, C.M. Rationalization of the effects of mutations on peptide and protein aggregation rates (2003) Nature, 424 (6950), pp. 805-808.

Clark, D.P., Pazdernik, N.J. Biotechnology: Applying the genetic revolution (2008) Elsevier Science & Technology, (ISBN-10: 0121755525 / ISBN-13: 9780121755522)

Clark, J.C., Wert, S.E., Bachurski, C.J., Stahlman, M.T., Stripp, B.R., Weaver, T.E., Whitsett, J.A. Targeted disruption of the surfactant protein B gene disrupts surfactant homeostasis, causing respiratory failure in newborn mice (1995) Proceedings of the National Academy of Sciences of the United States of America, 92 (17), pp. 7794-7798.

Crouch, E., Wright, J.R. Surfactant proteins A and D and pulmonary host defense (2001) Annual Review of Physiology, 63, pp. 521-554.

Cruz, A., Worthman, L.-A., Serrano, A.G., Casals, C., Keough, K.M.W., Pérez-Gil, J. Microstructure and dynamic surface properties of surfactant protein SP-B/dipalmitoylphosphatidylcholine interfacial films spread from lipid-protein bilayers (2000) European Biophysics Journal, 29 (3), pp. 204-213.

Dumon-Seignovert, L., Cariot, G., Vuillard, L. The toxicity of recombinant proteins in Escherichia coli: A comparison of overexpression in

BL21(DE3), C41(DE3), and C43(DE3) (2004) Protein Expression and Purification, 37 (1), pp. 203-206.

Egelhaaf, S.U., Van Swieten, E., Bosma, T., De Boef, E., Van Dijk, A.A., Robillard, G.T. Size and shape of the repetitive domain of high molecular weight wheat gluten proteins. I. Small-angle neutron scattering (2003) Biopolymers, 69 (3), pp. 311-324.

Frey, T.M. Incidence and prevention of ARDS: A measure of progress (2009) American Journal of Respiratory and Critical Care Medicine, 180 (11), p. 1158.

Gayen, A., Goswami, S.K., Mukhopadhyay, C.NMR evidence of GM1-induced conformational change of Substance P using isotropic bicelles (2011) Biochimica et Biophysica Acta - Biomembranes, 1808 (1), pp. 127-139.

Ghosh, S. Conformational study of papain in the presence of sodium dodecyl sulfate in aqueous medium (2005) Colloids and Surfaces B: Biointerfaces, 41 (2-3), pp. 209-216.

Goddard, T. D., and Kneller, D. G. SPARKY 3 (2005) University of California, San Francisco.

Goerke, J. Pulmonary surfactant: Functions and molecular composition (1998) Biochimica et Biophysica Acta - Molecular Basis of Disease, 1408 (2-3), pp. 79-89.

Griese, M. Pulmonary surfactant in health and human lung diseases: State of the art (1999) European Respiratory Journal, 13 (6), pp. 1455-1476.

Groat, R.G., Schultz, J.E., Zychlinsky, E. Starvation proteins in Escherichia coli: Kinetics of synthesis and role in starvation survival (1986) Journal of Bacteriology, 168 (2), pp. 486-493.

Günther, A., Schmidt, R., Nix, F., Yabut-Perez, M., Guth, C., Rosseau, S., Siebert, C., Grimminger, F., Morr, H., Velcovsky, H.G., Seeger, W. Surfactant abnormalities in idiopathic pulmonary fibrosis, hypersensitivity pneumonitis and sarcoidosis (1999) European Respiratory Journal, 14 (3), pp. 565-573.

Guyton, A.C. and Hall, J.E. Guyton & Hall textbook of medical physiology, Edition 11th (2006) Elsevier - Health Sciences Division (ISBN-10: 1416002138/ ISBN-13: 978-1416002130) pp. 496-497

Haagsman, H.P., Diemel, R.V. Surfactant-associated proteins: Functions and structural variation (2001) Comparative Biochemistry and Physiology - A Molecular and Integrative Physiology, 129 (1), pp. 91-108.

Halliday, H.L., Speer, C.P., Robertson, B. Treatment of severe meconium aspiration syndrome with porcine surfactant (1996) European Journal of Pediatrics, 155 (12), pp. 1047-1051.

Hallman, M., Glumoff, V., Rämet, M. Surfactant in respiratory distress syndrome and lung injury (2001) Comparative Biochemistry and Physiology - A Molecular and Integrative Physiology, 129 (1), pp. 287-294.

Hawco, M.W., Coolbear, K.P., Davis, P.J., Keough, K.M.W. Exclusion of fluid lipid during compression of monolayers of mixtures of dipalmitoylphosphatidylcholine with some other phosphatidylcholines (1981) Biochimica et Biophysica Acta - Biomembranes, 646 (1), pp. 185-187.

Hilty, C., Wider, G., Fernández, C., Wüthrich, K. Membrane protein-lipid interactions in mixed micelles studied by NMR spectroscopy with the use of paramagnetic reagents (2004) ChemBioChem, 5 (4), pp. 467-473.

James McKnight, C., Rafalski, M., Gierasch, L.M. Fluorescence analysis of tryptophan-containing variants of the LamB signal sequence upon insertion into a lipid bilayer (1991) Biochemistry, 30, (25), pp. 6241-6246.

Johnson, W.C. Analyzing protein circular dichroism spectra for accurate secondary structures (1999) Proteins: Structure, Function and Genetics, 35 (3), pp. 307-312.

Kang, J.H., Lee, M.K., Kim, K.L., Hahm, K.-S. The relationships between biophysical activity and the secondary structure of synthetic peptides from the pulmonary surfactant protein SP-B (1996) Biochemistry and Molecular Biology International, 40 (3), pp. 617-627.

Kiefer, H. In vitro folding of alpha-helical membrane proteins (2003) Biochimica et Biophysica Acta - Biomembranes, 1610 (1), pp. 57-62.

Korimilli, A., Gonzales, L.W., Guttentag, S.H. Intracellular localization of processing events in human surfactant protein B biosynthesis (2000) Journal of Biological Chemistry, 275 (12), pp. 8672-8679.

Krol, S., Ross, M., Sieber, M., Kunneke, S., Galla, H.-J., Janshoff, A. Formation of three-dimensional protein-lipid aggregates in monolayer films

induced by surfactant protein B(2000) Biophysical Journal, 79 (2), pp. 904-918.

Kurutz, J.W., Lee, K.Y.C. NMR structure of lung surfactant peptide SP-B11-25 (2002) Biochemistry, 41 (30), pp. 9627-9636.

Laws, D.D., Bitter, H.-M.L., Jerschow, A. Solid-state NMR spectroscopic methods in chemistry (2002) Angewandte Chemie - International Edition, 41 (17), pp. 3096-3129.

Lewis, J.F., Veldhuizen, R. The Role of Exogenous Surfactant in the Treatment of Acute Lung Injury (2003) Annual Review of Physiology, 65, pp. 613-642.

Lubec, G., Afjehi-Sadat, L. Limitations and pitfalls in protein identifications by mass spectrometry (2007) Chemical Reviews, 107 (8), pp. 3568-3584.

Marraro, G.A. Perspectives for use of surfactant in children and adults (2004) Journal of Maternal-Fetal and Neonatal Medicine, 16 (SUPPL. 2), pp. 29-31.

Mravljak, J., Konc, J., Hodoscek, M., Solmajer, T., Pecar, S. Spin-labeled alkylphospholipids in a dipalmitoylphosphatidylcholine bilayer: Molecular dynamics simulations (2006) Journal of Physical Chemistry B, 110 (51), pp. 25559-25561.

Munford, R.S., Sheppard, P.O., O'Hara, P.J. Saposin-like proteins (SAPLIP) carry out diverse functions on a common backbone structure (1995) Journal of Lipid Research, 36 (8), pp. 1653-1663.

Nilsson, M. The DOSY Toolbox: A new tool for processing PFG NMR diffusion data (2009) Journal of Magnetic Resonance, 200 (2), pp. 296-302.

Nogee, L.M., Wert, S.E., Proffit, S.A., Hull, W.M., Whitsett, J.A. Allelic heterogeneity in hereditary surfactant protein B (SP-B) deficiency (2000) American Journal of Respiratory and Critical Care Medicine, 161 (3 I), pp. 973-981.

Patthy, L. Homology of the precursor of pulmonary surfactant-associated protein SP-B with prosaposin and sulfated glycoprotein 1 (1991) Journal of Biological Chemistry, 266 (10), pp. 6035-6037.

Pérez-Gil, J. Structure of pulmonary surfactant membranes and films: The role of proteins and lipid-protein interactions (2008) Biochimica et Biophysica Acta - Biomembranes, 1778 (7-8), pp. 1676-1695.

Pochapsky, T.C., and Pochapsky, S.S. NMR for Physical and Biological Scientists (2007) Garland Science (ISBN-10: 9780815341031/ISBN-13: 978-0815341031).

Price, W.S. Pulsed-field gradient nuclear magnetic resonance as a tool for studying translational diffusion: Part 1. Basic theory (1997) Concepts in Magnetic Resonance, 9 (5), pp. 299-335.

Pujals, S., Giralt, E. Proline-rich, amphipathic cell-penetrating peptides (2008) Advanced Drug Delivery Reviews, 60 (4-5), pp. 473-484.

Ragin, A.D., Chmielewski, J. Probing essential residues for cellular uptake with a cationic nuclear localization signal sequence (2004) Journal of Peptide Research, 63 (2), pp. 155-160.

Rainey, J.K., Sykes, B.D. Optimizing oriented planar-supported lipid samples for solid-state protein NMR (2005) Biophysical Journal, 89 (4), pp. 2792-2805.

Reeve, C.A., Bockman, A.T., Matin, A. Role of protein degradation in the survival of carbon-starved Escherichia coli and Salmonella typhimurium (1984) Journal of Bacteriology, 157 (3), pp. 758-763.

Revak, S.D., Merritt, T.A., Hallman, M., Heldt, G., La Polla, R.J., Hoey, K., Houghten, R.A., Cochrane, C.G. The use of synthetic peptides in the formation of biophysically and biologically active pulmonary surfactants (1991) Pediatric Research, 29 (5), pp. 460-465.

Romano, D., Molla, G., Pollegioni, L., Marinelli, F. Optimization of human d-amino acid oxidase expression in Escherichia coli (2009) Protein Expression and Purification, 68 (1), pp. 72-78.

Ryan, M.A., Qi, X., Serrano, A.G., Ikegami, M., Perez-Gil, J., Johansson, J., Weaver, T.E. Mapping and analysis of the lytic and fusogenic domains of surfactant protein B (2005) Biochemistry, 44 (3), pp. 861-872.

Salditt, T. Lipid-peptide interaction in oriented bilayers probed by interface-sensitive scattering methods (2003) Current Opinion in Structural Biology, 13 (4), pp. 467-478.

Sanders, C.R., Sönnichsen, F. Solution NMR of membrane proteins: Practice and challenges (2006) Magnetic Resonance in Chemistry, 44 (7 SPEC. ISS.), pp. S24-S40.

Sarker, M. Structures and Interactions of Lung Surfactant Protein B (SP-B) Peptides (2010) PhD Thesis: Department of Physics & Physical Oceanography, Memorial University of Newfoundland.

Sarker, M., Rose, J., McDonald, M., Morrow, M.R., Booth, V. Modifications to surfactant protein B structure and Lipid interactions under respiratory distress conditions: Consequences of tryptophan oxidation (2011) Biochemistry, 50 (1), pp. 25-36.

Sarker, M., Waring, A.J., Walther, F.J., Keough, K.M.W., Booth, V. Structure of mini-B, a functional fragment of surfactant protein B, in detergent micelles (2007) Biochemistry, 46 (39), pp. 11047-11056.

Schram, V., Hall, S.B. SP-B and SP-C alter diffusion in bilayers of pulmonary surfactant (2004) Biophysical Journal, 86 (6), pp. 3734-3743.

Schurch, S., Possmayer, F., Cheng, S., Cockshutt, A.M. Pulmonary SP-A enhances adsorption and appears to induce surface sorting of lipid extract

surfactant (1992) American Journal of Physiology - Lung Cellular and Molecular Physiology, 263 (2 7-2), pp. L210-L218.

Seeger, W., Grube, C., Gunther, A., Schmidt, R. Surfactant inhibition by plasma proteins: Differential sensitivity of various surfactant preparations (1993) European Respiratory Journal, 6 (7), pp. 971-977.

Serrano, A.G., Pérez-Gil, J. Protein-lipid interactions and surface activity in the pulmonary surfactant system (2006) Chemistry and Physics of Lipids, 141 (1-2), pp. 105-118.

Shai, Y. Mechanism of the binding, insertion and destabilization of phospholipid bilayer membranes by α-helical antimicrobial and cell non-selective membrane-lytic peptides (1999) Biochimica et Biophysica Acta - Biomembranes, 1462 (1-2), pp. 55-70.

Shiffer, K., Hawgood, S., Haagsman, H.P., Benson, B., Clements, J.A., Goerke, J. Lung surfactant proteins, SP-B and SP-C, alter the thermodynamic properties of phospholipid membranes: A differential calorimetry study (1993) Biochemistry, 32 (2), pp. 590-597.

Sorensen, H. P., Mortensen, K. K. Soluble expression of recombinant proteins in the cytoplasm of Escherichia coli (2005) Microbial Cell Factories, 4(1) pp.1-8

Sreerama, N., Woody, R.W. A self-consistent method for the analysis of protein secondary structure from circular dichroism (1993) Analytical Biochemistry, 209 (1), pp. 32-44.

Sreerama, N., Woody, R.W. Computation and Analysis of Protein Circular Dichroism Spectra (2004) Methods in Enzymology, 383, pp. 318-351.

Sreerama, N., Woody, R.W. Estimation of protein secondary structure from circular dichroism spectra: Comparison of CONTIN, SELCON, and CDSSTR methods with an expanded reference set (2000) Analytical Biochemistry, 287 (2), pp. 252-260.

Sternin, E., Fine, B., Bloom, M., Tilcock, C.P., Wong, K.F., Cullis, P.R. Acyl chain orientational order in the hexagonal HII phase of phospholipid-water dispersions (1988) Biophysical Journal, 54 (4), pp. 689-694.

Stevens, T.P., Sinkin, R.A. Surfactant replacement therapy (2007) Chest, 131 (5), pp. 1577-1582.

Sueishi, K., Benson, B.J. Isolation of a major apoliprotein of canine and murine pulmonary surfactant. Biochemical and immunochemical characteristics (1981) Biochimica et Biophysica Acta, 665 (3), pp. 442-453.

Taneva, S.G., Keough, K.M.W. Dynamic surface properties of pulmonary surfactant proteins SP-B and SP-C and their mixtures with dipalmitoylphosphatidylcholine (1994) Biochemistry, 33 (49), pp. 14660-14670.

Tokieda, K., Whitsett, J.A., Clark, J.C., Weaver, T.E., Ikeda, K., McConnell, K.B., Jobe, A.H., Ikegami, M., Iwamoto, H.S. Pulmonary dysfunction in neonatal SP-B-deficient mice (1997) American Journal of Physiology - Lung Cellular and Molecular Physiology, 273 (4 17-4), pp. L875-L882.

Ueno, T., Linder, S., Na, C.-L., Rice, W.R., Johansson, J., Weaver, T.E. Processing of Pulmonary Surfactant Protein B by Napsin and Cathepsin H (2004) Journal of Biological Chemistry, 279 (16), pp. 16178-16184.

Veldhuizen, E.J.A., Waring, A.J., Walther, F.J., Batenburg, J.J., Van Golde, L.M.G., Haagsman, H.P. Dimeric N-terminal segment of human surfactant

protein B (dSP-B1-25) has enhanced surface properties compared to monomeric SP-B1-25 (2000) Biophysical Journal, 79 (1), pp. 377-384.

Veldhuizen, R., Nag, K., Orgeig, S., Possmayer, F. The role of lipids in pulmonary surfactant (1998) Biochimica et Biophysica Acta - Molecular Basis of Disease, 1408 (2-3), pp. 90-108.

Voorhout, W.F., Veenendaal, T., Haagsman, H.P., Weaver, T.E., Whitsett, J.A., Van Golde, L.M.G., Geuze, H.J. Intracellular processing of pulmonary surfactant protein B in an endosomal/lysosomal compartment (1992) American Journal of Physiology - Lung Cellular and Molecular Physiology, 263 (4 7-4), pp. L479-L486.

Walther, F.J., Hernandez-Juviel, J.M., Gordon, L.M., Sherman, M.A., Waring, A.J. Dimeric surfactant protein B peptide SP-B1-25 in neonatal and acute respiratory distress syndrome (2002) Experimental Lung Research, 28 (8), pp. 623-640.

Walther, F.J., Waring, A.J., Hernandez-Juviel, J.M., Gordon, L.M., Wang, Z., Jung, C.L., Ruchala, P., Clark, A.P., Smith, W.M., Sharma, S., Notter, R.H. Critical structural and functional roles for the N-terminal insertion sequence in surfactant protein B analogs (2010) PloS one, 5 (1): e8672.

Waring, A.J., Walther, F.J., Gordon, L.M., Hernandez-Juviel, J.M., Hong, T., Sherman, M.A., Alonso, C., Alig, T., Braun, A., Bacon, D., Zasadzinski, J.A. The role of charged amphipathic helices in the structure and function of surfactant protein B (2005) Journal of Peptide Research, 66 (6), pp. 364-374.

Whitsett, J.A., Weaver, T.E. Hydrophobic surfactant proteins in lung function and disease (2002) New England Journal of Medicine, 347 (26), pp. 2141-2148.

Whitsett, J.A., Wert, S.E., Weaver, T.E. Alveolar surfactant homeostasis and the pathogenesis of pulmonary disease (2010) Annual Review of Medicine, 61, pp. 105-119.

Wüstneck, R., Perez-Gil, J., Wüstneck, N., Cruz, A., Fainerman, V.B., Pison, U. Interfacial properties of pulmonary surfactant layers (2005) Advances in Colloid and Interface Science, 117 (1-3), pp. 33-58.

Wüthrich K. NMR of Proteins and Nucleic Acids (1986) John Wiley & Sons. (ISBN-10: 0471828939, ISBN-13: 978-0471828938), pp.234-238

Yu, H. Extending the size limit of protein nuclear magnetic resonance (1999) PNAS 96 (2), pp. 332-334.

Zaltash, S., Palmblad, M., Curstedt, T., Johansson, J., Persson, B. Pulmonary surfactant protein B: A structural model and a functional analogue (2000) Biochimica et Biophysica Acta - Biomembranes, 1466 (1-2), pp. 179-186.

Supplemental materials

Supplementary figure 1.

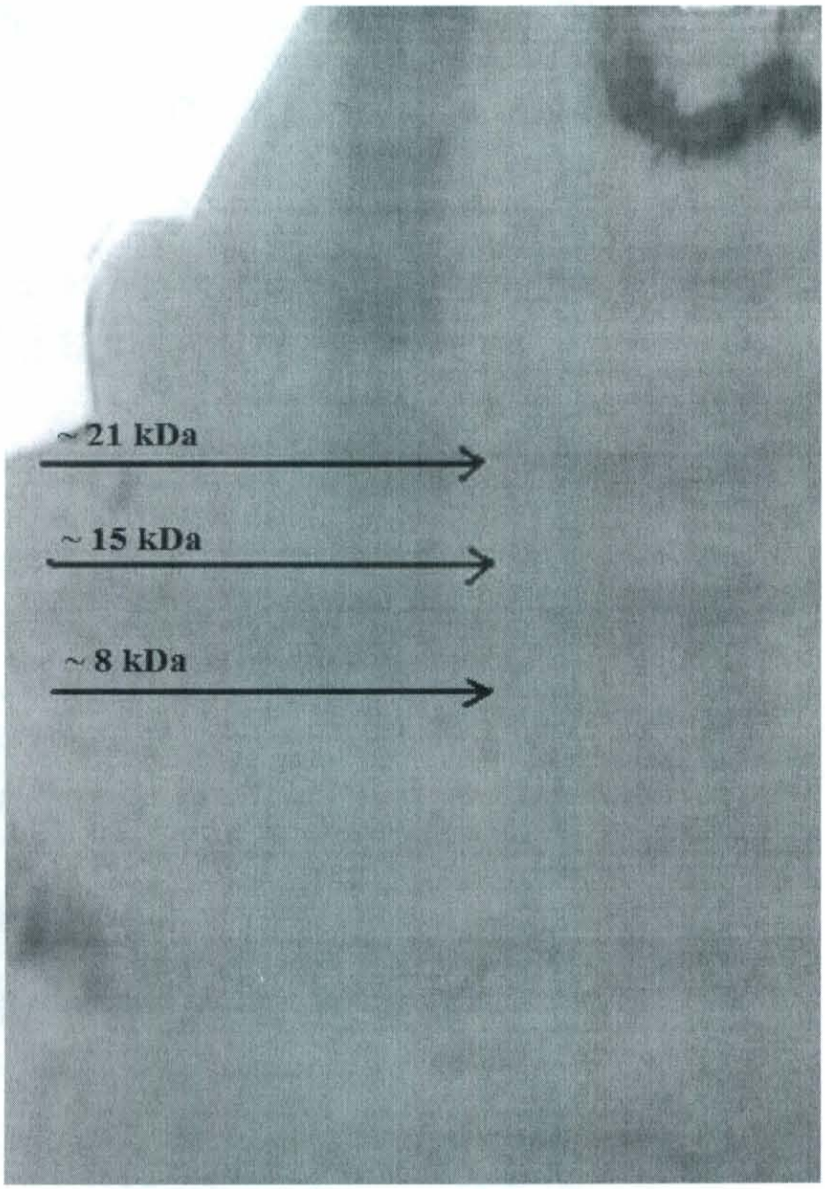

Figure S1. SDS-PAGE gel, Comassie stained of purified SN-SP-B. While we were expecting only one band (~27 kDa for SN-SP-B), three bands were detected in the purified sample after column chromatography